Investigation of optical wireless for employment within a vehicular environment

Zaiton Abdul Mutalip

A thesis presented for the degree of

Doctor of Philosophy

School of Engineering

March 2016

To my family, for their unconditional support

Table of Contents

Table of Contents ..... **i**

List of figures ..... **vi**

List of tables ..... **x**

Acronyms ..... **xiii**

Acknowledgements ..... **xv**

Declaration ..... **xvi**

Abstract ..... **xvii**

Publications associated with this research work ..... **xx**

Chapter 1 : Introduction **1**

1.1 General overview 1

1.2 Motivation 3

1.3 Contribution to knowledge 4

1.4 Outline of the thesis 5

Chapter 2 : Background Research and Related Work **7**

2.1 Introduction 7

2.2 Overview of Optical Wireless Communication Systems 7

2.2.1 Optical Wireless Mathematical Model 8

2.2.2 Optical Wireless Channel Model 8

2.2.3 Optical Wireless configurations 12

2.2.4 Modulation Format 13

2.3 Overview of Automotive Network 16

2.4 Wired Intra Vehicle Communication Networks 18

2.4.1 Controller Area Network (CAN) 20

2.4.2 Time-triggered CAN (TTCAN) 20

2.4.3 Local Interconnect Network (LIN) 20

2.4.4 Time-Triggered Protocol (TTP) 21

2.4.5 Byteflight 21

2.4.6 FlexRay 21

2.4.7 MOST 22

2.4.8 IDB-1394 22

2.5 Wireless Intra Vehicle Communication Networks 22

2.5.1 Wi-Fi 23

2.5.2 Bluetooth 24

2.5.3 Ultra-Wideband (UWB) 24

2.5.4 ZigBee 25

2.5.5 Radio-Frequency IDentification (RFID) 25

2.5.6 Optical Wireless 25

2.6 Common Wireless Intra Vehicle Network Requirements 26

2.6.1 Bandwidth Requirements 27

2.7 OW in Intra Vehicle Environment 28

2.8 Issues and Design Challenges 29

2.9 Conclusion 30

Chapter 3 : Transmitter and Receiver Design 32

3.1 Introduction 32

3.2 The basic system 32

3.2.1 The basic system requirement 33

3.3 Optical wireless transmitter and receiver design 33

3.3.1 Optical source 33

3.3.2 Optical detector 35

3.3.3 Bandwidth calculation 35

3.3.4 Infrared LED driver 39

3.3.5 Pre-emphasis 42

3.3.6 Front-end 44

3.4 Precautions 48

3.5 Performance study of the system designed 48

3.6 System Noise Analysis 50

3.7 Conclusion....52

Chapter 4 : Channel Characterization – Line-of-Sight Transmission 54

4.1 Introduction....54

4.2 Ideal LOS link....55

4.3 The tubes....58

4.4 Channel measurement setup....61

4.5 Channel characterisation by measurements....61

4.5.1 Divergence angle....61

4.5.2 Frequency response....63

4.5.3 Optical power....68

4.6 Conclusions....78

Chapter 5 : Channel Characterization – Non Line-of-Sight Transmission 80

5.1 Introduction....80

5.2 NLOS Channel model....81

5.3 Reflection characteristics....81

5.4 Received power....82

5.5 Straight tubes....82

5.5.1 Received optical power at different transmission angles....83

5.5.2 Path loss....85

5.6 Bend tube measurements....87

5.6.1 Plastic tubes....90

5.6.2 Metal tubes 95

5.7 Conclusions 111

Chapter 6 : Digital System Transmission – a prototype 113

6.1 Introduction 113

6.2 Methodology 114

6.3 Eye pattern 119

6.3.1 SNR 141

6.3.2 Relationship between SNR, Q-factor and BER 143

6.4 Conclusion 149

Chapter 7 : Conclusions and future work 151

7.1 Summary of the work 151

7.2 Improvements and suggestions for further work 155

References 157

Appendix A 167

Appendix B 169

Appendix C 184

List of figures

Figure 2-1 OW communication system 8

Figure 2-2 Lambertian reflection pattern [19] 9

Figure 2-3 Typical Phong's reflection pattern [19] 10

Figure 2-4 OW link configurations [39] 13

Figure 2-5 Embedded Automotive Subsystems 17

Figure 2-6 Intra-vehicle networks 19

Figure 2-7 Common In-vehicle Network Protocols [56] 20

Figure 3-1 OW communication system 33

Figure 3-2 Fundamental transmitter 36

Figure 3-3 Fundamental receiver 37

Figure 3-4 SFH205F CV characteristic 38

Figure 3-5 Relative response of VISHAY VSLY5850 39

Figure 3-6 Analogue drive circuit 40

Figure 3-7 Darlington IRLED driver 41

Figure 3-8 Darlington IRLED driver normalised response 42

Figure 3-9 IRLED transmitter with pre-emphasis 43

Figure 3-10 Normalised response of the system 44

Figure 3-11 High-impedance front-end receiver with amplifier 47

Figure 3-12 Waveforms of the test signal 49

Figure 3-13 Optical power intensity at a distance 50

Figure 4-1 LOS link model [94] 55

Figure 4-2 Vertical assessment scenarios 57

Figure 4-3 Representative tubes 58

Figure 4-4 Reflection coefficient measurement setup 60

Figure 4-5 Channel measurement experimental setup 61

Figure 4-6 Divergence angle 62

Figure 4-7 Determination of the number of reflections in a straight tube. 62

Figure 4-8 Circular cardboard tube normalised response 64

Figure 4-9 Circular plastic tube normalised response 64

Figure 4-10 Circular mild steel tube normalised response 64

Figure 4-11 Square aluminium tube normalised response 65

Figure 4-12 Square aluminium tube normalised response 65

Figure 4-13 Circular aluminium tube normalised response 65

Figure 4-14 Circular galvanised aluminium tube normalised response 66

Figure 4-15 Square mild steel tube normalised response 66

Figure 4-16 Free space normalised response 66

Figure 4-17 Normalised response at 0.5 metre range 69

Figure 4-18 Normalised response at 1 metre range 70

Figure 4-19 Radiometric output power for different IRLED forward currents. 71

Figure 4-20 Photometric output power for different IRLED forward currents.....71

Figure 4-21 Received optical power plotted against separation distance. 73

Figure 4-22 Received optical power plotted against tube diameter at 0.5 metre and 1 metre range. 75

Figure 4-23 Received optical power plotted against reflection coefficient at 0.5 metre and 1 metre range.....76

Figure 4-24 LOS path loss at different separation distances.....77

Figure 5-1 Transmitter and receiver orientation experimental setup.....83

Figure 5-2 Received power at different angles (0.5 metre distance). 84

Figure 5-3 Received power at different angles (1 metre distance). 84

Figure 5-4 Path loss at different angle (0.5 metre distance). 85

Figure 5-5 Path loss at different angle (1 metre distance). 86

Figure 5-6 Array of four IrLEDs arrangement. 88

Figure 5-7 Frequency response of array IrLEDs transmitter 88

Figure 5-8 Array of four IrLEDs transmitter circuit.....89

Figure 5-9 Experimental materials bent through different angles – Plastic. 90

Figure 5-10 Normalised response of plastic tube. 91

Figure 5-11 Waveforms of B1.....92

Figure 5-12 Waveforms of B2.....92

Figure 5-13 Waveforms of B3.....93

Figure 5-14 Waveforms of B4.....93

Figure 5-15 Experimental setup for identifying best angle selection. 95

Figure 5-16 Waveforms of best angle selection. 96

Figure 5-17 Determination of the number of reflections in 20 mm bent tube. 98

Figure 5-18 Circular mild steel tube captured waveform at 30° bend.....99

Figure 5-19 Received optical power plotted against number of reflections. 108

Figure 5-20 Signal to noise ratio (measured using power meter). 109

Figure 5-21 Signal to noise ratio (measured using photo meter). 109

Figure 5-22 Calculated path loss (based on measurement using power meter) 110

Figure 5-23 Calculated path loss (based on measurement using photo meter) 110

Figure 6-1 Pulse waveform at the oscillator input, and the system output. 115

Figure 6-2 Pulse waveform at the receiver output.....116

Figure 6-3 SNR at the receiver at different frequency.....142

Figure 6-4 relationship between BER and Q-factor. 145

Figure 6-5 relationship between BER and SNR.....146

List of tables

Table 2-1 Main properties of OW configurations [42] 13

Table 2-2 Comparison between PPM, DPPM and DPIM [50] 15

Table 2-3 Common wireless network drawbacks 27

Table 2-4 Network bandwidth requirements.....28

Table 3-1 Technical features of optical sources and detectors.....35

Table 4-1 experimental materials 59

Table 4-2 power loss.....63

Table 5-1 Received optical power for plastic tubes.....94

Table 5-2 Consequent path loss for plastic tubes. 94

Table 5-3 Experimental metal tube bends.....97

Table 5-4 Estimation number of reflections in bent tubes 98

Table 5-5 Square aluminium tube normalised response and waveforms 100

Table 5-6 Square aluminium tube normalised response and waveforms 102

Table 5-7 Circular aluminium tube normalised response and waveforms.....104

Table 5-8 Circular galvanised aluminium normalised response and waveforms.....106

Table 6-1 Transmitted and received pulse with eye pattern at different frequency .118

Table 6-2 Free space transmission: back-to-back - transmitted and received pulse with eye pattern at different frequency 120

Table 6-3 Free space transmission: 1 metre distance - transmitted and received pulse with eye pattern at different frequency 121

Table 6-4 Transmission within 35mm circular mild steel tube at 30° bend - transmitted and received pulse with eye pattern at different frequency.....123

Table 6-5 Transmission within 35mm circular mild steel tube at 45° bend - transmitted and received pulse with eye pattern at different frequency.....124

Table 6-6 Transmission within 35mm circular mild steel tube at 60° bend - transmitted and received pulse with eye pattern at different frequency.....125

Table 6-7 Transmission within 40 mm square aluminium tube at 30° bend - transmitted and received pulse with eye pattern at different frequency.....126

Table 6-8 Transmission within 40 mm square aluminium tube at 45° bend - transmitted and received pulse with eye pattern at different frequency.....127

Table 6-9 Transmission within 40 mm square aluminium tube at 60° bend - transmitted and received pulse with eye pattern at different frequency.....128

Table 6-10 Transmission within 20 mm square aluminium tube at 30° bend - transmitted and received pulse with eye pattern at different frequency 129

Table 6-11 Transmission within 20 mm square aluminium tube at 45° bend - transmitted and received pulse with eye pattern at different frequency 130

Table 6-12 Transmission within 20 mm square aluminium tube at 60° bend - transmitted and received pulse with eye pattern at different frequency 131

Table 6-13 Transmission within 20 mm circular aluminium tube at 30° bend - transmitted and received pulse with eye pattern at different frequency 132

Table 6-14 Transmission within 20 mm circular aluminium tube at 45° bend - transmitted and received pulse with eye pattern at different frequency 133

Table 6-15 Transmission within 20 mm circular aluminium tube at 60° bend - transmitted and received pulse with eye pattern at different frequency 134

Table 6-16 Transmission within 35 mm circular galvanised aluminium tube.....135

Table 6-17 Transmission within 35 mm circular galvanised aluminium tube.....136

Table 6-18 Transmission within 35 mm circular galvanised aluminium tube.....137

Table 6-19 Transmission within 40 mm square mild steel tube.....138

Table 6-20 Transmission within 40 mm square mild steel tube.....139

Table 6-21 Transmission within 40 mm square mild steel tube.....140

Table 6-22 performance summary.....147

Acronyms

CAN	Controller Area Network
DD/IM	Direct Detection / Intensity Modulation
DH-PIM	Double-Pulse Interval Modulation
DPIM	Digital Pulse Interval Modulation
DPPM	Differential Pulse-Position Modulation
ECU	Electronics Control Unit
EM	Electromagnetic
FM	Frequency Modulation
FOV	Field of View
IrDA	Infrared Data Association
IRLED	Infrared Light Emitting Diode
LAN	Local Area Network
LED	Light Emitting Diode
LIN	Local Interconnect Network
LOS	Line of Sight
MAC	Medium Access Control
MOST	Media Oriented Systems Transport
MSM	Multiple-Subcarrier Modulation
NLOS	Non Line of Sight
OOK	On Off Keying
SNR	Optical Signal to Noise Ratio
OW	Optical Wireless
OWC	Optical Wireless Communication

PM	Pulse Modulation
PPM	Pulse Position Modulation
RF	Radio Frequency
RFID	Radio-Frequency Identification
RMS	Root Mean Square
RZ	Return to Zero
SNR	Signal to Noise Ratio
SSM	Single-Subcarrier Modulation
TDMA	Time Division Multiple Access
TTP	Time-Triggered Protocol
TTCAN	Time-Triggered CAN
UWB	Ultra-Wide Band
V2I	Vehicle-to-Infrastructure
V2V	Vehicle-to-Vehicle

Acknowledgements

First of all, I thank Allah, for giving me knowledge and strength to complete this PhD thesis. The completion of the thesis would not be possible without the support and encouragement of many individuals. I thank all the people who have supported me throughout my PhD course.

I am very grateful to the Ministry of Higher Education of Malaysia (MOHE) and Universiti Teknikal Malaysia Melaka, Malaysia (UTeM) for providing me with a scholarship. I would not have completed a PhD without this financial assistance. I wish to express my gratitude to The University of Warwick for the facilities for this research.

I would like to extend my sincere thanks my research advisor, Professor Roger J. Green, Dr Mark S. Leeson and Dr Matthew Higgins for their guidance, ideas patient advising, understanding and continuous support.

In addition, I wish to thank the secretaries and technical assistants in the engineering department, for assisting me in many different ways. Kerrie, Ian, Will and Huw deserve special mention.

Last but not least, without my family's endless love, this quality research work would not be possible. Thanks for the 'dua', love, patience, and encouragement.

Declaration

This thesis is submitted in partial fulfilment for the degree of Doctor of Philosophy under the regulations set out by the Graduate School at the University of Warwick. This thesis is solely composed of research completed by ZAITON ABDUL MUTALIP, except where stated, under the supervision of Professor Roger J. Green, Dr Mark S. Leeson and Dr Matthew Higgins, between the dates of January 2012 and March 2016. No part of this thesis has been previously submitted to the University of Warwick or any other academic institution for admission to a higher degree.

Zaiton Abdul Mutalip
March 2016

Abstract

The substantial increase in powerful electronic systems and functions has produced significant implications for the vehicular industry, where the amount of wiring infrastructure has increased the vehicle weight, weakened performance, and made adherence to reliability standards difficult. Eventually, connecting the electronics infrastructure was mostly complicated and costly in vehicular domain systems. Thus, little research has been conducted to explore appropriate wireless technologies that may be suitable with the emerging network standard within the context of vehicular networks.

This thesis describes an in-depth investigation of deploying an optical wireless communication system within the vehicular environment, particularly in confined spaces. A wide variety of measurements has been performed using tubes of various materials and geometries, in a laboratory setup. The principle objective is to provide a primary knowledge of optical wireless channel characterization within a laboratory vehicular setting. The work presented is a study on directed line-of-sight (LOS) and non-LOS (NLOS) links, and focuses on frequency response, power efficiencies, and path losses in different experimental settings. Further, a variety of experimental settings was used in respect to different receiver/transmitter orientations and various bent tubes angles in order to investigate the channel conditions. The noise analysis,

SNR, path loss and the eye pattern for the digital system prototype designed were also analysed.

The system requirement for the LOS link were based on the transmission of the sinusoidal signal at a distance of 1 m with 13 MHz signal and approximately 15.6 dB SNR. Successful demonstration of the OWC within smaller size and high reflection coefficient material are promising. In addition to good transmitter and high sensitivity receiver.

The NLOS link also demonstrated a good indication, both in straight tube with angled transmitter/receiver orientation and bend tubes. Detail studies on NLOS link with pulse signal transmission, which replicates a digital system transmission with 54.48 mW or 44.58 mW/cm^2 output power,6 MHz signal transmission with the aim of 10^{-4} to 10^{-6} BER. Although, the operational functionality of digital system has successfully demonstrated, however achieving the desired BER is a bit difficult with the designed system. Further improvement on the highly sensitive receiver design, a proper modulation scheme is required in order to improve the quality of the transmitted signal in terms of SNR and BER.

The study also suggested that the transmission within the metal tubes is better than in plastic tubes in addition to minimum bend angle, smaller tube diameter and high reflective coefficient. Transmission within 20 mm circular aluminium tube and 35 mm galvanised aluminium tube are the best so far.

Finally, based on the initial viability results, it was seen that it is possible to implement an optical wireless communication infrastructure within the vehicular environment. Experimental validation of the system proposed shows that achieving high data rates is not a problem with the use of high brightness, high power LEDs as this system is

going to be implemented within the vehicle chassis, thus the eye safety constraints should not be a limiting factor. Therefore, in this study, optical wireless transmission within the vehicular environment is proposed, solving the problems of vehicular networking systems.

Publications associated with this research work

The following papers have been published as a result of the work contained within this thesis.

Conference Paper

R. J. Green, Z. Rihawi, Z. A. Mutalip, M. S. Leeson, and M. D. Higgins, "Networks in automotive systems: The potential for optical wireless integration," in Transparent Optical Networks (ICTON), 2012 14th International Conference on, 2012, pp. 1–4

Book Chapter

M. D. Higgins, Z. Rihawi, Z. A. Mutalip, R. J. Green and M. S. Leeson, "Optical Wireless Communications in Vehicular Systems", Communication in Transportation Systems, O. Strobel (ed.), IGI Group, ISBN 978-14-666-2976-9, Chapter 7, pp. 209-222, 2013.

Journal Paper

Z. S. Rihawi, Z. A. Mutalip, M. S. Leeson, M. D. Higgins and R. J. Green, "Free Space Optical Communications in Vehicular Networks Using Rectangular Guiding Models", Photonics Technology Letters, vol. 28, no. 13, pp. 1430-1433, 2016.

Chapter 1: Introduction

1.1 General overview

Automotive manufacturers constantly explore, improve and develop advanced inventions to satisfy buyers' requirements, and rigid regulation in terms of performance, safety, fuel utilization proficiency, and more latterly ecological regulations. In parallel, rapid advances in execution and reliability of electronic embedded frameworks has emerged in the course of recent decades. Such execution and dependability empowers manufacturers to actualize complex vehicle control frameworks, which they are trying to accomplish by the utilization of out-dated mechanical control frameworks. Progress in suitable electronic control frameworks is being used to help drivers control decisively the vehicle through capacities, for example, steering, traction, stability, braking, suspension, or motor control [1][2][3].

Consequently, a vehicle consists of numerous numbers of circuits, sensors, and many other electrical components. Thus, communication is necessary amongst these circuits and functions of the vehicle. If all of the electrical devices, sensors, switches and motors in the vehicle are gathered together, the resulting quantity of cabling and

networks is large. Thus, networking provides a more effective method for complex in-vehicle communications. An in-vehicle communication system is an electronic network that interconnects all electrical and electronic components inside the vehicle.

The advancement of electronic systems has significant implications for automotive engineering. Previously, one particular electronic element was connected to another by single, point-to-point wiring. As the electronic content increased, the wiring increased, resulting in the increase of the vehicle weight, weakened performance, increased fuel consumption, and it has become harder to achieve the reliability standards required, as a result [1][2][3]. Several standards have been initiated by the Society of Automobile Engineers (SAE), International Standards Organization and International Electrotechnical Commission (ISO/IEC). These were developed for vehicular communication and protocols requirements and may be referred to by the interested reader [4][5]

In automotive communications, two areas that are getting considerable attention are the protocols and technologies that support x-by-wire applications, such as, for example, Flexray, and the protocols and technologies intended for telematics and wireless applications. X-by-wire is a technology that has replaced conventional mechanical connections with the use of electrical or electro-mechanical systems to execute vehicle functions. Automotive telematics is defined as any wireless information or communications service involved in a vehicle. There are several applications aggressively pushing for the usage of wireless communications in automotive systems, for both for inter- and for intra-vehicle communications [6][7].

References [6] and [8] presented the most commonly-used wireless protocols for inter-/intra-vehicle communications, namely Bluetooth, ZigBee, UWB, Wi-Fi and Wi-Max. These wireless networks behave differently under different conditions and are

evaluated by the performance and reliability of the protocols. All the systems exploit radio frequency (RF) methods, which offer flexibility, new abilities, but also RF vulnerability. Regrettably, other communication devices (wrist radios and personal locators) using similar frequencies can interfere with the transmission. Also, Federal Communications Commission (FCC) licenses may be required thus limiting the choices and making them costly whilst offering lower speed compared to infrared transmission.

Optical wireless communications (OWC) are now beginning to be introduced into vehicular applications, offering various advantages, for instance, immunity from electromagnetic interference, flexibility, great bandwidth capability, as well as less weight than copper cable/wire systems used for communication and control. Another important highlight of OWC is their low power consumption [9], [10], [10].

1.2 Motivation

The work by other researchers in the use of OWC within the vehicle are limited to the use in the cabin of the vehicle, and focus on the distribution of entertainment data, which was proposed as early as 1998 [11][12]. To the extent of the author's knowledge, there is no work in the open literature describing extensive research, or ongoing research developments currently being studied by others, concerning the transmission of an optical wireless signal in small confined spaces, such as in tubes, nor are there theoretical models and/or simulations precisely focused on it.

Understanding of the behaviour of such networks is critical in designing, simulating, and analysing any intra-vehicle optical wireless system; gathering experimental data on these channels is, therefore, essential. This has motivated the author to investigate

further the performance of optical wireless communication in confined spaces, particularly in hollow tubes.

1.3 Contribution to knowledge

Most of the existing research has concentrated on the use of OWC within the cabin of the vehicle, and has not incorporated any experimental results. All the previous discussions and conclusions were based on analytical models and simulation results. To fulfil the research objectives, diverse aspects of the research were addressed. The primary research intention presented in this work is an experimental investigation of OWC implementation within the vehicular environment. Based on the extensive channel measurements and verifications, the novelty of this research includes:

- In general, OWC links in an automotive environment is still relatively new, and there is much space that needs to be explored practically. The work within this thesis contributes to primary knowledge on intra-vehicle communications, and is the first step towards the generation of a general theory for communication within a vehicle chassis.
- A practical and cost-effective demonstration model illustrating the use of OWC signal transmission through hollow tubes for LOS and NLOS environment has been developed. The relative response and effective modulation bandwidth of the IRLED has been presented practically. Then, the electrical signal-to-noise ratio (SNR) of the desired system has been analysed.
- The OWC channel through the line-of-sight (LOS) transmission has been characterised. Firstly, the characteristics of IR reflections on different materials were studied. Then, the study of the effects of various system parameters on

channel frequency response and path loss within the LOS environment was undertaken.

- The OWC channel through the non-line-of-sight (NLOS) transmission within a vehicle has been characterised. The study has concentrated on the effects of various system parameters on channel frequency response and path loss within the NLOS environment. Furthermore, the number of reflections within the tubes at different bending angles was estimated.
- An experimental proof-of-concept of an OWC link for employment within a vehicular environment, within the chassis of a vehicle, particularly in hollow tubes, was demonstrated for the first time, showing significant potentials for the deployment thereof.
- A mathematical expression for the received optical power density for the case of specific materials and geometries has been determined.
- A practical approach for determining the best angle selection to outline the orientation of the transmitter for the highest level of received signal power was investigated.
- The SNR and path loss for the NLOS environment at three different bending angles was determined.

The findings are believed to be useful for designing, predicting and evaluating the OWC system's abilities, and to open up a new scope in OWC applications, specifically within the vehicular environment.

1.4 Outline of the thesis

The work presented in this thesis is divided into 7 chapters and are structured as

follows:

- Chapter 1 introduces the area of optical wireless communication systems and defines the perspectives of this research.
- Chapter 2 presents an overview of optical wireless communications and describes various transmission techniques within automotive networks in general. This chapter focuses on the intra-vehicle communication networks and also discusses different issues related to the implementation of optical wireless communication systems within an automotive environment.
- Chapter 3 describes the experimental apparatus and the construction of the transmitter and the receiver. A transmitter and a receiver have been designed and implemented using infrared LEDs. The system design is presented its capabilities are also shown, including the noise analysis.
- Chapter 4 describes the experimental procedures and results obtained using straight tubes, which represent the line-of-sight (LOS) transmission situations in confined spaces. It also includes a discussion regarding the frequency response, power efficiencies, and path losses in different experimental settings.
- Chapter 5 details experimental procedures and result obtained for the non-line-of-sight (NLOS) transmission using straight and bending tubes. The chapter also details the performance of the system.
- Chapter 6 presents a prototype of digital system transmission in an NLOS setting to emulate a real environment. The study has concentrated on metal tubes only, and the experimental results of the proposed prototype network are presented.
- Finally, in chapter 7, conclusions and suggestions for future directions and areas for potential research are presented.

Chapter 2: Background Research and Related Work

2.1 Introduction

Nowadays, the growing requirements for wireless communication technologies have gained substantial attention mostly because of the increasing needs for short range and high-speed communications. Maintaining and reconfiguring a wired system is inconvenient and costly. Thus, finding better and more efficient techniques to transmit information is essential. Wireless technology offers flexibility and responses in comparison to the disadvantages of a wired system. Optical wireless technology is currently one of the newest solutions being considered to achieve implementation of a high-speed wireless LAN.

This chapter provides an overview of the optical wireless communication system approach, with a focus on the indoor applications, as well as advantages that makes OW a strong candidate for the vehicular communication applications. The chapter also outlines existing vehicular communication networks.

2.2 Overview of Optical Wireless Communication Systems

Although the ideal model for in-house OWC was first proposed in 1979 [13], extensive research has taken place concerning the channel capacity, channel modelling and

modulation techniques, all of which are still evolving to suit specific applications. Indoor OWC has gained remarkable popularity due to the huge unregulated bandwidth it can provide, with an availability of low cost transmitters and receivers, all of which makes it acceptable for indoor communications.

2.2.1 Optical Wireless Mathematical Model

Figure 2-1 OW communication system

A mathematical model for the OW communication system shown in Figure 2-1 may be represented by Eq. 2-1 below

$$y(t) = R * x(t) + n(t) \tag{2-1}$$

where $y(t)$ is the signal current generated at the front-end of the receiver, $x(t)$ represents the transmitted optical pulse, $n(t)$ represents the noise at reception, R represents the O/E conversion efficiency at the photodetector terminal and '$*$' denotes the convolution operation.

2.2.2 Optical Wireless Channel Model

Much research has been conducted for propagation characteristics in confined spaces, such as indoor, heating, ventilation and air conditioning (HVAC), mine and tunnel,

and metal pipes. The focus of the research concentrates on other wireless technologies except for within the indoor environment [14][15][16]. Furthermore, the propagation characteristics of the above mentioned environments is not ideal. HVAC ducts are not totally confined as there are ventilation openings, the size of the mines and tunnels is too large and in metal light pipes the focus is only on the surface interaction of powder substrates in the material (for controlled gas environment) [15][17][18].

A Lambertian model has often been used to provide and approximate description of the fundamental channel modelling in indoor OWC environment. The model of Lambert is utilized to effectively approximate irregular reflection patterns and reflected IR signals without privileging any specific direction. The model is described by [19][20][21][22]

$$R(\theta) = \rho R_i \frac{1}{\pi} \cos(\theta_o) \tag{2-2}$$

where ρ is the surface reflection coefficient, R_i is the incident optical power and θ_o is the angle observed. The expression demonstrates that the shape of the reflection pattern does not does not rely on upon the incidence angle. This makes the model simple and easy to actualize in software.

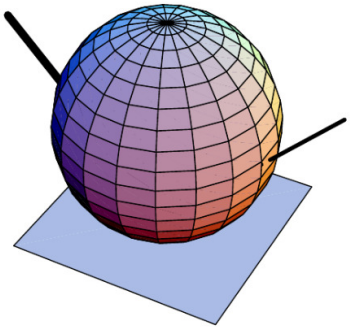

Figure 2-2 Lambertian reflection pattern [19]

Figure 2-2 illustrates a Lambertian reflection model [19], with the thicker line

representing the incidence direction and the thinner line identifying the direction of specular reflection.

The Lambertian is not the only option to estimate accurately the reflection pattern of smooth surfaces and around the specular reflection direction as the model of Phong fits quite well. This considers an accumulation of diffuse and specular components, where the ratio of each part depends totally on the surface attributes. Eq. 2-2 from the Lambert model is used to represent the diffuse component, meanwhile the specular component takes into account the incidence angle (θ_i) and the observation angle. Thus, the Phong model is best described as [19][23][24][25]

$$R(\theta_i, \theta_o) = \rho \frac{R_i}{\pi}\{r_d \cos(\theta_o) + (1 - r_d)cos^m(\theta_i - \theta_o)\} \quad (2\text{-}3)$$

where ρ is the surface reflection coefficient, R_i is the incident optical power and r_d is the percentage of incident signal that is reflected diffusely (assumes between 0 and 1). m controls the directivity of the specular component of the reflection.

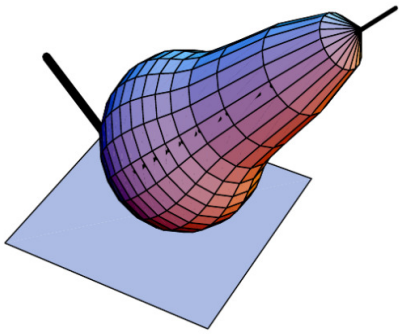

Figure 2-3 Typical Phong's reflection pattern [19]

Figure 2-3 represents a typical reflection pattern using Phong's model [19], which is described by $R(45°, \theta_o) = \frac{0.5}{\pi}\{cos(\theta_o) + cos^{45.3}(\theta_o - 45°)\}$ $(\theta_i = 45°)$. The bolder line represents the incidence direction, and the less bold line represents the direction of specular reflection $\theta_r = 45°$. As Phong's model depends on both θ_o and

θ_i, it is thus more complex and requires significantly higher computational time compared to the model of Lambert.

Modelling of reflection patterns within a specified confined space takes into account the assumption of purely diffuse reflections and an ideal Lambertian source. In addition, indoor environments sizes and shapes with different surface properties, and different transmitter and receiver specifications would also be essential factors in determining the channel model. [26]

A significant amount of work is available concerning the channel characterization, covering both practical measurements and simulation methods for indoor systems. Investigation of the channel characteristics under different optical configurations in various conditions has been performed. Experimental work carried out in [27], [28], [29], [30] and [31] measured the channel properties over high bandwidth and characterized the frequency response. Commonly examined characteristics are the channel impulse response, frequency response, path loss, optical power distributions, SNR, and RMS delay spread.

Work from previous research has also outlined a number of simulation methods for indoor OWC to characterize the nature of the channel, as such discussed in the following subsection [32].

2.2.2.1 Recursive Method

The recursive method for replicating several reflections was introduced by [33]. This technique was mainly developed to find the effect of multiple reflections without considering the temporal spread.

2.2.2.2 Statistical Model

The statistical model for the indoor channel was introduced by [34]. This model is developed based on the approximation of the RMS delay spread, τ_{rms}, and the mean excess delay τ_m, of the *h(t).* The τ_{rms} and τ_m values are then contrasted with the Rayleigh or Gamma distributions to fit with the impulse response curve.

2.2.2.3 Dustin Algorithm

This algorithm is the quicker way of computing multipath dispersion due to wall reflections on an indoor diffuse link [35].

2.2.2.4 Monte Carlo Algorithm

This scheme is the improved version of the Dustin Algorithm, where this scheme also takes into account the evaluation of specular reflections [36]. In [37], this scheme was modified, where the influence of each ray traced, and each bounce to the receiver, were each calculated.

2.2.2.5 Iterative Site Based Modelling

This is the newest method for the indoor wireless impulse response approximation. The method is capable of interpreting multiple reflections of any order [38].

2.2.3 Optical Wireless configurations

Figure 2-4 shows six indoor OWC configurations, depending on the degree of directionality of the transmitter and receiver [39]. Diffuse links are the easiest to use, as they do not require line-of-sight (LOS), and are the most robust [40].

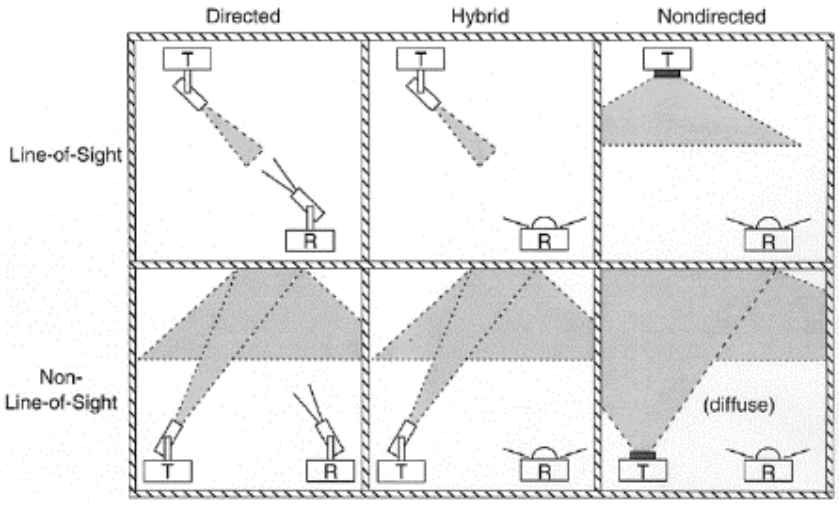

Figure 2-4 OW link configurations [39]

Table 2-1 outlines the main properties of OW configurations [42]. A diffuse link is believed to be the best option for intra-vehicle network. Although diffuse links suffer higher path lost and require high transmitter power [41], it is expected that this will not be an issue for intra-vehicle networks over short distances, and in small confined spaces.

Table 2-1 Main properties of OW configurations [42]

Type of link	Tx FOV	Rx FOV	Type of connection	Major advantage	Major disadvantage	Implementation
Directed	Narrow	Narrow	LOS	High speed	Shadowing	Complex
Diffuse	Wide	Wide	Reflections	High coverage	Low speed	Simple

2.2.4 Modulation Format

Various modulation schemes and multiple access techniques have been implemented in optical wireless systems, depending on the applications. Different considerations must been taken into account when selecting the modulation technique to meet each application requirement. Amongst numerous techniques, basic modulation schemes

widely adopted for indoor wireless modulation are: on-off keying (OOK), pulse modulation (PM) and sub-carrier modulation [39][43][44][45].

2.2.4.1 On-Off Keying (OOK)

OOK is the straightforward modulation format in terms of hardware implementation and integration. OOK balances between complexity and performance [44][46]. In conditions where OOK is incapable of providing the power efficiency required, pulse modulation is an alternative modulation scheme in optical wireless communication.

OOK could be implemented in many ways, including non-return-to zero (NRZ) and return-to-zero (RZ) format. OOK signals are extremely popular for both simplicity and bandwidth efficiency. The standardized transmitted pulse is of the form [47][48]

$$p(t) = \begin{cases} 1 & for\ 0 \leq T_b \\ 0 & elsewhere \end{cases} \quad (2\text{-}4)$$

where T_b is the bit interval. NRZ contains no discrete spectral components for a truly random input. Thus, it requires either non-linear clock recovery or line coding which works against bandwidth efficiency.

The RZ signal spectrum has discrete spectral components at the bit rate. Hence, clock recovery is straightforward and it does not requires additional clock. The transmitted pulse for a 50% duty cycle RZ signalling is represented as [47] [49]

$$p(t) = \begin{cases} 1 & for\ 0 \leq {}^{T_b}/_{2} \\ 0 & elsewhere \end{cases} \quad (2\text{-}5)$$

2.2.4.2 Pulse Modulation (PM)

PM provides high-speed digital transmission with higher power efficiency compared to OOK but does require a more complex system [44]. There are three types of PM: Pulse-Position Modulation (PPM), Differential Pulse-Position Modulation (DPPM) and Digital Pulse Interval Modulation (DPIM).

Table 2-2 summarises the properties of PPM, DPPM and DPIM in terms of peak-to-average power ratio, bandwidth requirement and throughput [50] . Among those three, PPM is broadly utilized in indoor optical wireless communications, as it offers higher average power efficiency. PPM delivers a reduction in average power requirement in contrast to OOK. For the IEEE 802.11 infrared physical layer standard and Infrared Data Association (IrDA) serial data links, PPM is the chosen modulation scheme [51][48].

Table 2-2 Comparison between PPM, DPPM and DPIM [50]

Modulation format	PPM	DPPM	DPIM
peak-to-average power ratio	2^M	$\frac{2^M+1}{2}$	$\frac{2(2^{M-1}+2\alpha+1)}{3\alpha}$
Bandwidth requirement (Hz)	$\frac{2^M R_b}{M}$	$\frac{(2^M+1)R_b}{2M}$	$\frac{(2^{M-1}+2\alpha+1)R_b}{2M}$
Throughput	M	$\frac{M2^{M+1}}{2^M+1}$	$\frac{M2^{M+1}}{2^{M-1}+2\alpha+1}$

In this table, M represents the number of bits/symbol, α is the number of pulses in the header and R_b represents data bit rate.

2.2.4.3 Sub-Carrier Modulation

Sub-carrier modulation techniques for OW links have been proposed in [52]. This

modulation scheme is being used when data rates exceed 100 Mbit/s, as it is relatively immune from multipath dispersion. Single-Subcarrier Modulation (SSM) and Multiple-Subcarrier Modulation (MSM), are other techniques suitable for OWC systems [52][53].

Other than the above-mentioned modulation schemes, Differential Pulse Position Modulation (DPPM), Digital Pulse Interval Modulation (DPIM), Double-Pulse Interval Modulation (DH-PIM), and the combination of OFDM with any other access scheme, are modulation methods suitable for optical wireless communication, which could be the alternatives of PPM, because of their improved performance in terms of power and bandwidth efficiencies [54].

2.3 Overview of Automotive Network

Vehicular communication networks can be classified as either (1) inter-vehicle networks, or (2) intra-vehicle networks. Inter-vehicular communication occurs when the vehicle communicates with the outside world. This type of communication can be further categorized as (1) vehicle-to-vehicle (V2V) communication, and (2) vehicle-to-infrastructure (V2I) communication. The research in this area is rapidly growing, due to significant advances in mobile and wireless communication technologies.

On the other hand, intra-vehicle networks is the communication networks that generates function within a vehicle. Currently, the main intra-vehicular communication is wired and network-based. Advancement in inexpensive high performance wireless LAN technology has made wireless intra-vehicular communication popular. A remarkable amount of research has been undertaken to exploit the diverse technologies that can be provided to improve the safety and comfort

of the passenger wirelessly [1].

The automotive subsystem is generally divided into five main domains, as shown in Figure 2-5. The Powertrain domain serves to control the engine and transmission system. It performs complex and frequent data exchange, so therefore it requires a high network bandwidth and reliability to retain a real-time control mechanism in order to maintain strict timing requirements [6][7].

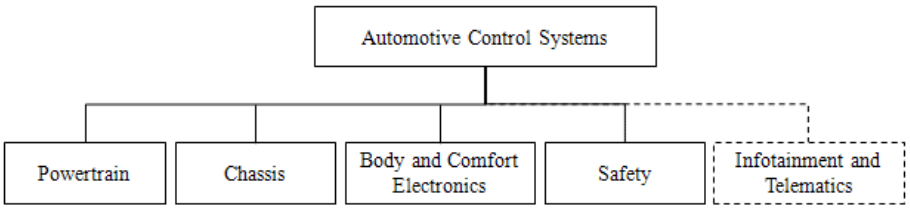

Figure 2-5 Embedded Automotive Subsystems

The Chassis domain is responsible for controlling the suspension, steering and braking. It is also involved with real-time safety-critical applications, and thus requires on-time data exchange. Therefore, it requires a high bandwidth, reliable- and flexible network [6][7].

The Body and Comfort Electronics domain is mostly responsible for comfort functions. This domain is made up of air conditioning, lighting, wiper, cruise control, locks and so on. The Body and Comfort Electronics domain does not require a high bandwidth network. A low cost network could be used for these applications, as the communications are mainly depending on driver/passengers action [6][7] .

The Safety domain concerns with the driver and passengers safety. Although it

involves impact- and rollover sensors, airbags, and seat belts, this network still requires reliable and high-speed data transmission [6][7].

The Infotainment and Telematics domain deals with multimedia and mobile communications, as well as vehicle monitoring systems and location devices [1]. The Infotainment and Telematics devices in a vehicle represent a different class of applications that require high data rates to transmit data, music and video streams. Thus, Media Oriented Systems Transport (MOST), and IDB-1394, which interconnect infotainment and telematics devices, will not be discussed further in this thesis.

All these domains are controlled by an electronics control unit (ECU), which exchanges data and information amongst up to 70 ECUs in one vehicle [1]. As function of a vehicle are getting more complex, and there are increasing expectations for high data rate demands for automotive networking, better networking schemes were becoming issues.

2.4 Wired Intra Vehicle Communication Networks

Most of the automotive subsystems are safety-critical. Thus, to interconnect these subsystems, some thought needs to be given to the bandwidth, flexibility, security and reliability requirements across the whole "network of networks".

From an engineering point of view, the high number of existing networks should be reduced; therefore, new networking technologies are being studied to produce fewer and more general automotive networks. The basic requirements for automotive networks are outlined as follows [7][55]:

- Increasing driving comfort and driver/passengers security.
- Reducing the size of the wiring harness in order to increase reliability,

serviceability and external noise immunity, plus reduce the system cost, weight and installation processes.

- Improving common sensor data to eliminate the redundant sensors such as speed sensor, and engine temperature sensor.
- Flexible networking which allows more functions to be added through software changes.

There are few, in-vehicle communication network types and protocols utilized as a part of vehicles by different makes. Common in-vehicle network protocols are summarized in Figure 2-6 and Figure 2-7.

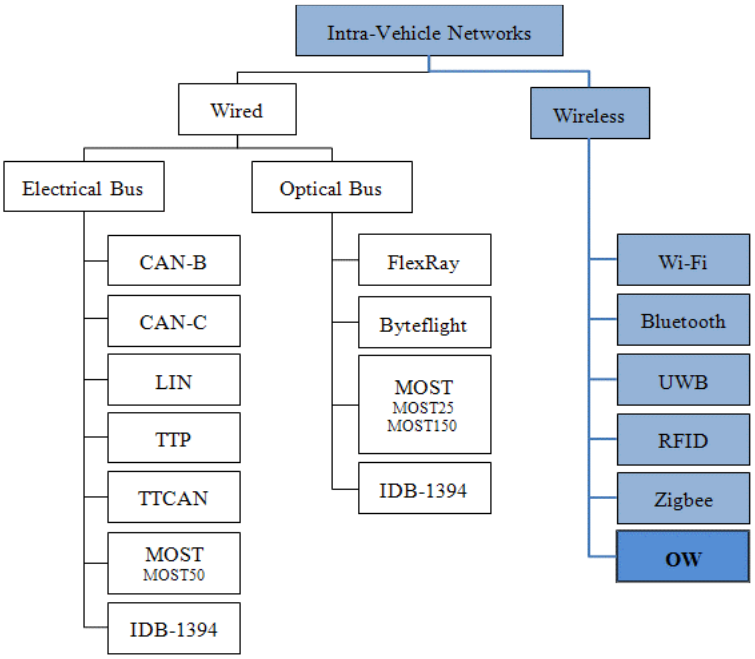

Figure 2-6 Intra-vehicle networks

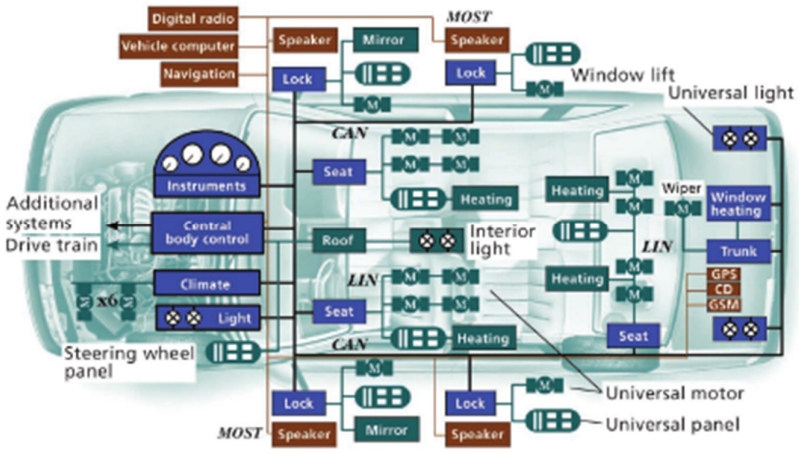

Figure 2-7 Common In-vehicle Network Protocols [56]

2.4.1 Controller Area Network (CAN)

The CAN protocol is the most common inexpensive low-speed serial bus standard used for in-vehicle networks. CAN offers flexible and efficient bandwidth utilization, and a robust, simple and cheap communication network [57]. CAN versions support different data rates, such as 125 kbit/s and 1 Mbit/s, respectively for low- and high speed CAN. Normally CANs are used for the engine management system, ABS/EPS, electronics transmission, as well as body comfort, and convenience electronics networking in the Drivetrain and Comfort/Convenience domains [58][59].

2.4.2 Time-triggered CAN (TTCAN)

TTCAN has been developed, based on CAN, to make it more applicable to safety-critical applications. TTCAN is being used in engine management and transmission systems, and x-by-wire applications. TTCAN uses a bus topology network, able to handle maximum data rate up to 1 Mbit/s [60].

2.4.3 Local Interconnect Network (LIN)

LIN is a low speed serial bus network (25 kbit/s), and can be considered as an

alternative to a low speed CAN [55]. Normally LIN is used alongside CAN, as it compliments it. LIN is used mainly in simple applications in the Comfort/ Convenience Electronics area (sensor and actuator) over a single wire transmission. It provides a master-slave protocol, and can be used for five different frame types covering unconditional, event-triggered, random diagnostic, and user-defined conditions [1].

2.4.4 Time-Triggered Protocol (TTP)

The TTP was developed as a time-triggered event solution. It is available in two forms, TTP/A and TTP/C. TTP/A will be an expert/slave TDMA convention, whilst TTP/C is a completely disseminated TDMA protocol. TTP/A is not currently used in the automotive industry, whereas TTP/C is used for fault-tolerance applications, with a star- or bus topology. This protocol ensures that no single fault is likely to occur. The specific transfer data rate is unspecified, but typically up to 10 Mbit/s [61][62].

2.4.5 Byteflight

This optical data bus was designed for time- and safety-critical applications, and is able to carry 10 Mbit/s of data. It is deployed mainly in safety-related applications, especially for airbags (airbag sensor network). Due to its flexibility, Byteflight is also being used in the Body and Comfort Electronics domain [56]. This high performance protocol combines time- and event driven control mechanisms, and is based on a single point-to-point link. This optical data bus system has been expanded to be part of the FlexRay protocol [63].

2.4.6 FlexRay

FlexRay is a general-purpose high-speed, fault-tolerant protocol, developed for time- and safety-critical applications. The objective of the development of FlexRay has been

to complement CAN in higher bandwidth and reliable applications. It was deployed across all domains, especially in x-by-wire systems. It is a protocol that combines time- and event-triggered control mechanisms, and uses a comparatively high data rate at a maximum of 20 Mbit/s. It has a flexible topology in which it can be organised as a bus, a star, or a multiple star, for either optical- or electrical physical layers [64].

2.4.7 MOST

MOST is a high-speed multimedia technology used to transport multimedia information signals through plastic optical fibre (MOST25, MOST150), or electrical wire (MOST50, MOST150) physical layers. A maximum data rate for each of the MOST versions is 25 Mbits/s, 50 Mbits/s, and 150 Mbits/s for MOST25, MOST50 and MOST150, respectively [65].

2.4.8 IDB-1394

IDB-1394 is a vehicular version of a multimedia bus for all automotive applications based on IEEE 1394. IDB-1394 system used for in-vehicle multimedia and telematics are capable of transferring up to 400 Mbit/s, and are expected to reach 1600 Mbit/s in the near future. The advantages of IDB-1394 are it allows isochronous and asynchronous data transfer. Isochronous is a real time data transmission for high-speed camera and video streaming. IDB-1394 is a genuine challenger for MOST technology [66].

2.5 Wireless Intra Vehicle Communication Networks

In recent years, research in intra-vehicle communication systems has become an attractive field, especially in new architecture based on wireless networks. This has

been as a result of more sensors and integrated networks being added, which has increased the complexity and weight of the cabling. Thus, other alternatives have been investigated, and a wireless network shows great promise in the solution to this problem. Generally, there are a few potential wireless networks that are being thought-through for intra-vehicle applications, such as Ultra-Wide Band (UWB), ZigBee, Wi-Fi, and optical wireless. [65]

Wireless vehicle communication technologies and protocols have the prospect to bolster numerous new and innovative applications. These innovations can significantly improve the safety, comfort, and convenience value of new vehicles, as well as infotainment and telematics functions. Positive progressions in the next generation vehicle communications will allow communication globally around the world, the embedded devices and with each other, making each vehicle a communications hub [8].

2.5.1 Wi-Fi

In wireless sensor networks, Wi-Fi is only used to perform a particular function in collecting sensor data for long distance data transmission. Currently, Wi-Fi is widely used in inter-vehicle communication [61][67]. Amongst all other wireless networks in a vehicle, Wi-Fi is the most mature technology used. Unfortunately, its complexity has led to the use of other available wireless technologies.

There are some weaknesses in using the Wi-Fi for an intra-vehicle wireless network, which could affect the performance and reliability of the network itself. The performance can degrade due to harsh operating condition, including motion, congestion, crash, and interference.

2.5.2 Bluetooth

The use of the Bluetooth in a vehicle is divided into two levels, being the user devices level and the system level. At the user device level, this network provides seamless connection for user-portable multimedia devices, telematics, and mobile electronic devices such as laptops, digital cameras, mobile phones, and hands-free accessories within the vehicle. In contrast, at the system level, Bluetooth functions similarly to any other copper-based vehicle control network such as CAN. Potential usage of Bluetooth for automotive control system has been presented in [10].

The major drawback of Bluetooth is that the device always need to be "on" to alert for available networks to join, and it requires longer battery life, resulting in regular charging being required [8][68][69]. Operating over relatively short transmission distances is also one of the points why this protocol has not been considered for vehicle networks.

2.5.3 Ultra-Wideband (UWB)

UWB is a short-range wireless communications low transmission power, mainly operated in an indoor- or confined environment. UWB is usually used for in-vehicle sensing, telematics, multimedia and infotainment domains, in addition to vehicular radar systems [70][71][72].

Limitation or drawbacks of UWB come from the challenge of designing a small antenna for any applications. Moreover, a UWB receiver tends to be affected by the in-band interference originating from other radio signal sources. Unfortunately, this problem is not an interest in general as it is normally integrated into mobile platform that are synchronised with a variety of other radios [73].

2.5.4 ZigBee

ZigBee technology has been developed, based on the IEEE 802.15.4 specifications. Due to its open standard, low power and low cost characteristics, it becomes an attractive wireless technology options other than Bluetooth and Wi-Fi. ZigBee is suitable for low data rate and low power consumption applications [74].

Currently, most of ZigBee commercial applications are hybrid with RF systems and are related to the inter-vehicle communications, such as vehicle-to-vehicle and vehicle-to-infrastructure links [75]. Unfortunately, systems based solely on ZigBee are still in early stage and not commercially available for intra-vehicle networks. Furthermore, the data rate of ZigBee is only 20 – 250 kbit/s, thus not suitable for the transmission of control system signals.

ZigBee has been created particularly to allow low power utilization and years of battery life [69].

2.5.5 Radio-Frequency IDentification (RFID)

RFID system is one of the potential wireless technologies that use a transponder attached to the objects to be acknowledged. The transponder communicates via RF to a reader attached to a system to be detected. RFID was proposed for use in wireless sensor networks. Unfortunately, there are several issues needed to be considered when using this technology as the reader and the tag must be in a fixed location, can only detect signal from nearest tag and large power loss. [76]

2.5.6 Optical Wireless

OWC is based on the optical radiation to convey information in free space. OW physical layer relies on wavelengths ranging from 800 – 3000 nm band. OW holds numerous advantages in automotive context as it could provide high-speed

transmission at low cost, immune to electromagnetic interference, use unregulated spectrum, as well as using small components that leads to low power consumption [77].

2.6 Common Wireless Intra Vehicle Network Requirements

Reference [78] suggested three network requirements for wireless intra-vehicle as follows:

- Requirement 1: high-speed information transfer is required for the intra-vehicle network, starting from a few hundred Mbps or more.
- Requirement 2: preferable secure transmission distance around 100 metres, to cater for large sized vehicles such as aeroplanes and long train.
- Requirement 3: low equipment, installation and maintenance cost, in order to introduce the technology to the commercial passenger car.

Existing wireless standards-based technology are not by any means applicable for intra vehicular wireless networks since most of these standards have not been produced for the intra-vehicle applications, therefore the technical specializations do not match the necessities (either overkill or falls short).

The drawbacks of current wireless network for intra-vehicle application are as in Table 2-3.

Table 2-3 Common wireless network drawbacks

Wireless technology	Drawbacks
RFID	Costly RFID readers. Incompatible for reliability and latency requirements as adopt simple physical layer waveform and MAC protocol design.
Bluetooth	Complex system, costly and high power requirement. Interfere with Wi-Fi signal as operated in the same frequency as Wi-Fi standard.
ZigBee	Low data rate

2.6.1 Bandwidth Requirements

As stated earlier, each subsystem in vehicle requires different communication requirements. The Society of Automotive Engineers (SAE) has outlined intra-vehicle communication networks based on bandwidth and functions of the networks [7]:

- Class A represents low speed/low cost networks with transmission capacity less than 10 kbit/s. Class A is dedicated to the Body and Comfort Electronics domain. LIN is an example in this class.
- Class B operates from 10 to 125 kbit/s, and is utilized for general data exchange (i.e. instrument cluster, vehicle speed) and some Body domain networks that need faster transmission rate. CAN-B is the main example of this class.
- Class C is for high-speed networks represented by CAN-C. The network in this class works from 125 kbit/s to 1 Mbit/s. Powertrain and Chassis domains are normally in this class.
- Class D is also for high-speed network dedicated for Infotainment and Telematics domain. Class D operates up to greater than 1 Mbit/s. MOST and

Bluetooth is the main examples.

Table 2-4 summarizes the network bandwidth requirements in each vehicle domains. Based on Table 2-4, the bandwidth required for the research ranges from 100 kbit/s to 22 Mbit/s, depending on the control signal requirement.

Table 2-4 Network bandwidth requirements

	Powertrain	Chassis	Body and Comfort Electronics	Safety	Infotainment and Telematics
Bandwidth	500 Kbit/s	500 Kbit/s	100 Kbit/s	22 Mbit/s	10 Mbit/s
Number of ECU	3 – 6	6 - 10	14 - 30	4 - 12	11 - 12
Safety requirements	High	high	low	low	Very high
Bus topology	Bus	bus	bus	ring	star
BER	Varies from 10^{-4} (aggressive environment) to 10^{-6} (benign environment) [79]				$\leq 10^{-10}$ [80]

2.7 OW in Intra Vehicle Environment

The implementing of OW technology in vehicular environment originates from the idea of reducing the weight of a spacecraft. The study of optical wireless technology for intra-satellite communications has begun since 1991. The need of reducing spacecraft weight, low power consumption and immune to EM interference is the contributing factors that directed to the used of optical wireless. NANOSAT-01 is a project developed by INTA implemented the communication between sensors and on-board data handling using diffuse optical wireless links, is the first optical wireless

intra-satellite link in orbit in 2005. OPTOS launched in 2010 is the latest spacecraft, which communicates mostly using optical wireless-CAN [12].

Broadband optical wireless communications for personal and broadcast in-flight communication and entertainment services has been proposed in [40].

The utilization of OW in the car context has been proposed in [9], several pathways are possible to transfer light such as: doors (point to point link), the engine compartment (MIMO execution should be expected in this case) and the inner cockpit of the vehicle (where unstable obstacles can be available such as passengers). The latest study about optical wireless channel in the car cabin is presented in [81], where power and bandwidth distribution in different parts of the car are characterised. The rapid improvement of optical wireless communication and LEDs technology in the visible spectrum has widened the future of implementing this innovation in the vehicle with the intention of replacing CAN.

2.8 Issues and Design Challenges

Besides eye-safety requirement issue, several other factors require highest attention in this research. Main critical aspect to be looked into is the exchange of data in between ECU, since more cross-area data exchanges are required. Moreover, communication between this ECU requires high-speed, event-triggered and time-triggered communication [1]. Detailed analysis on the LED as a transmitter should be focused as it has limited modulation bandwidth, which is the limiting factor to achieve high transmission rates [82]. A communication protocol also plays an important issue [83]. Precise receiver specifications are also required as multipath propagation arises by the reflection on car body metal and could distort waveform [84]. Noise is also an issue

that need extra consideration.

In the actual deployment of OW networks in the vehicle, many challenging problems must be addressed. Since, high mobility of the vehicles, connectivity must be ensured and channel must be managed efficiently. Furthermore, these problems are worsen by the harsh wireless environments in which these networks operated, where wireless transmission may fail due to many reasons, including channel fading, collisions, obstruction and interference [11].

Rapid development of intra-vehicle OW communication and LEDs advancement in the visible spectrum has widened the future of actualizing this technology in the vehicle with the intention of replacing CAN. Thus, it is believed that this new type of transmission has better prospective to be investigated and developed.

2.9 Conclusion

In this chapter, an overview of indoor OWC and communication networks in the vehicular environment were briefly discussed. The significant advantages of OWC such as high-speed transmission at low cost, resistance to electromagnetic impedance, utilisation of small components that prompts low power utilization and not having to design a system around other competing RF systems, offer valuable potential for implementation in vehicular environment.

The chapter also outlined a secure vehicular communication network for example the CAN, TTCAN, LIN, TTP, Byteflight, FlexRay, MOSt and IDB-1394, which integrates passive and active interaction of cabin, chassis, powertrain and safety domain that builds up current in-vehicle communication systems.

Current research on intra-vehicle optical wireless communication concentrated on the

computer simulation of received power and bandwidth availability of an OWC system, mainly in the cabin of the vehicle. No experimental research has been done within the chassis of the vehicle.

Most communications systems could either be bandwidth efficient, power efficient, or cost efficient. Bandwidth efficiency sets the highest priority, which describes the ability of a modulation scheme to accommodate data within a limited bandwidth. In indoor OWC, NRZ OOK is commonly used. However, in this thesis, the RZ OOK signalling is used, as it offers the simplest transmitter and receiver design and easiest integration in the IM/DD modulation. Setting up a practical demonstration prototype does not aiming for the extreme bandwidth, but setting up the system at required link distance is more important at this earliest phase. Thus, power efficiency is a more important factor in system design consideration. The pulse duration in the RZ OOK is lower than the bit duration, hence giving an improvement in power efficiency over NRZ OOK.

Chapter 3: Transmitter and Receiver Design

3.1 Introduction

As discussed in the previous chapter, most of the wireless technology for intra vehicle communication is not designed to operate within a confined spaced. Moreover, implementation of optical wireless is limited to the communication between the vehicle to the outside world and only within the cabin of the vehicle. The objective of this research is to study the prospect of implementing OW concept within the chassis of the vehicle. Thus, attaining maximum range or extreme bandwidth is not the important factor as for many systems employing OW, but setting up a basic, cost-effective, and practical transmission system within the vehicle environment is the core interest. Hence, this chapter concentrates on the development of the transmitter and receiver combination, based on an infrared LED as the transmitter, as a tool for exploring the channel characteristics.

3.2 The basic system

Figure 3-1 shows the block diagram of an intra-vehicle optical wireless transmitter and receiver, which is closely related to the free space optical wavelength, aside from the operational wavelengths.

Figure 3-1 OW communication system

3.2.1 The basic system requirement

The objective of this chapter is to develop a transmitter and receiver to be used as a measuring tool for this research. There are a few requirements set for the system design, such as:

Transmission distance	:	1 metre
Bandwidth	:	10 Mbits/s
SNR	:	≈ 10 dB
BER	:	10^{-4} to 10^{-6}

The system requirements set for this thesis is based on the intra-vehicular network bandwidth requirement, as stated in Table 2-4. The bandwidth requirement is from 100 kbit/s up to 22 Mbit/s based on the application. Since the main idea of this system is to replace the network represented by CAN-C and is not safety critical, the bandwidth is set at 10 Mbit/s. While for the SNR value, 10 dB was set based on that for an indoor environment, as at this optimal threshold value, minimum noise is produced. Shorter distances were set since the vehicle size limits the needed. The BER expected from the system designed is between 10^{-4} to 10^{-6}.

3.3 Optical wireless transmitter and receiver design

3.3.1 Optical source

Nowadays, a wide variety of commercial off-the-shelf LED's and Laser diodes are

available for use in optical wireless communications. A few aspects need to be considered, before choosing the right optical source, such as spectral width, power radiated, half power angle, and maximum modulation operating frequency. In this instance, an IrLED was the preferred option for the following reasons:

- Reliability - the LED is more reliable and robust, thus increasing device lifetime.
- An IrLED can be modulated (turned off and on) at high enough speeds

Choosing the correct IRLED is a particular challenge. A few parameters play an important role in selecting an appropriate IrLED:

- Switching speed
- Wavelength selection
- Divergence angle
- Optical output power

However, the market availability of preferable IrLEDs is limited, so therefore there must be a trade-off between these parameters.

In the proposed system, the preferable IRLED for the transmitter was OPTEK OP280V as it has fast switching speed with a rise time (t_r) and fall time (t_f) of 100 ps. Unfortunately, the output power density of such an individual device is too low, being around 2.5 mW/cm^2. In order to use this, a transmitter with an array of such IrLEDs needs to be designed. However, the efficiency and modulation bandwidth of the system will be limited by using this configuration [8].

The next suitable type of IRLED for the transmitter is VISHAY VSLY5850. Although the switching speed is greater than that of the OPTEK OP280V, it has a significantly better radiant power of 600 mW/sr. Furthermore, VSLY5850 offers the widest

bandwidth in the market at 850nm peak wavelength. The divergence angle also plays an important role in the IRLED transmission, where smaller divergence angle gives greater concentration, thus the transmission power density is high. The VSLY5850 has angle of half intensity of ± 3°.

3.3.2 Optical detector

The receiver design has been constructed using an OSRAM SFH205F silicon PIN photodiode with an active area of 2.65mm^2, a zero-voltage depletion capacitance of 10pF, a half angle of ±60° and responsivity of approximately 1 A/W at the chosen operational wavelength of 980nm.

3.3.3 Bandwidth calculation

The channel capabilities of the system were calculated based on optical source and optical detector features that are shown in Table 3-1.

Table 3-1 Technical features of optical sources and detectors.

Feature	VSLY5850	SFH205F
Device	High Speed Infrared Emitting Diode	Silicon PIN Photodiode with Daylight Blocking Filter
Wavelength at peak emission	850 nm	900 nm
Half angle	± 3°	± 60°
Active chip area	-	7.02 mm^2
Switching times Ie from 10% to 90% and from 90% to 10% ; I_F = 100 mA, R_L = 50 Ω	10 ns	20 ns
Radiant intensity I_F = 100 mA; tp = 20 ms	600 mW/sr	-
Noise equivalent power	-	0.039 pW / Hz^{½}

The SFH205F modulation bandwidth was calculated as= $0.35/\tau_r = 0.35/20$ ns = 17.5 MHz. Thus, the system bandwidth will be limited by the optical detector to around 17.5 MHz, in addition to other electronic device limitations and conversion constraints.

A simple experimental setup was developed to determine the real capability of the IRLED. A basic optical wireless transmitter circuit was setup as shown in Figure 3-2, and the receiver as in Figure 3-3, and were constructed for the experiment.

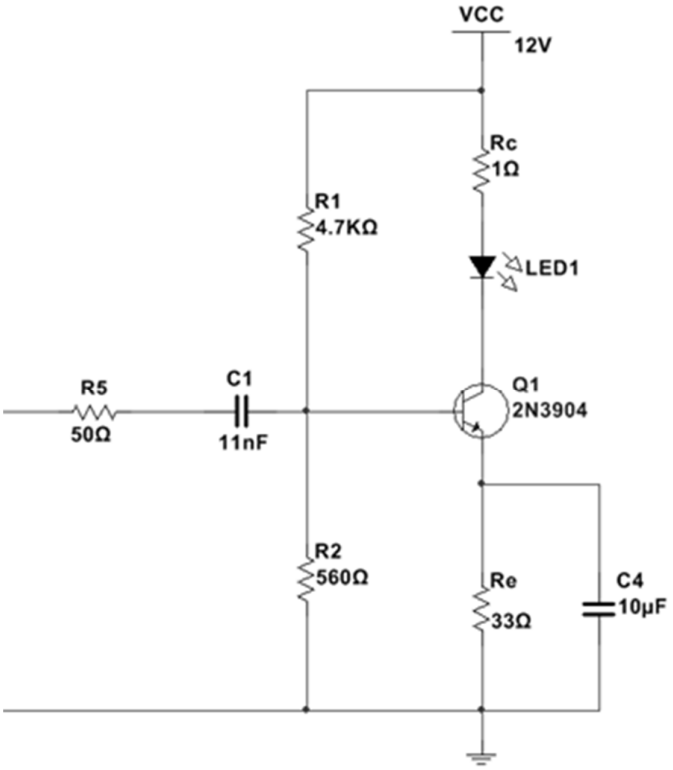

Figure 3-2 Fundamental transmitter

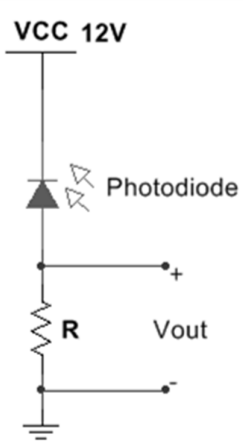

Figure 3-3 Fundamental receiver

The value of the resistor R in Figure 3-3 needed to be carefully calculated to ensure that the receiver bandwidth is more prominent than the IRLED transmission capacity. The bandwidth of the receiver also depends on the photodiode's internal capacitance. The CV characteristic of the SFH205F was determined using a Boonton Electronics Capacitance meter as in Appendix A, and the results are tabulated as in Figure 3-4. The internal capacitance of the photodiode is about 10pF for a 12 volts bias voltage. A lower value of R, at the receiver circuit is chosen for adequate data transfer capacity of the receiver, which is required to be higher than the LED upper 3 dB cutoff frequency, without sacrificing the receiver sensitivity.

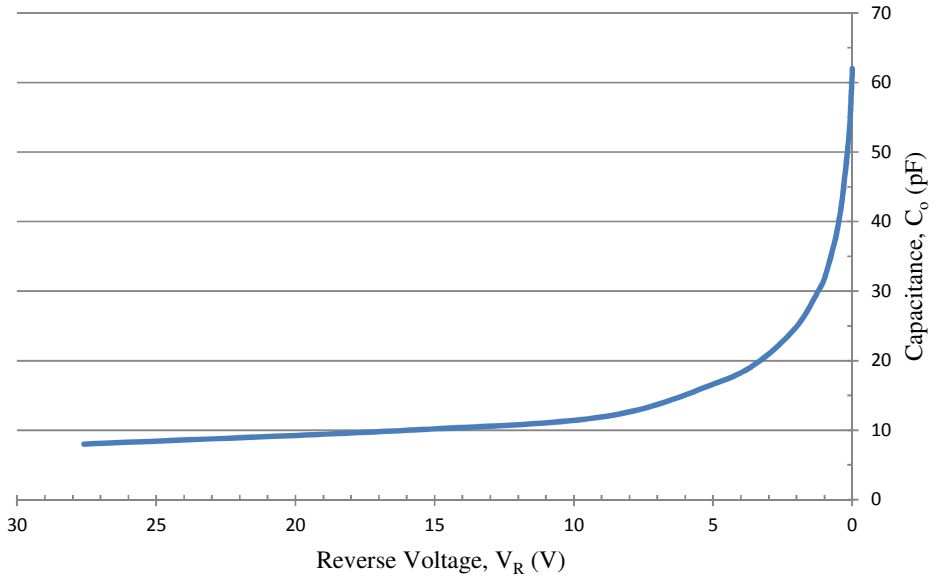

Figure 3-4 SFH205F CV characteristic

The relative response of the VSLY5850 is presented in Figure 3-5. The normalised responses in the graph were calculated based on the standard dB formula of $20\log_{10}(P_r/P_t)$ and were normalised to their respective peak values. The test proved that the effective modulation bandwidth of the IRLED is only up to 15 MHz at 10 cm range. The calculated bandwidth based on the datasheet is under the optimum testing condition. Supplying more current to the device could increase the bandwidth of the test system; unfortunately, it also heats up the IRLED and consequently shortens its lifetime.

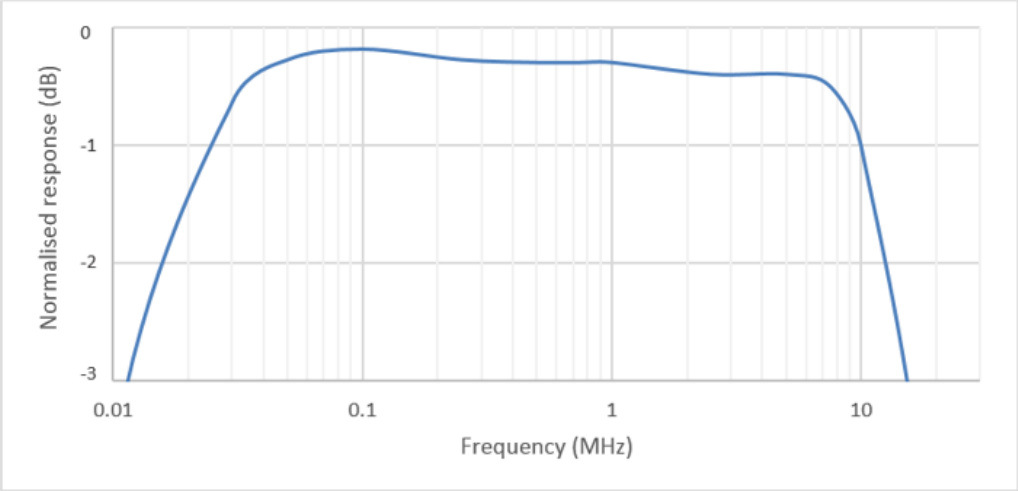

Figure 3-5 Relative response of VISHAY VSLY5850

3.3.4 Infrared LED driver

The purpose of the driver circuit is to transform the data voltage signal at the transmitter into a modulation current appropriate for an IRLED source. The transmitter could be either analogue or digital, depending on the application. Since analogue signals are commonly used in most systems, and can be used for digital modulation as well, the IRLED driver design was based on this form.

There are two possible high-speed drive circuits for analogue transmission presented in Figure 3-6. The common emitter configuration changes over an input base voltage into a collector current to turn the IRLED on, whereas the Darlington pair configuration is normally used to reduce the effect of amplifier input impedance loading the source, effectively acting as a kind of current amplification.

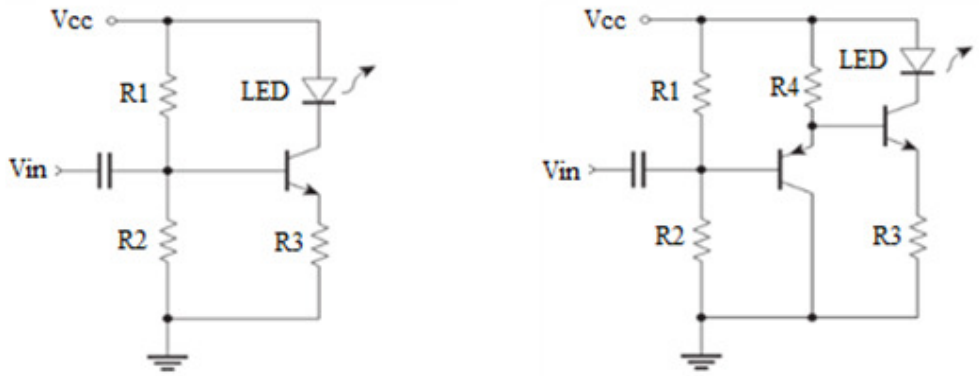

(a) CE configuration drive circuit (b) Darlington pair drive circuit

Figure 3-6 Analogue drive circuit

In order to attain the highest data rate, the IRLED should not be completely turned off. This will speed up the process of creating minority carries in the junction, and avoid "slow start" mechanisms, such as the need to fill traps and interface states in the semiconductors. An adequate bias level must be chosen to turn on the IRLED in a control to avoid these mechanisms. The Darlington pair drive circuit has the ability to enhance the switching current capabilities, and this configuration is thus more suitable to drive high radiance IRLED at higher frequencies, thereby increasing the transmission power and therefore the overall range.

To drive the IRLED, the transmitter utilising the Darlington IRLED driver, as shown in Figure 3-7, was used. The IRLED driving current was given by the transistor Q1 collector current, which was controlled by the resistor R7. The value of R7 had to be precisely estimated to guarantee appropriate current flow through the IRLED under all normal operating conditions. The function of the Q2 transistor was to ensure that the IRLED was not fully OFF during the operation, in order to enhance a higher switching

rate. The bias resistors R4 and R5, which forward the bias current to the emitter base junction to switch the transistor to its ON state, controlled the DC base current.

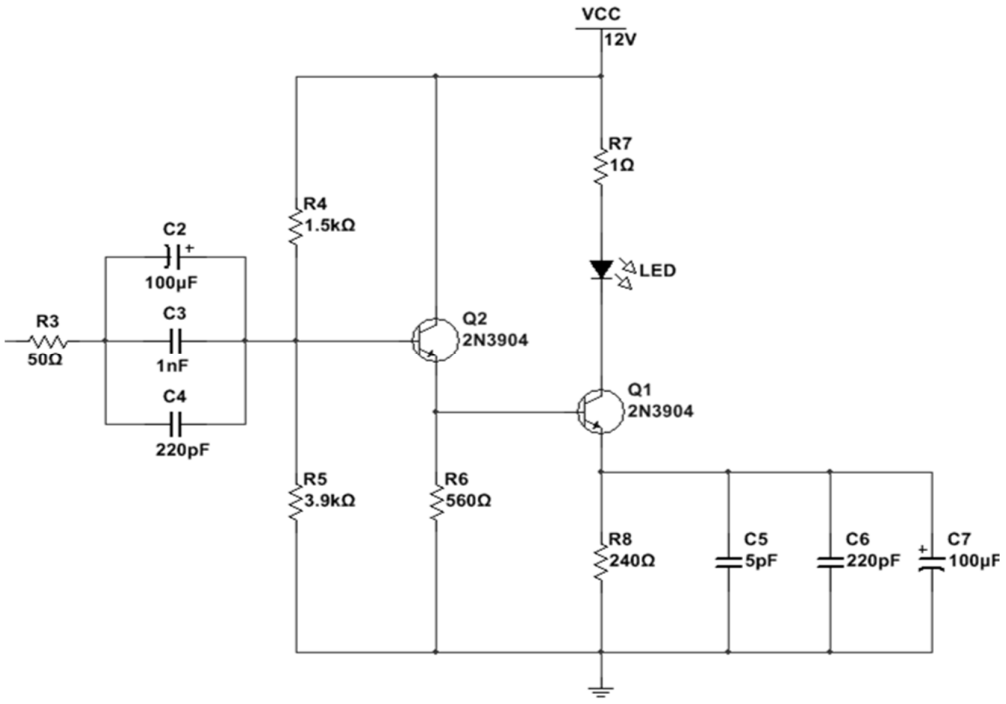

Figure 3-7 Darlington IRLED driver

The basic experiment, as explained in Section 3.2 was repeated and the effective modulation bandwidth found, using the Darlington IRLED driver, greatly reduced to 1 MHz, as shown in Figure 3-8. The normalised response in the graph was again calculated using the dB formula given above and also normalised to their respective peak values. This demonstrated that the effective modulation bandwidth was reduced significantly when more gain and higher transmitted powers were achieved, commensurate with the usual trade-off between transmitted power (gain) and bandwidth.

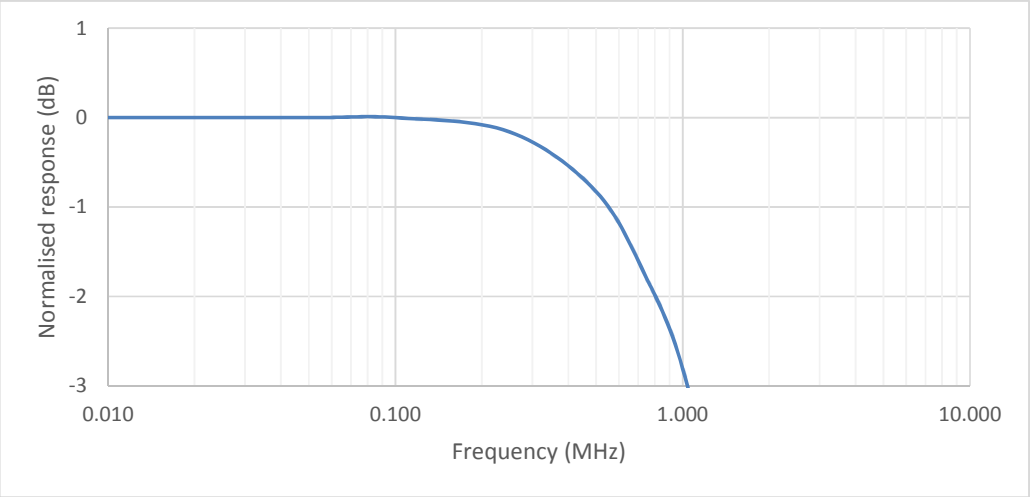

Figure 3-8 Darlington IRLED driver normalised response

3.3.5 Pre-emphasis

The modulation bandwidth of the IRLED transmitter can be enhanced by using pre-emphasis. By utilizing the passive frequency pre-emphasis technique shown in Figure 3-9, the modulation bandwidth of the system was improved significantly.

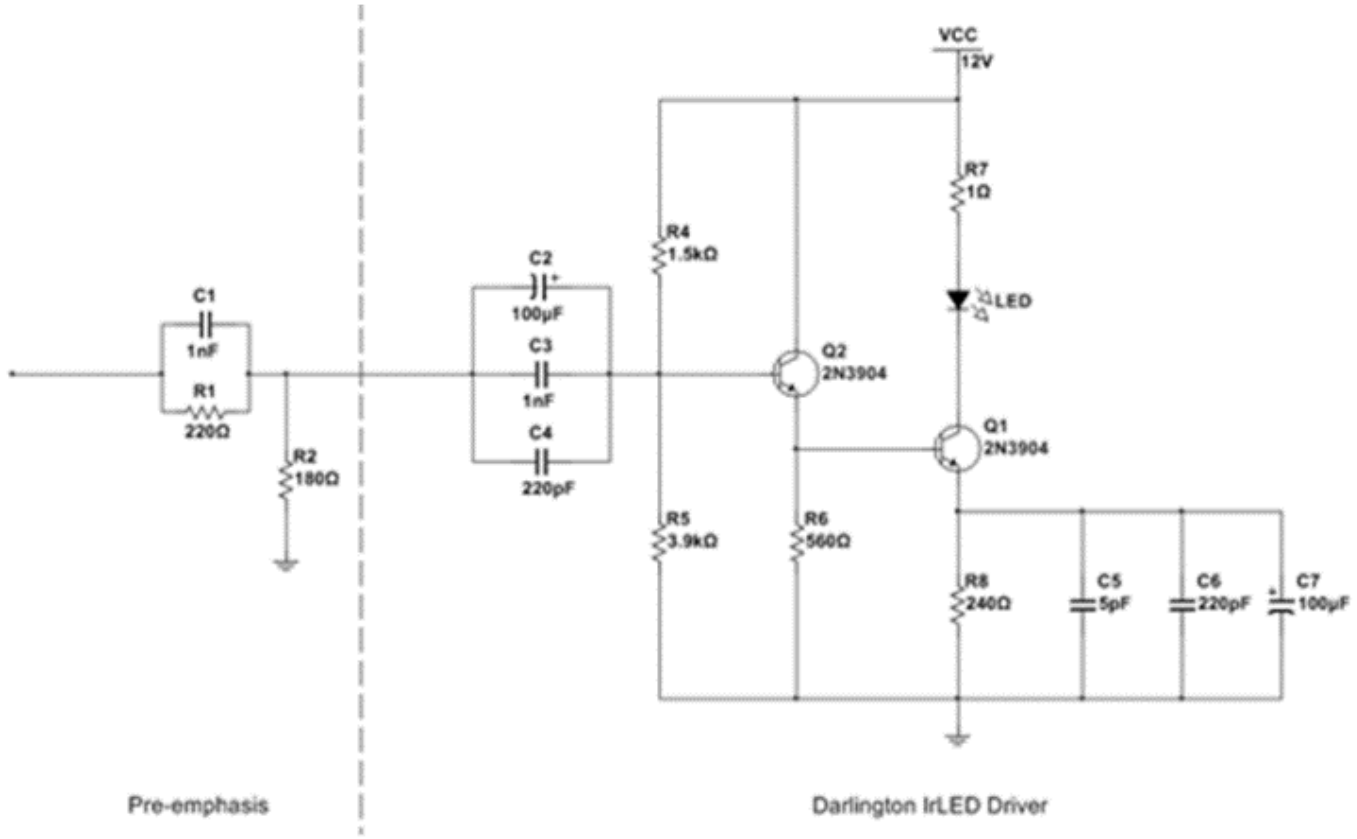

Figure 3-9 IRLED transmitter with pre-emphasis

The normalised response of the system is shown in Figure 3-10 with 13 MHz achievable modulation bandwidth. A small peak in the response at higher frequencies is caused by reasons such as (1) resonance due to stray capacitance, (2) the difficulties of getting the exact corner frequency needed, (3) the interaction of the frequency responses of other devices in the system.

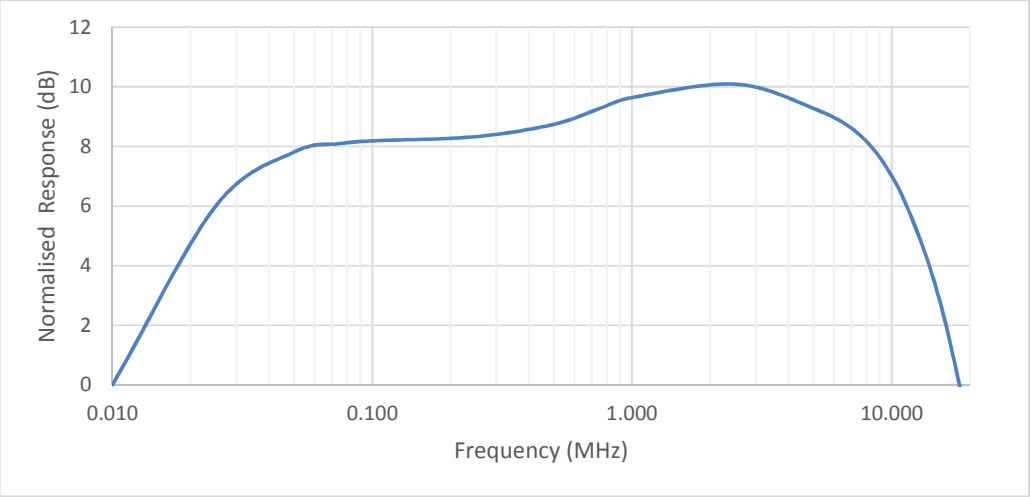

Figure 3-10 Normalised response of the system

3.3.6 Front-end

Due to the constraints of optoelectronics, there are limitations on transmitting high power optical signals, thus an optical wireless communication system overall performance is determined mostly by the receiver performance [85][86].

A high impedance front-end was used at the receiver is shown in Figure 3-11. The photodiode used was the SIEMENS SFH 205F with a built-in daylight filter. The current-to-voltage conversion in the pre-amplifier was set by load resistor, R1. The idea of a high impedance front end was to give the photodiode as high a load

impedance as possible, so that the current signal from the photodiode will generate as high a signal voltage as possible across the load resistance in series with the photodiode. Then, the subsequent high impedance presented by the amplifier does not reduce the effect of this high resistance load, and consequently reduce the voltage generated by the photodiode signal current. However, because of photodiode capacitance, a higher effective load impedance increases the front-end time constant, and thus lowers the receiver bandwidth since this is given by $(2\pi R_L C_T)^{-1}$, where $R_L$is the load resistance (R1 in Figure 3-11) and C_T is the total capacitance associated with the photodiode and the amplifier.

Photodetector bandwidth limitation are based on two principals; bandwidth associated with the carrier transit time or RC time constant. This thesis only concerns the bandwidth restricted by the latter [87][88]. Bandwidth is related to integration time by the formula

$$\Delta f = \frac{1}{2\pi\tau} \tag{3-1}$$

where τ is the integration of time or "time constant" of the system in seconds. The time constant, τ is the time for the photodetector (or the system) takes to reach a value of $(1 - e^{-1}) \cong 60\%$ of its steady state value [89].

Therefore, in this particular case, R1 was set to a relatively low value in order to maintain a good bandwidth for the front end as a whole. Loading the current-source with a large impedance maximised the amount of voltage developed at the amplifier input and thus reduced the amplifier noise sources.

The op-amp AD8072JN is a current feedback amplifier with 100 MHz bandwidth, 500 V/μs of slew rate, along with settling to 0.1% of full output in 25 ns, and with a gain flatness of 0.1 dB from low frequencies up to 10 MHz. This op-amp is very useful in

high-speed, general-purpose applications. A current feedback amplifier was chosen because given the limited choices of the feedback impedance, it offered faster operation, fast slew rates and fixed bandwidth versus gain in addition to the capability to retain high full power of bandwidth at much higher gain. The first stage amplifier gain was 13, as this was the maximum gain allowable for the op-amp with the limitation of the feedback resistor. A small source of DC bias for the non-inverting op-amp was provided by R2 to R4.

A second stage amplifier with a gain of 7.8 was added to the circuit as shown in Figure 3-11 below, so that the output voltage was high enough to be detected at a range of one metre.

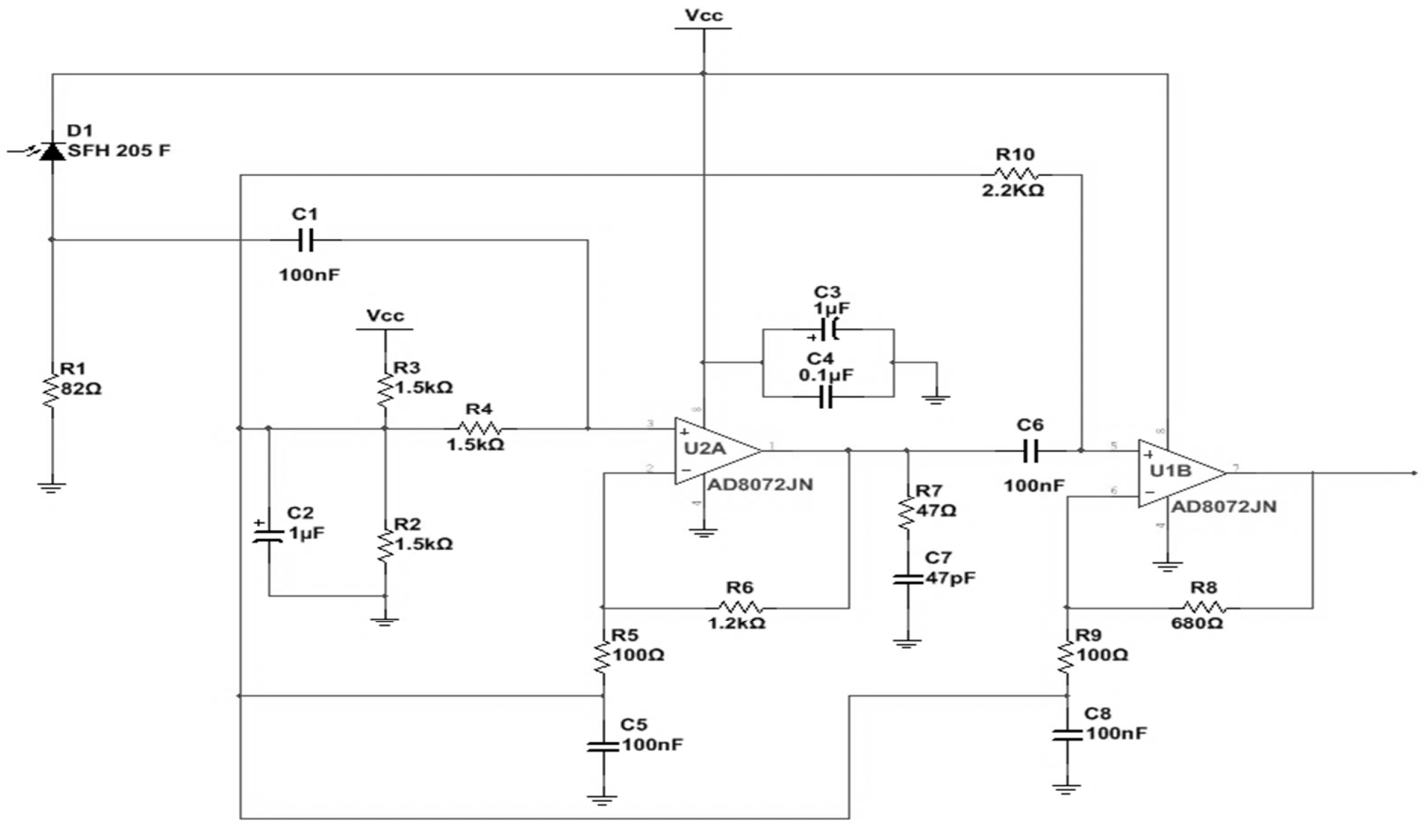

Figure 3-11 High-impedance front-end receiver with amplifier

3.4 Precautions

The system was designed to operate at high frequencies, therefore the circuit tended to pick up interfering signals via power supplies and earth loops.

Although OW systems have much less potential for interference with RF-sensitive electronic systems, a few precautions have been considered to keep EMI to the lowest level possible. It was believed that these steps could prevent the present of spurious signals from interfering with the system operation. The steps taken are as follows:

- using capacitive decoupling to reduce low frequency feedthrough,
- using shielded power cables,
- placement of the circuit in a shielding box.

3.5 Performance study of the system designed

The functionality of the system designed has been verified by sending a continuous wave (CW) signal at a range of 0.25 metres within a free space controlled environment. This environment was created by covering the transmission channel with a thick black cloth to prevent external optical and infrared sources such as ambient light. The signal was sent at various frequencies, and the quality of the signal received was very good over a satisfactory frequency range, as shown in Figure 3-12 (a) – (d).

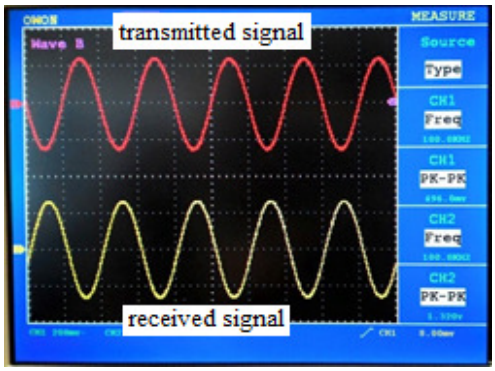

(a) 100 kHz

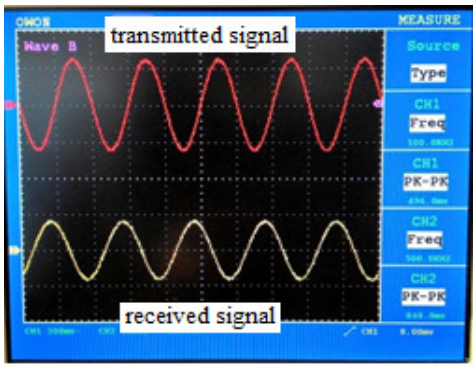

(b) 500 kHz

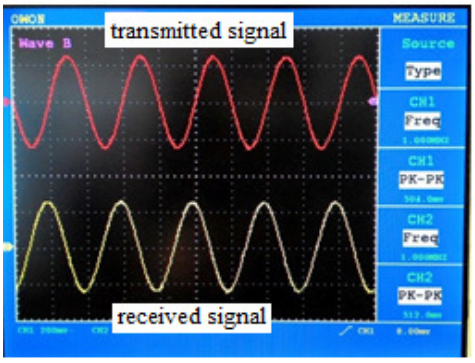

(c) 1 MHz

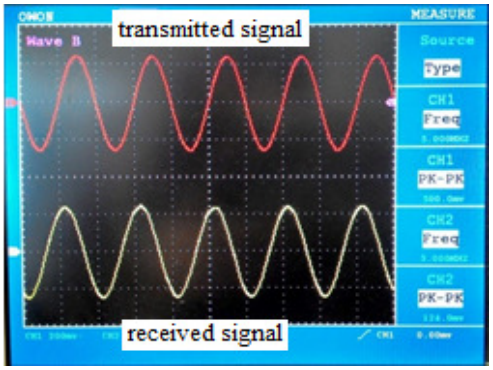

(d) 5 MHz

Figure 3-12 Waveforms of the test signal

The received power was measured using an Ealing research radiometer/photometer as in Appendix A, and the results were tabulated in Figure 3-13. Under free space transmission, the optical power intensity decreased dramatically over distance.

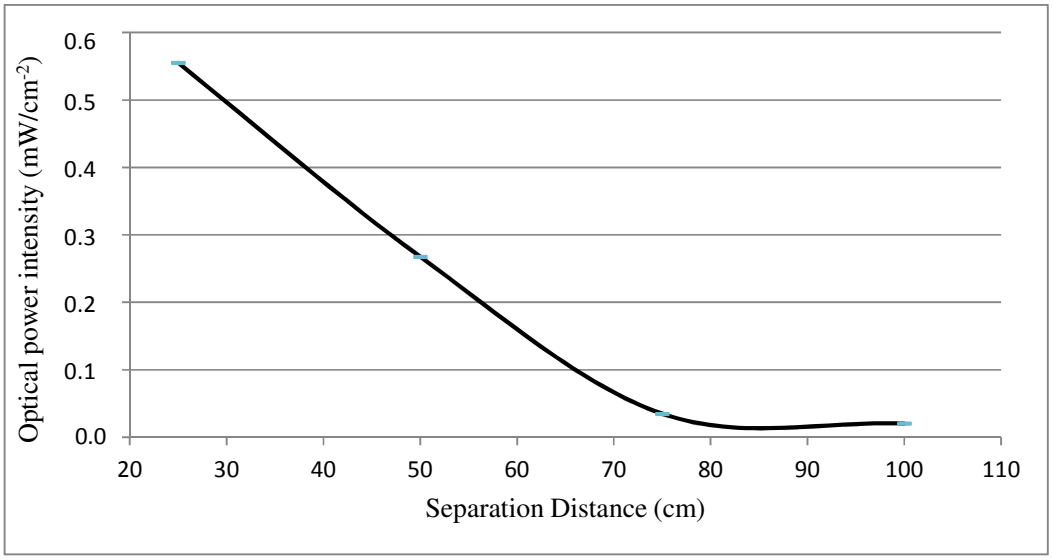

Figure 3-13 Optical power intensity at a distance

3.6 System Noise Analysis

In optical wireless communication systems, noise comes from two sources, namely internal and external. A detailed noise source analysis was thoroughly given in [90]. There was only small amount of ambient light existing at the opening end of the configurations, which covered with black cardboard iris. The transmission for free space tests was also performed under controlled condition, which considerably minimised noise contributions from daylight, and fluorescent light. The external noise was determined in fact to be negligible, and was ignored in this particular set of experiments.

Major sources of noise, which affect the system sensitivity, come from the internal circuitry itself. The noise generated in the receiver was one of the main areas of interest in this study. Different photodetector noises that appear are thermal noise, shot noise and dark current noise. However, only shot noise in the photodetector, thermal noise in the resistance and amplifier noise will be examined.

The shot noise comes from the statistical uncertainty in photon arrival rate, which can be represented in terms of voltage source or current source. The mean square value of shot noise current has the following form [91][88][87][92]:

$$I_{ns} = 2qI_pB \tag{3-2}$$

where q is the electronic charge in Coulombs, I_{ns} is the RMS noise current, I_p is the photocurrent generated in Amperes, and B is the electrical bandwidth, in Hertz, over which the noise is measured.

The second noise source is the thermal noise of the shunt resistance, which is otherwise called as Johnson noise, and is given by [91][88][87][92]:

$$I_{th} = (4kTB/R)^{1/2} \tag{3-3}$$

where I_{th} is the thermal noise current in Amperes, k is the Boltzmann's constant, T is the temperature in Kelvin, B is the effective bandwidth in Hertz, and R is the load resistance in Ohms.

Amplifier noise also assumes an essential element of the receiver noise analysis and is given by three terms. The first two are in the form of the photodiode shot noise and the load resistance Johnson noise as described above. The third term comes from the input voltage noise of the amplifier, due to the shot noise of the input bias current, and the Johnson noise of the feedback resistor both of which are directly linked to the frequency bandwidth. This may be combined into an equivalent input noise current, designated I_{amp}. Thus, the total noise current generated by a receiver is given by [92], [93]:

$$I_N = \left[I_{ns}^2 + I_{th}^2 + I_{amp}^2\right]^{1/2} \tag{3-4}$$

Since the noise sources described are uncorrelated, they must add in a sum-of-squares manner, as shown in the equation above.

The main performance analysis for the receiver concentrates on the signal to noise ratio (SNR). The SNR of the system is determined by measuring the peak value of the signal and dividing this by RMS noise. The ratio was calculated using the Equation 3-4.

$$SNR = 20\log\frac{(S+N)_{pk-pk}}{N_{pk-pk}} \quad (3\text{-}5)$$

The distance between the transmitter and receiver was set at 0.5 metres under controlled free space transmission conditions. The noise was measured to be approximately 2mV RMS, and the calculated signal to noise ratio was 15.6 dB.

3.7 Conclusion

This chapter discussed the details procedure for the transmitter and receiver design. A continuous wave signal was used to demonstrate the functionality of the system designed.

Based on the system design, it can be deduced that parameters obtained were as follows.

		Expected system design	System parameters obtained
Transmission distance	:	1 metre	1 metre
Bandwidth	:	10 Mbits/s	13 Mbits/s
SNR	:	≈ 10 dB	≈ 15.6 dB
BER	:	10^{-4} to 10^{-6}	Refer to Chapter 6

From the measurement, the target bandwidth obtained is far better than expected. Furthermore, a bit rate of 3Mbit/s was obtained from the expected system design. The 15.6 dB SNR value was obtained from the measurement. The SNR needs to be as high as possible since higher SNR values obtained means that the system will offer better transmission performance. Thus, a better system has been designed; unfortunately, the value of SNR will be degraded as the distance increases. Other possible reasons for SNR degradation might come from the idea that the performance of OWC systems is limited by the power constraint at the transmitter, by receiver sensitivity and by limits on the available optical gain.

The BER parameters will be covered in Chapter 6.

Furthermore, the IRLED, other electronic devices and the receiver itself, limited the modulation bandwidth of the system. However, there is a trade-off between the modulation bandwidth and the system gain. All measurements from this point forward will be based on a 13 MHz bandwidth system, without using any lens or concentrator.

Chapter 4: Channel Characterization – Line-of-Sight Transmission

4.1 Introduction

The design of a wireless communication system in a narrow confined space using an infrared signal carrier needs extensive understanding regarding the behaviour of the infrared channel itself. This involves channel measurements under different environments and using different optical arrangements for a clearer understanding of the OW channel characteristics, in this case, in representing tubes to emulate the kind of spaces, which might be available in vehicular applications. Such measurements could thus provide an in-depth understanding of the channel behaviour under different environments. Measurements are also essential in providing required knowledge about reflections and noises that are encountered in actual application of this system. For example, the performance of the system will generally be affected by transmit- or receive angles, the physical geometry of the channels, and the materials from which the channel are made. The effects of these factors are essential subjects for investigation for optical wireless communications within vehicular applications. The aim of this chapter is to understand the behaviour of an optical wireless system in representative straight tubes (line-of-sight link) at first, and to investigate the practicality and explore the performance of a realistic system design, based on a physical demonstrator, build for the purpose.

4.2 Ideal LOS link

In practice, LOS channels are preferable in indoor OW transmission because optimum channel condition are provided using direct links, meaning the best transmission performance in terms of power and bandwidth being made available. Ideally, LOS may be described as the link condition without fading, for which the theoretical channel model can be expressed as Equation 4-1.

$$R(x) = S(x) * H(x) + n(x) \qquad (4\text{-}1)$$

where $R(x)$ is the received signal, $S(x)$ is the transmitted signal, $H(x)$ is the channel response, $n(x)$ denotes the total channel noise (defined as the sum of both shot noise and thermal noise) and * represents the convolution operator. For the purpose of this study, the noise sources only originate from origins within the transmitter and due to front-end aspects of the receiver itself, as the transmission in being done in the tube, and external light sources do not affect the link, unlike an open-air free space link.

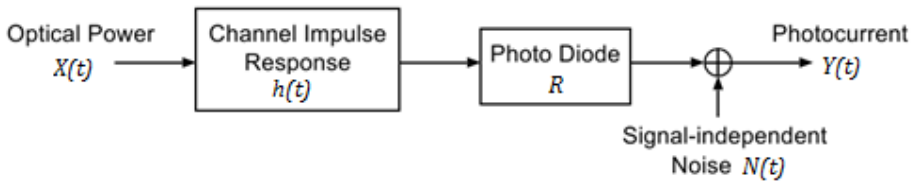

Figure 4-1 LOS link model [94]

Figure 4-1 presents the mode of the LOS channel as a baseband linear system, with $X(t)$ being the instantaneous input power, $Y(t)$ being the output current, $h(t)$ being the channel impulse response, R being the photodetector responsivity and $N(t)$ being the additive noise.

The channel could also be described in terms of its frequency response [39]

$$H(f) = \int_{-\infty}^{\infty} h(t) e^{-j2\pi f t}\, dt \tag{4-2}$$

which is the Fourier transform of $h(t)$. It is usually relevant to model the channel $h(t) \leftrightarrow H(f)$ as fixed, since it commonly changes only when the transmitter, receiver or reflecting elements are moved by relatively significant amounts, such as a few centimetres in the practical case.

Frequency response is the fundamental characterisation investigated here in this study. The transmission in the tubes has virtually unlimited bandwidth in principle, excluding the limitations due to the optoelectronic circuitry at the transmitter and the receiver, that is, the useful bandwidth usually is limited by the electronic parts that build up the transmitter and receiver, rather than by the optical components. Thus, the frequency responses of the systems investigated were determined by characterising the OW transmission channel in the representative tubes.

The channel characterization relates the transmitted and received optical power via [39]

$$P_r = H(0) P_t \qquad (W) \tag{4-3}$$

where, P_t is the transmitted optical power, P_r is the received optical power and $H(0)$ is the path loss. Path loss is defined as the integration of the channel impulse response $h(t)$ considering the reflections from the walls, ceiling, and other objects as [95][96].

$$H(0)\text{dB} = -10 \log_{10} \int_{-\infty}^{\infty} h(t) dt \tag{4-4}$$

This estimation is particularly accurate in the LOS link, as in Figure 4-2.

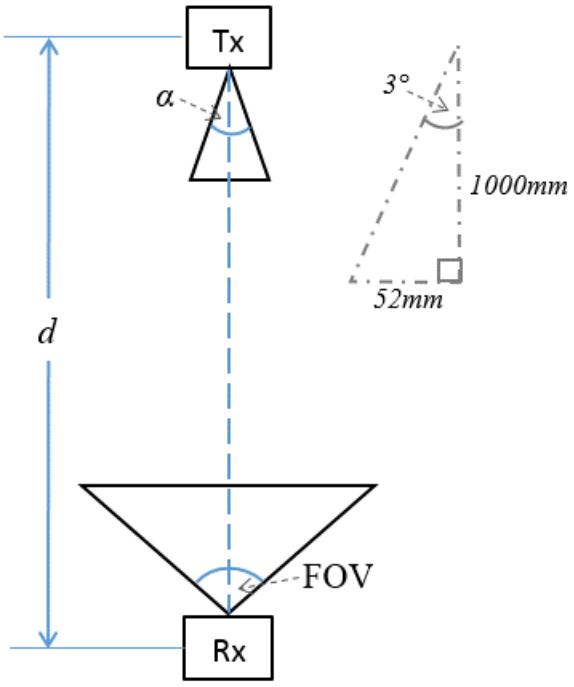

Figure 4-2 Vertical assessment scenarios

For the geometrical link, the LOS channel path loss is defined [39]

$$H(0)_{LOS} = \frac{A_{PD}}{d^2} R_0(\varphi)\cos(\psi) \tag{4-5}$$

where, A_{PD} is the PD active area, d is the distance between transmitter and receiver, φ is the angle with respect to the transmitter, ψ is the angle with respect to the receiver and $R_0(\varphi)$ is the transmitter radiant intensity given by Equation 4-5 [39].

$$R_0(\varphi) = \left[\frac{n+1}{2\pi}\right]\cos^n(\varphi) \qquad (W/sr) \tag{4-6}$$

$$n = \frac{\ln 2}{\ln(\cos\alpha)} \tag{4-7}$$

where, α is the transmitter beam angle, mode number n of the Lambertian radiation pattern determines the beam width.

4.3 The tubes

The OW channel measurements were carried out in nine different environments, as shown in Figure 4-3 and listed in Table 4-1.

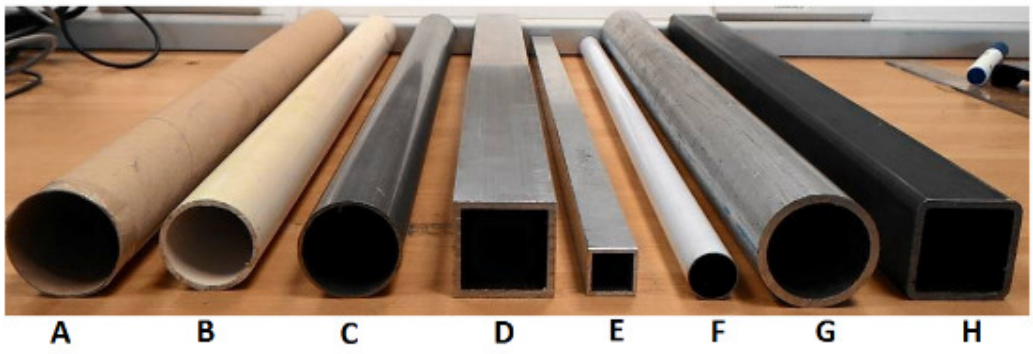

Figure 4-3 Representative tubes

The controlled free space (indicated as I) were used as a benchmark for the measurement in various tubes. The inner tube were not coated/painted, as this will affect the way IR interact on the tested materials. Types and thickness of inner coat/paint will act differently and thus will not provide the desired results.

Table 4-1 experimental materials

Items	Material	Dimension	Measured reflection coefficient
A	Circular cardboard tube	40mm diameter	0.1
B	Circular plastic tube	35mm diameter	0.1
C	Circular mild steel tube	35mm diameter	0.3
D	Square aluminium 6082 tube	40mm x 40mm	0.3
E	Square aluminium 6082 tube	20mm x 20mm	0.3
F	Circular aluminium tube	20mm diameter	0.4
G	Circular galvanised aluminium tube	35mm diameter	0.2
H	Square mild steel tube	40mm x 40mm	0.1
I	Free space (controlled environment)		

The reflection coefficient in Table 4-1 is the ratio of the amplitude reflected wave of the material and the amplitude of the incident wave on a silver glass mirror (assumed to have perfect reflection) as

$$\text{reflection coefficient}_{measured} = \frac{V_{material}}{V_{mirror}} \tag{4-8}$$

where $V_{material}$ is the reflected voltage of the material under test and $V_{mirror}$is the reflected voltage of the silver glass mirror. This coefficient is essential in characterizing the tubes and is measured using simple measurement procedures as illustrated in Figure 4-4(a). The values of the reflection coefficient measured are considerably lower than the expected values. The surface roughness of the inner side of the material is probably the major factor in this as it was not possible to determine the surface roughness appropriately, and inner material could be coated for protection purposes.

The ideal condition is to carry out the measurement at normal incidence, unfortunately

taking consideration of the geometrical shape, size and angle of half intensity of the emitter and photodiode, it is impossible. As reflection coefficient varies with angle, higher at normal incidence and larger at wider angle, thus having a small angle of incidence is an advantage. The emitter and photodiode was placed side by side to achieve as smallest angle of incidence as possible, and the measured angle of incidence was 30^0.

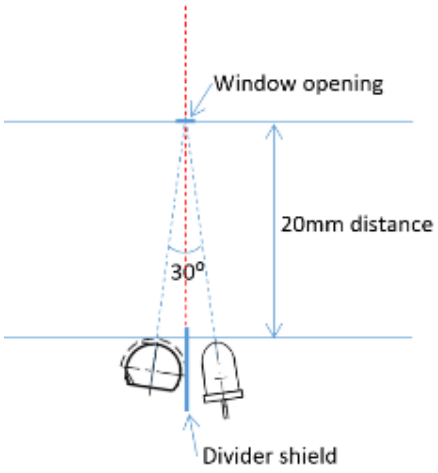

(a)

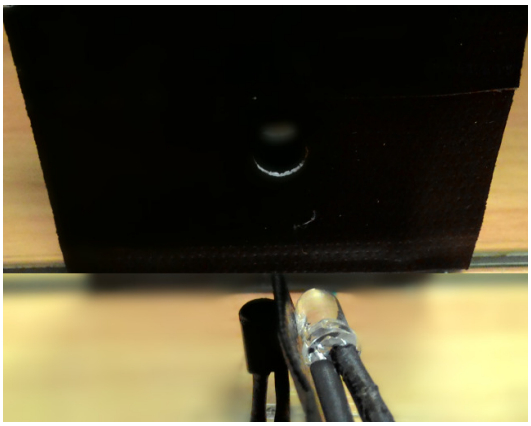

(b)

Figure 4-4 Reflection coefficient measurement setup

A thick (1mm) black cardboard was used as a shield to isolate the beam getting into the receiver. The shield chosen was opaque to the IR beam. The same cardboard with a 5mm diameter circular opening, as in Figure 4-4(b) was placed on the tube under test circular opening will be reflected back to the receiver. Thus, the detector was constrained to look at the one point corresponding to a symmetrical incident of reflection.

4.4 Channel measurement setup

The experimental setup for the channel measurement was as in Figure 4-5, where the transmitter and the receiver were aligned in the centre of the tube. The system was measured using a continuous wave (CW) modulated source at different frequencies (ranging from 10 KHz to 35 MHz) in different tubes of length 0.5 metre and 1 metre.

Figure 4-5 Channel measurement experimental setup

4.5 Channel characterisation by measurements

This section concentrates on the channel characterisation for the line-of-sight (LOS) transmission. The measurements for the transmission within the tubes were compared with transmission in the free space as characterized in Chapter 3. Three criteria were considered to quantify the characteristic of the transmission: the frequency response, the optical power, and the path loss.

4.5.1 Divergence angle

Geometrical calculations were undertaken to determine how much transmitted light would have entered the photodiode. Based on Figure 4-6, the divergence angle was calculated, and at a distance of 1 metre the amount of light which entered the photodiode was determined.

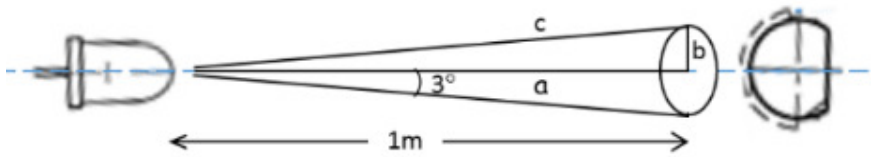

Figure 4-6 Divergence angle

The half-viewing angle is 3°, thus $\cos 3 = a/c = 1/c$. Therefore,$c = a/0.999 = 1.001$. Now, $\sin 3 = b/c$, thus $b = 0.052 \times 1.001 = 0.052\, m = 52\, mm$.

Based on the calculated divergence angle and the inner dimension of the tubes, the number of reflections in each tube could be calculated, as indicated in Figure 4-7, using the following formula:

$$\tan 3° = \frac{r}{d}$$

$$\therefore d = \frac{r}{\tan 3°}$$

$$\text{Number of reflections} = \frac{length\ of\ tube}{2d}$$

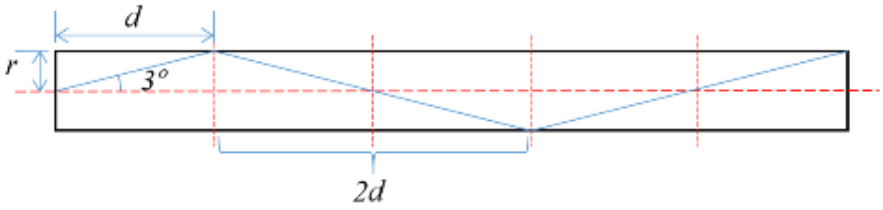

Figure 4-7 Determination of the number of reflections in a straight tube.

In a 20 mm diameter tube, the number of reflections was three, whereas in the 35 mm and 40 mm tubes, the number of reflections was only one. The diameter of the tubes determined the number of reflections occurring within theme and was also related to

the reflection coefficient of the material. Transmission in lower reflection coefficient tubes could be improved by using a smaller tube diameter.

Table 4-2 shows the percentage of power loss at the end of each tube opening, before entering the receiver. The losses were mainly due to the number of reflections occurring within the tubes. The loss percentage varied between 1.11% and 1.17% depending on the reflection coefficient and the inner diameter of the tube. This shows that only approximately 98% of the transmitted power can enter the receiver. Additionally, the use of a narrow beam transmitter also helped to concentrate the power into the receiver.

Table 4-2 power loss

	A	B	C	D	E	F	G	H	I
No of reflections	1	1	1	1	3	3	1	1	0
loss percentage	1.17%	1.16%	1.14%	1.16%	1.14%	1.11%	1.13%	1.17%	1.17%

4.5.2 Frequency response

Channel frequency responses are based on the frequency profiles obtained at 0.5 and 1 metre distances. The transmitter and the receiver are aligned to obtain the highest received signal, and remain at the same position throughout the process. The normalised response for each of the tube at different transmission distances is plotted in Figure 4-8 through to Figure 4-16.

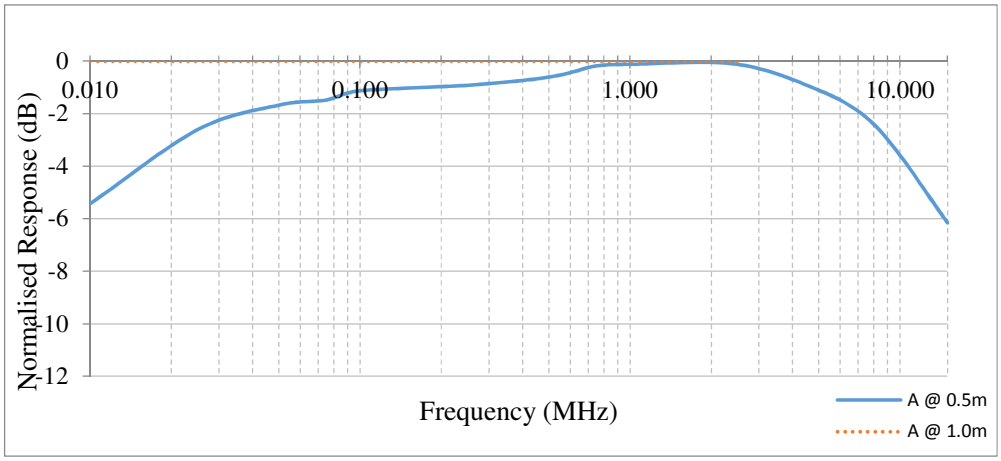

Figure 4-8 Circular cardboard tube normalised response

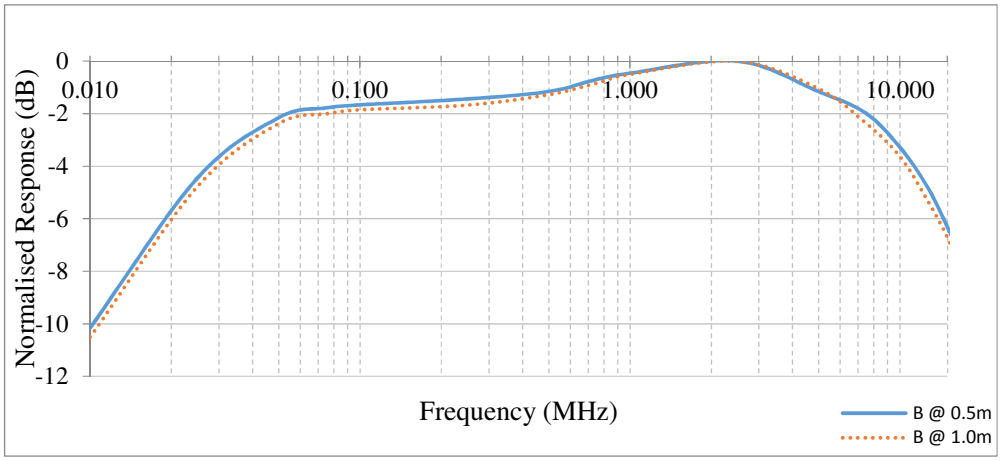

Figure 4-9 Circular plastic tube normalised response

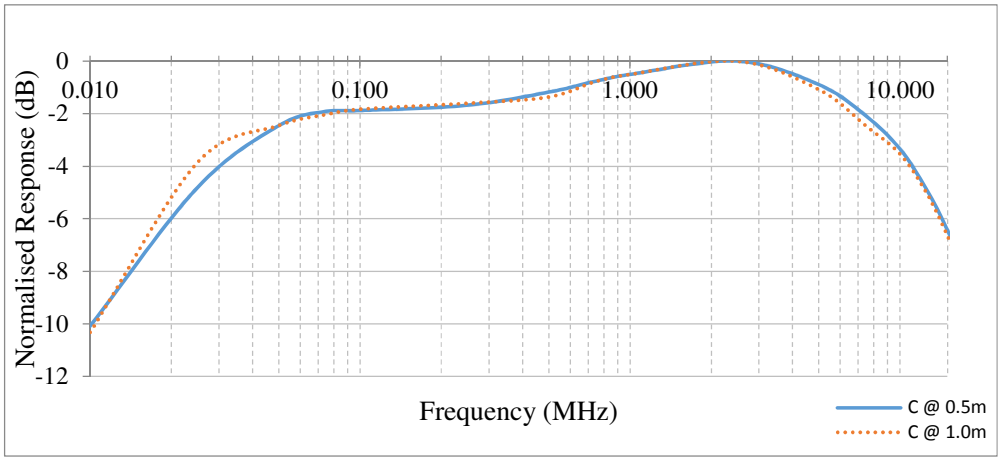

Figure 4-10 Circular mild steel tube normalised response

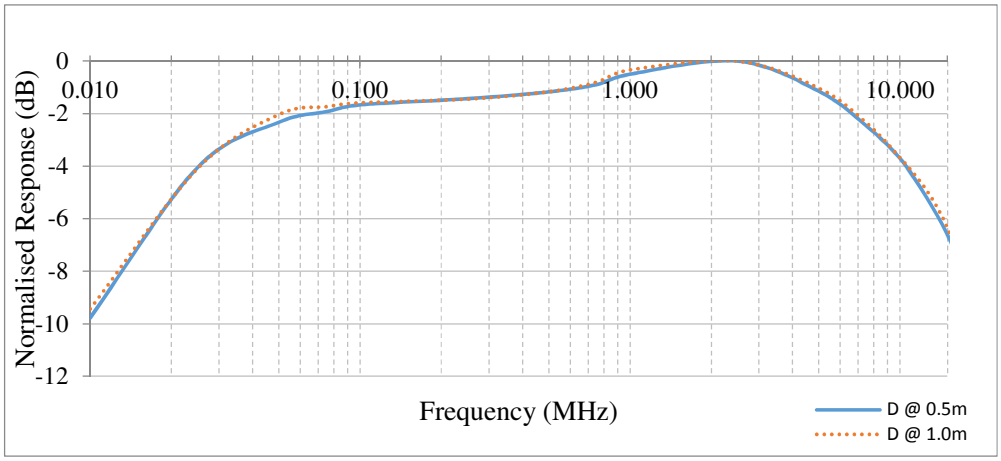

Figure 4-11 Square aluminium tube normalised response

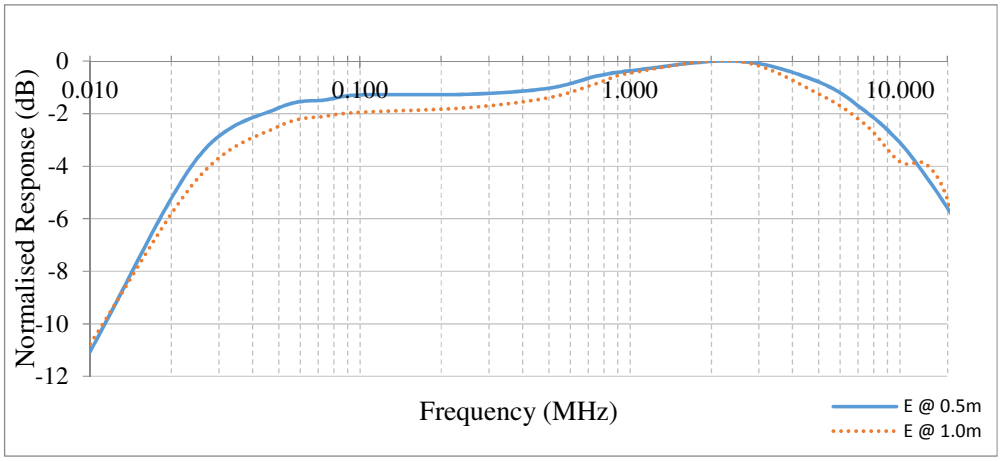

Figure 4-12 Square aluminium tube normalised response

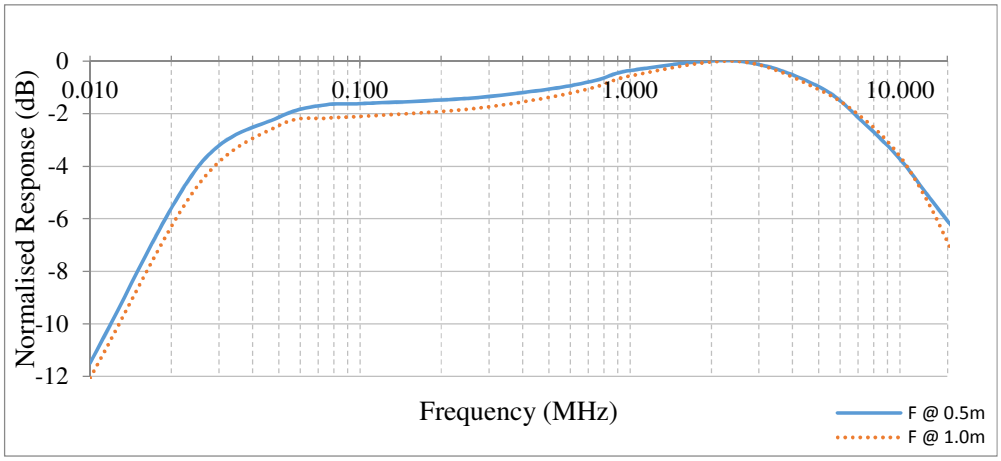

Figure 4-13 Circular aluminium tube normalised response

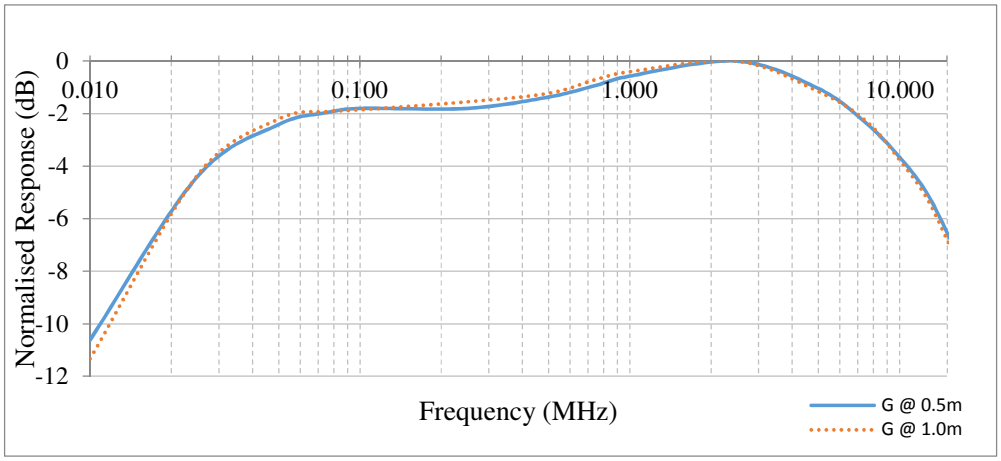

Figure 4-14 Circular galvanised aluminium tube normalised response

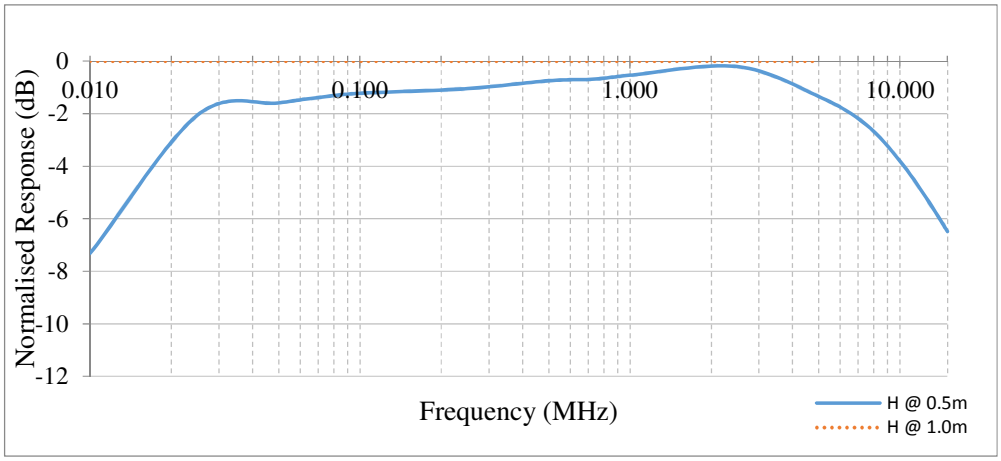

Figure 4-15 Square mild steel tube normalised response

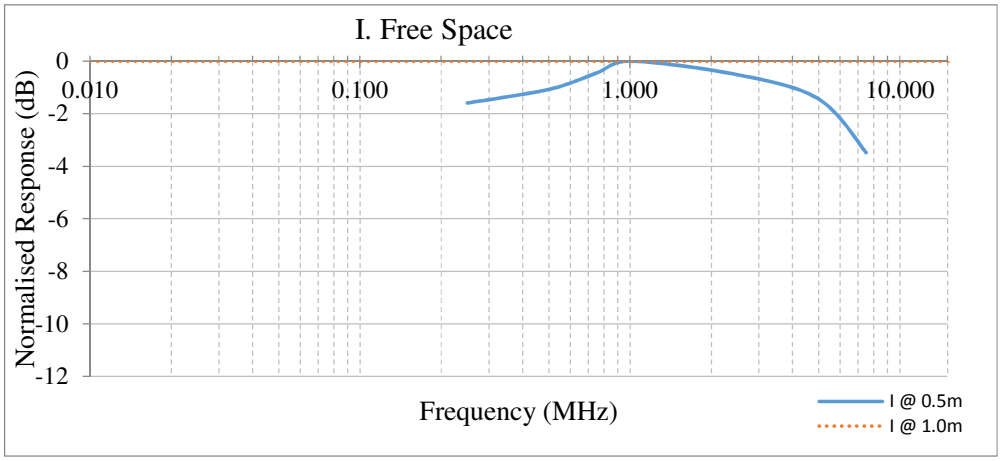

Figure 4-16 Free space normalised response

For all the plots, the normalised response has the same pattern and the 3-dB cut-off frequency is about 13 MHz from the constant relative response, except for the transmission in circular cardboard tube, square mild steel tube and free space. The transmission for the 0.5 m cardboard tube is acceptable, unfortunately for the 1 m transmission, there was no signal detected at the receiving end. The same occurred within the transmission in the square mild steel tube - there was no signal detected at the receiving end for a 1 m distance.

The surface condition of the materials plays an important role in reflecting of the signal. All the tubes with shiny inner surface will specularly reflect light efficiently. While the matt or dark inner surfaces diffuse light reflection in broad range of directions and the received signals are hardly detected at the receiving end as the distance between the transmitter and receiver is substantial in terms of wavelengths.

A weak signal is detected in free space transmission, as the signal power has been dispersed to different angle and absorbed by the thick cloth used to cover the testing area (controlled environment), and does not benefit from reflections in transmission as in the controlled setup.

Figure 4-17 and Figure 4-18 show the only difference for the transmission within the tubes, which is the relative response gain. They show that the materials with a high reflection coefficient receive a much higher power compared to the ones with a lower reflection coefficient. The worst power received is the transmission over free space where weak signal were detected in 0.5 m distance and no signals were detected in 1 m transmission distance.

From the plots, the circular aluminium (F) and galvanised aluminium (G) tubes have the highest response. Although the reflection coefficient of the circular aluminium

tube is high, the inner diameter of the tube is small. This demonstrates that the inner dimension of the tube also plays an important role for better transmission as it also determines how many reflections occur within it. The transmission could be improved either by using high reflective coefficient material or by using a small tube diameter.

Clearly, the shape of the frequency response is almost identical, and the only difference is in the amplitude of the received signal. The response at 0.5 metre and 1 metre are almost the same. Unfortunately, for the free space transmission, the received signal is weak at 0.5 metre, and no detectable signal was received over a 1 metre range.

4.5.3 Optical power

4.5.3.1 Transmitted optical power

The most relevant parameter for wireless transmission is the radiometric optical power, in Watts. However, this parameter was not provided in the data sheet. Therefore, measurements were executed to estimate the transmitted optical power, P_t in watts for the particular IRLED. The IRLED radiometric powers for the devices used were measured using a Thor Labs power meter with an S314C power sensor as in Appendix A. This thermal power sensor is designated for broadband optical power measurements of 100 μW to 200 W power sources. The thermal sensor coating has a flat spectral response over a wide range of wavelengths. The transmitted power was measured, back-to-back, in between the IRLED and the S314C sensor. The power measured increased relatively linearly at different IRLED forward currents, as shown in Figure 4-19. The photometric power outputs were also measured using an Ealing photometer, as in Figure 4-20, which gives a proportional indications of the radiometric power detected.

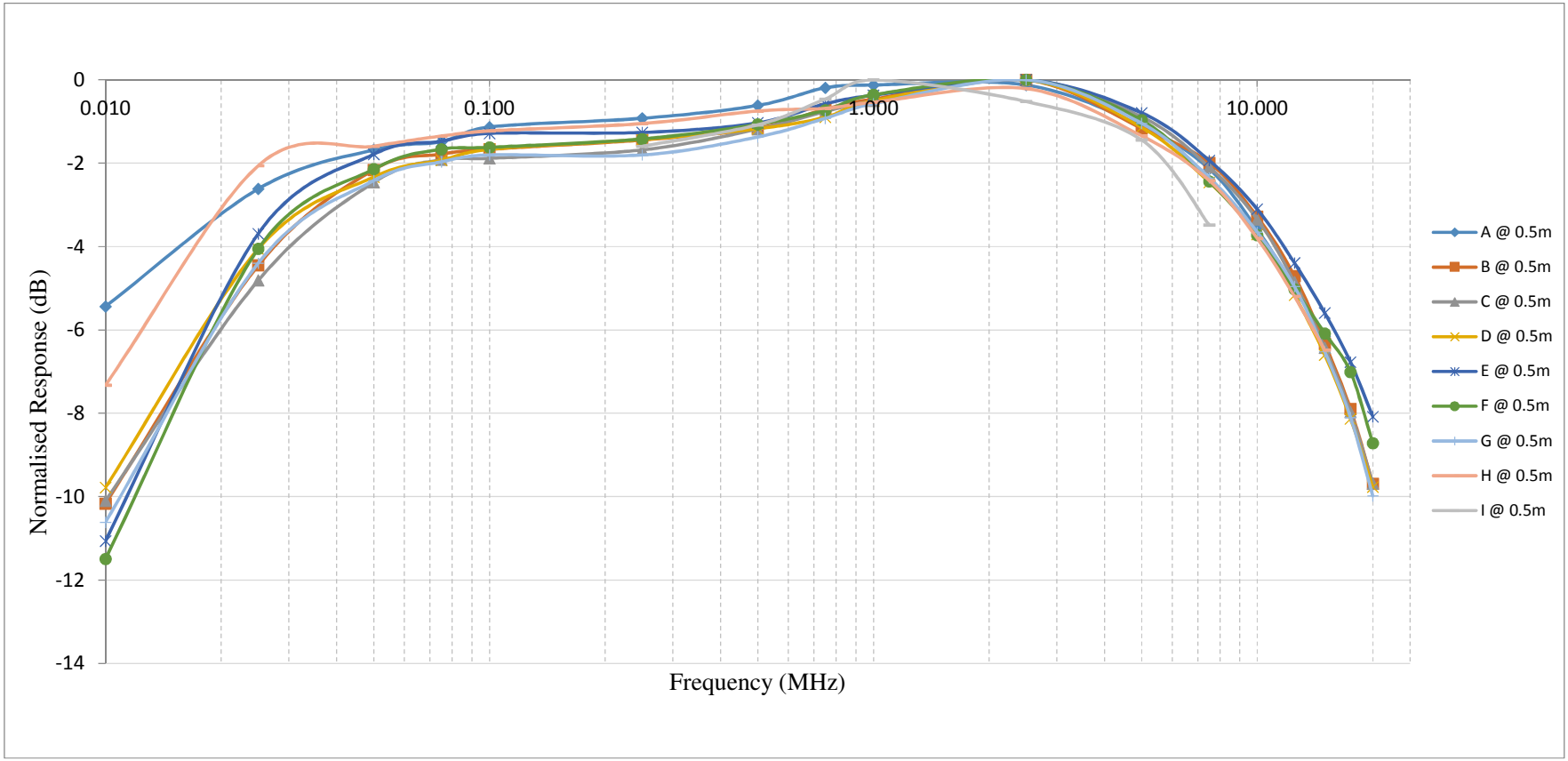

Figure 4-17 Normalised response at 0.5 metre range

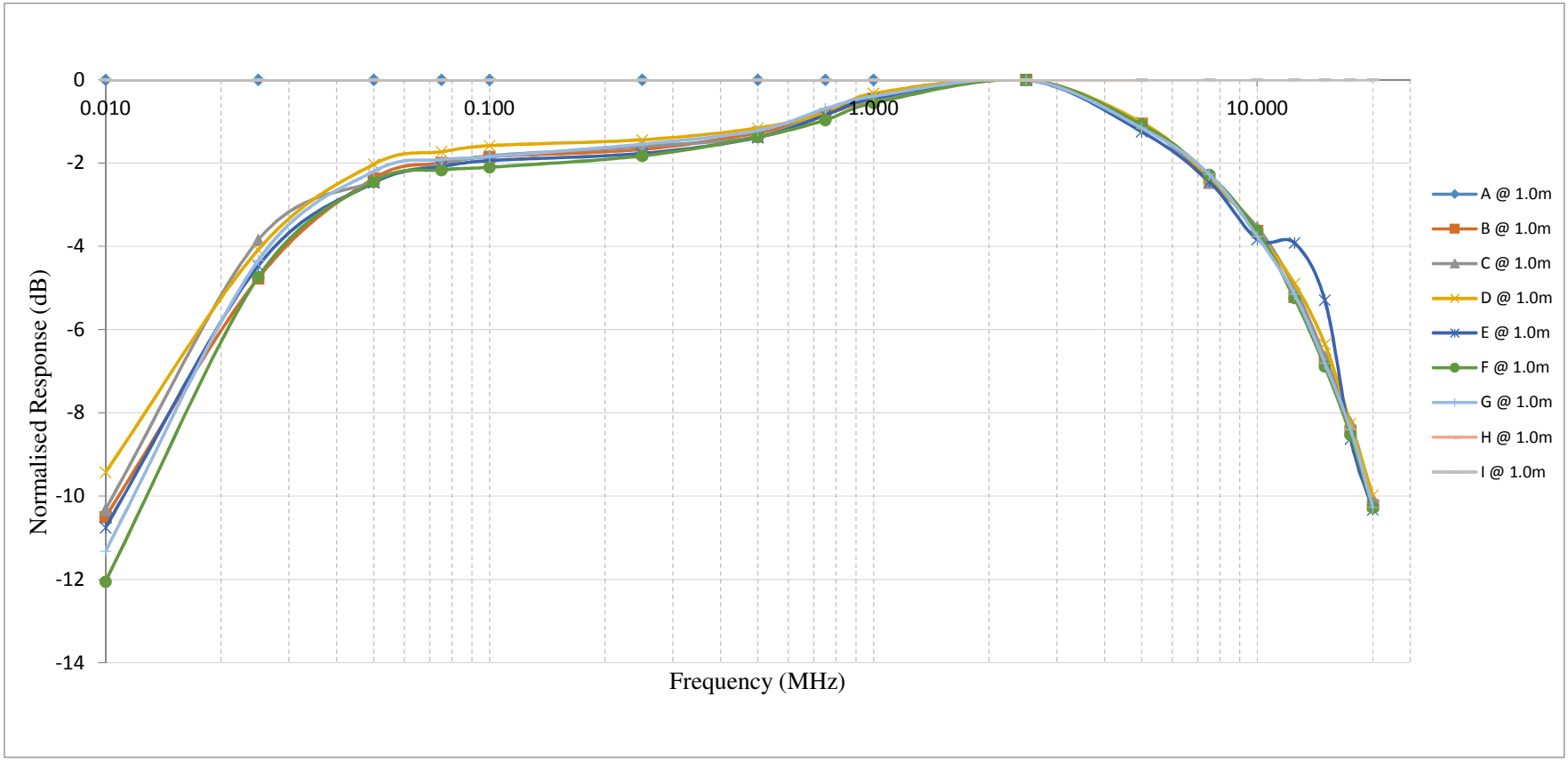

Figure 4-18 Normalised response at 1 metre range

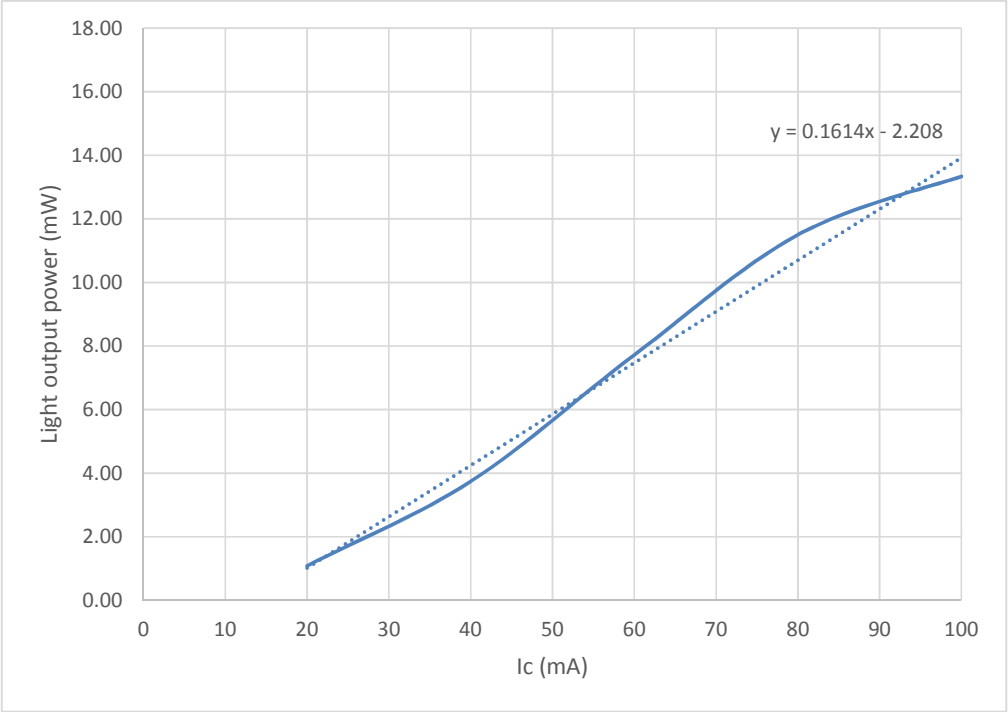

Figure 4-19 Radiometric output power for different IRLED forward currents.

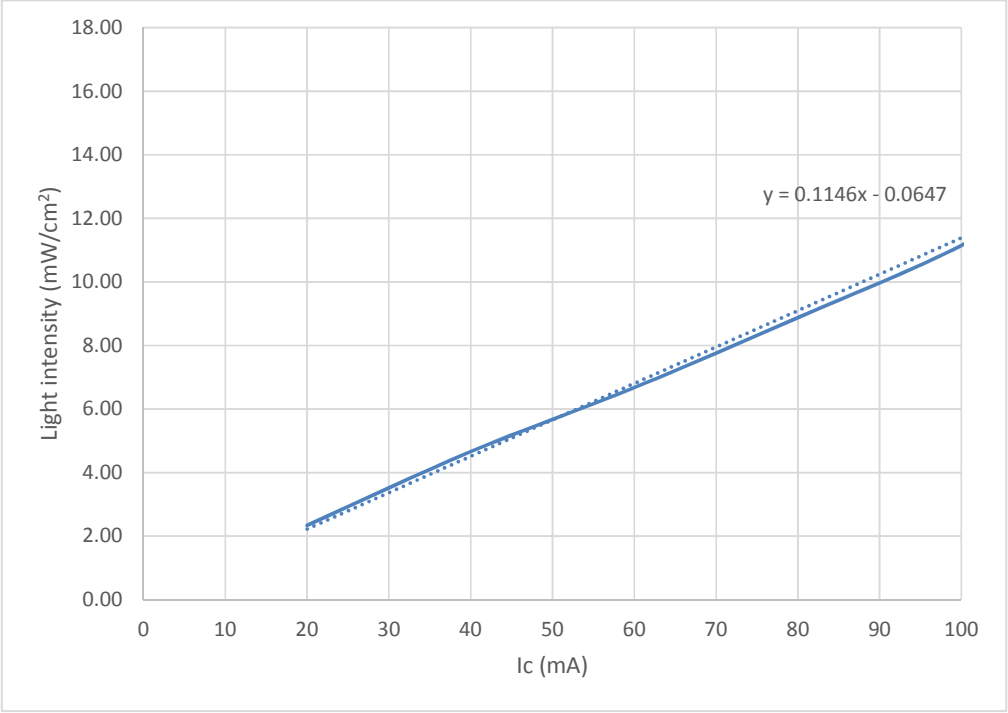

Figure 4-20 Photometric output power for different IRLED forward currents.

4.5.3.2 Optical power received

Based on the number of reflections discussed in Section 4.5.1, a channel model based on reflection presented in reference [24] was developed. According to the Lambert-Phong pattern model based on reflection described in the reference, the intensity of Lambert pattern was specified by Equation 4-9 and Equation 4-10 , which represents the incident optical power [24].

$$P(\theta, \emptyset, m) = \frac{P_{Tx}(m+1)}{2\pi} cos^m \theta \tag{4-9}$$

where θ is the angle between the initial direction of the beam and the direction of maximum power, $\emptyset$ represent the azimuth angle, m is the Lambert exponent defining the width of the beam and P_{Tx} is the transmitted optical beam power.

$$P_p = \frac{A^R}{d^2} P(\theta, \emptyset, m) \cos\varphi \text{rect}\left(\frac{\varphi}{FOV}\right) \tag{4-10}$$

in which A_R is the photodiode detecting surface area, d is the distance between the emitter and the receiver, φ incident angle of incident light, and FOV is the field of view.

Experimental measurements were obtained to discover the received optical power and the path loss for the demonstration scenario. Figure 4-21 illustrates the optical power received over distances based on the power transmitted in Section 4.5.1. The measurement was done using the Ealing photometer. The received power drastically reduced as the distance increased. The detected optical power measured in each tubes are different depending on the size, geometry and the reflection coefficient of the tubes at a given range, as will be discussed in the following section. Smaller tubes dimensions gave a high-detected optical power compared to larger tubes. Based on the plot, the tubes with smaller dimensions and with high reflection coefficients give

better performance.

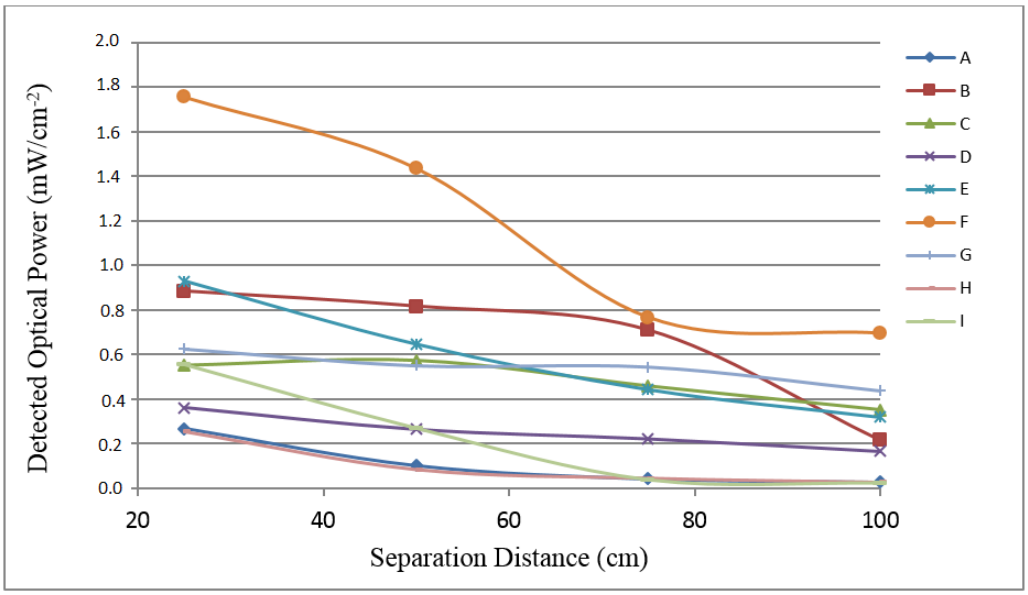

Figure 4-21 Received optical power plotted against separation distance.

Figure 4-22 tabulates the received optical signal for 20 mm, 35mm and 40 mm diameter tubes at 0.5 metre and 1 metre ranges. The plot shows that the optical power received is higher in a smaller tube diameter and in shorter tube range. As the tube diameter and the distance increases, the optical power detected weakens accordingly. In the 20 mm tube, the circular aluminium tube offers higher optical power received compared to the square aluminium tube. The change in the geometrical shape of the tube might also reflect the result of the angle of incidence in the square tube that has a sudden change instead of a gradual change in the circular tube. Furthermore, the light rays might still be contained in the tubes rather than increasing the fraction of light as a result of reflections in a wide range of directions and some might be reflected back. The results for the 35 mm tube are contradictory for 0.5 metre and 1 metre ranges. At 0.5 metres, the next to the lowest optical power received was in circular plastic,

circular mild steel and circular galvanised aluminium tubes, but at a range of 1 metre, the order was circular galvanised aluminium, circular mild steel and circular plastic tubes. This is as the circular galvanised aluminium and circular mild steel tubes have better reflection properties compared to the circular plastic tube. This shows that highly reflective surfaces such as circular galvanised aluminium tubes are suitable for longer transmission ranges. In the 40 mm tube, the detected optical powers for circular cardboard and square mild steel tubes are very similar at 0.5 metre and 1 metre ranges, as the reflection coefficient is nearly the same, as shown in Figure 4-23.

Figure 4-23 tabulates the received optical signal against reflection coefficient at 0.5 metre and 1 metre ranges. The optical power received is higher at larger reflection coefficient and decreases accordingly as the reflection coefficient gets smaller. From the plot, the circular aluminium tube with smaller diameter size and higher reflection coefficient has highest detected received signal at 0.5 m and 1 m separation ranges. The plot also proves that the tubes with smaller diameter produced higher detected signals at the receiving end. This results from the advantages of smaller tube diameters having higher reflection coefficient values, in addition to smooth shiny surfaces.

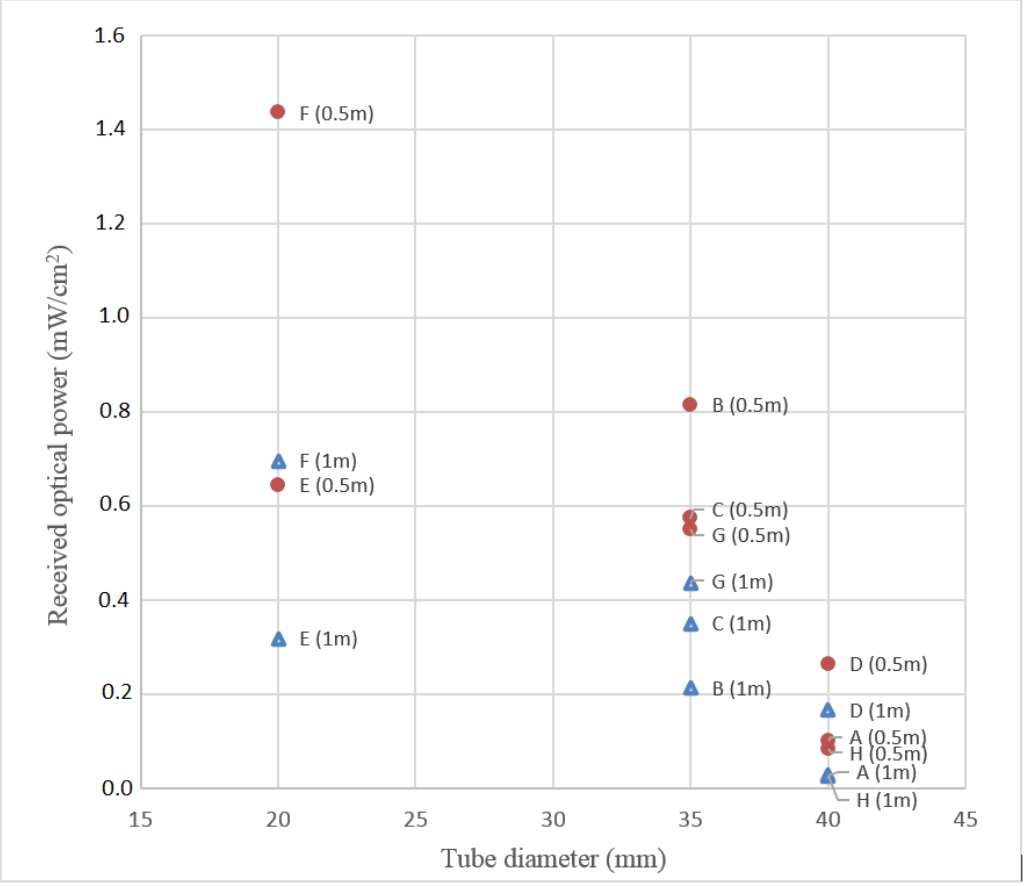

Figure 4-22 Received optical power plotted against tube diameter at 0.5 metre and 1 metre range.

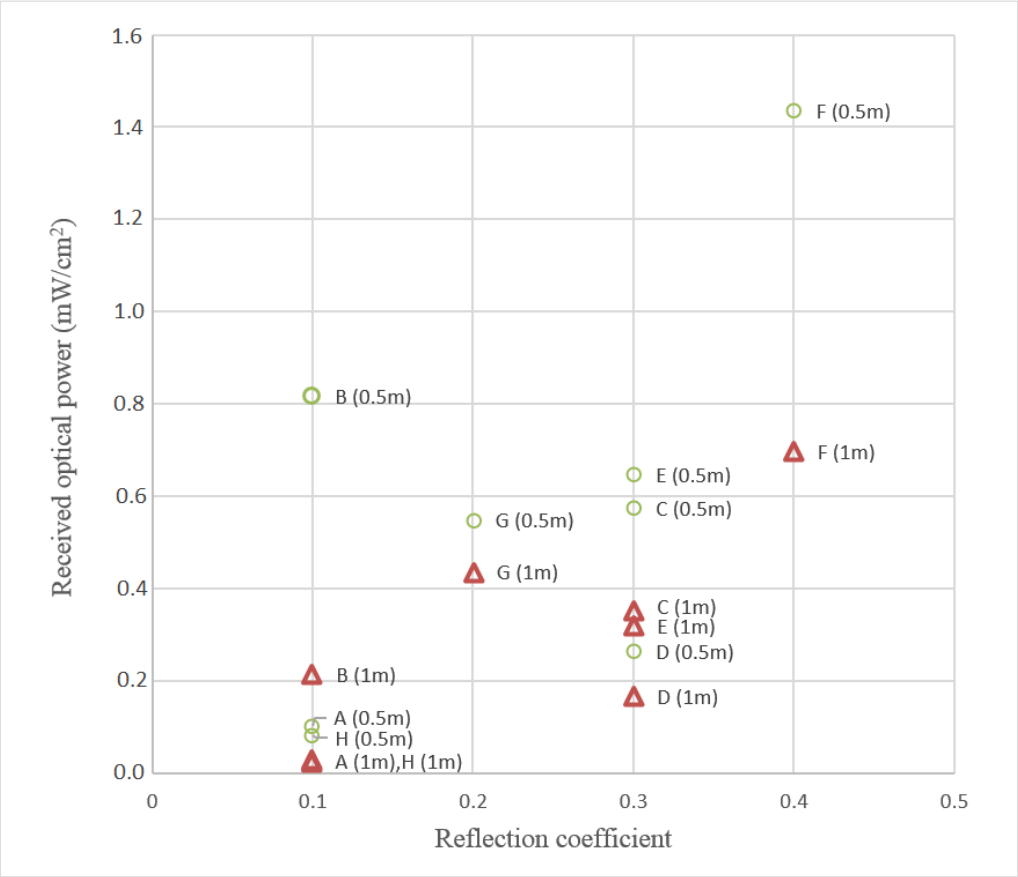

Figure 4-23 Received optical power plotted against reflection coefficient at 0.5 metre and 1 metre range.

4.5.3.3 Path loss

In optical wireless communications, the concept of path loss is used to characterize how the power of the transmitted signal varies as a function of distance. The path loss is defined by the following equation [97]

$$P_L(dB) = -10 \log_{10} \frac{P_R}{P_T} \tag{4-11}$$

where P_R is the received power and P_T is the transmitted power.

The measured LOS path losses are illustrated in Figure 4-24. The path loss is very different in different tubes at the same link distances. Path loss increased linearly for all of the tubes, and the tubes with a small diameter have the lowest path loss. The path loss for the free space situation deteriorates rapidly after a distance of 0.5 metre, as well as for the cardboard and steel tubes. In other tubes, the optical beams still could be measured at the receiving end, even though the received signal was weaker over the distance.

The path loss increases rapidly in free space, plastic tubes and mild steel tubes as the optical waves are diffusely reflected by light coloured object (plastic tube) and absorbed by dark objects (free space, under controlled conditions, and mild steel tubes).

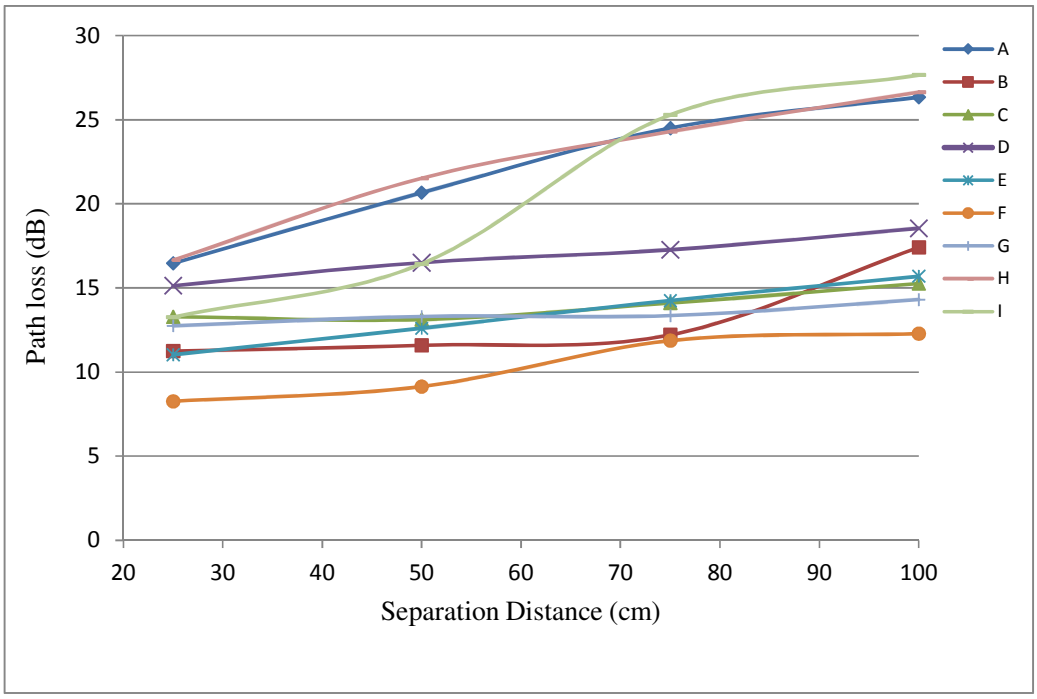

Figure 4-24 LOS path loss at different separation distances

4.6 Conclusions

In this chapter, the channel properties of the LOS demonstration system were described by the following parameters: the material reflection properties, frequency response and path loss.

The reflection coefficient of each of the tubes was measured in order to investigate the effect of the materials parameter during the transmission of light signal within the test tubes. The measured reflection coefficients were considerably lower than the expected values, as they were measured based on the test conditions (circular or square shapes) instead of a flat piece of material. The result might have slight differences as the angle of incidence and the way light reflected and composition of combination of specular and diffuse reflection may differ and affect the findings.

The number of reflections within each test tube was also estimated based on the light reflection law and divergence angle. The highest number of reflections within these straight test tubes is 3, which occurred within the smallest tube sizes (20mm circular and square aluminium tubes). Only 1 reflection was estimated to happen within the other test tubes.

The upper and lower 3-dB frequencies for LOS transmission in the tubes are nearly the same. It can be concluded that the tubes do not significantly change the frequency response, when the bandwidth of the optoelectronics is linked to 13 MHz. The only effect that the tubes have so far is because of the differences of reflection coefficient and geometry of the tubes relative to beam spreading, and acceptance angle of the receiver. The limitation of the transmission comes from other factors, such as the optoelectronic devices at the transmit end, and at the receiver itself.

The size, geometry and reflective properties of the tubes mainly determine the received

signal power level at any point. The experimental works proved that transmission through small tube with higher reflection coefficient was great. As the tube diameter increased the detected optical power get worsen. Further, the received optical power also deteriorates in the lower reflection coefficient tube.

Analysis on the received optical power within different tubes size proved that smaller test tubes, with high reflection coefficients have higher detected optical signals at the receiving end.

The experimental work also demonstrated very large path loss results for large distance links, demonstrating that, at greater ranges, the link is very much power-limited. The detected optical power is related to the path loss. A high-powered source is necessary at longer ranges, especially with large tube diameter with low reflection coefficient where the path loss becomes very large.

Thus, this chapter suggested that transmission using optical wireless communication technology within smaller in size and high reflection coefficient material are promising in straight tubes, in addition to the need for a good transmitter and high sensitivity receiver.

Chapter 5: Channel Characterization – Non Line-of-Sight Transmission

5.1 Introduction

LOS systems are capable of high transmission capacity, however they have the problem of alignment in practical communication links. Non-Line-of-sight (NLOS) systems, in contrast, permit roaming but offer lower bandwidths. NLOS communication systems rely on the reflections of light from any diffusely-reflecting surfaces which have been illuminated from elsewhere [98]. However, multipath dispersion arising from surface reflections can degrade the performance of an NLOS system, in terms of SNR and potential data rates. This chapter aims demonstrate that OW systems can operate around confined spaces and corners, and, in order to assess the performance of NLOS systems, the effect of representative different tube configurations were set up, using the types of configurations as below:

(1) Straight tubes with angle transmitter and receiver orientation

(2) Bending tubes at different angles

Furthermore, in any diffuse system, the position of the transmitter plays a critical role in the power levels at various point along any tube or route otherwise defined.

5.2 NLOS Channel model

In the NLOS case, the light redirected by any reflecting object is taken into account. The received power in the NLOS case is commonly given by [99]

$$P_r = H_{LOS^{(0)}} P_t + H_{NLOS^{(0)}} P_t \tag{5-1}$$

$$P_r = H_{LOS^{(0)}} P_t + P_t \sum_{\text{ref}} H_{\text{ref}^{(0)}} \tag{5-2}$$

where $H_{LOS^{(0)}P_t}$ is the average received power of the unobstructed LOS path, and $H_{NLOS^{(0)}P_t}$ is the channel DC gain on LOS and reflected path $H_{\text{ref}^{(0)}}$. The noise considered comes from the noise sources, which were discussed in Section 3.6.

5.3 Reflection characteristics

The reflection attributes of the surfaces rely upon on few aspects, for example, material surface properties, wavelength of the incident radiation, and the angle of incidence. The shape of reflection pattern is controlled by the irregularity of the surface in respect to the wavelength. According to [13], the Rayleigh criterion is best used to determine whether a surface is smooth or rough. A smooth surface reflects incident rays in a very predictable manner, in agreement with the laws of reflection. A surface may be assumed as smooth, if [13]

$$\zeta < \frac{\lambda}{8 \sin(\theta_i)} \tag{5-3}$$

where ζ is the maximum height of the surface irregularities, λ the wavelength of the incident radiation and θ_i the angle of incidence with respect to the surface.

A surface is assumed rough when $\zeta > 0.1\mu m$. This demonstrates that the majority of the surfaces are rough for the mentioned λ value, yielding diffuse reflection patterns, in this manner supporting the utilization of a Lambertian reflection pattern in channel models.

5.4 Received power

This investigation is closely interrelated to the work on indoor environments, therefore the power distribution profile in a tube was related to the power distribution profile of optical wireless communication in a room. Some of the established algorithms used to estimate the impulse response are: the recursive method [33], the statistical approach [34], the DUSTIN algorithm [35], the ceiling bounce model [100], Monte Carlo simulation [36], the Modified Monte Carlo Scheme [37], and Iterative, Site-Based Modelling [38]. Every one of these models was constructed just with respect to the single transmitter circumstance.

The recursive method is commonly employed, as it concurs well with empirical results and recursive methods are able to compute the impulse response for any number of reflections. This allows accurate power distribution analysis and impulse response analysis. However, the results from the simulation are not always the best, as the approach is based on the idealized transmitter, reflector and receiver models.

5.5 Straight tubes

This section describes measurements that were performed to explore the effect of changing the transmitter or receiver orientation angle on the transmission link. The infrared channel was characterized by measuring the detected optical power intensity

using photometer. The experimental setup was as in Figure 5-1. Only the transmitter or the receiver was rotated in steps of 15° each time. By rotating the transmitter/receiver angle, the number of reflections/bounces occurring in the tubes increases and did not comply with the one calculated in Section 4.5.1.

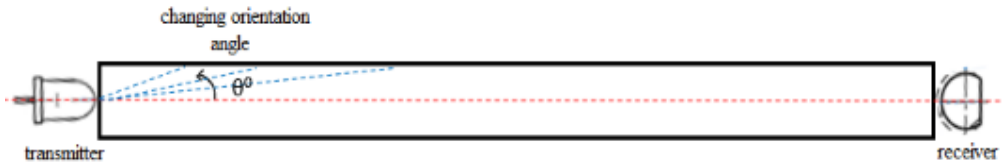

Figure 5-1 Transmitter and receiver orientation experimental setup.

5.5.1 Received optical power at different transmission angles

The results for the transmission medium at 0.5 metre and 1 metre distances were determined, as Figure 5-2 and Figure 5-3 respectively. The plot illustrates that the power intensity reduced as the angle increases. Similar trends were obtained for both 0.5 metre and 1 metre separation distances. The received signal was good at transmission angles less than 15°. As the transmission angle increased, the received power detected decreased significantly. The detected optical power intensity was high for the highest reflection coefficient materials and for smaller cross sections, and vice versa.

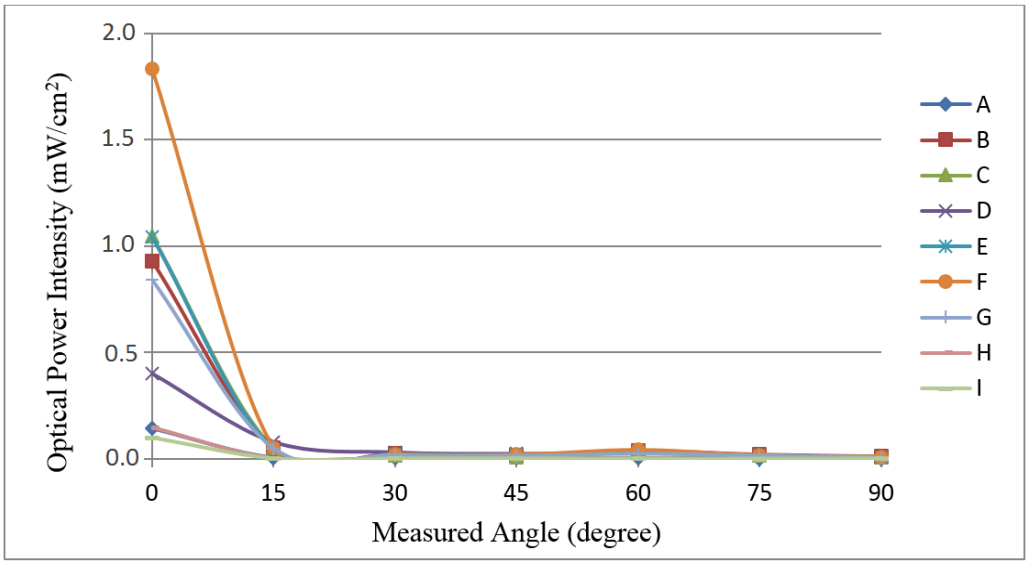

Figure 5-2 Received power at different angles (0.5 metre distance).

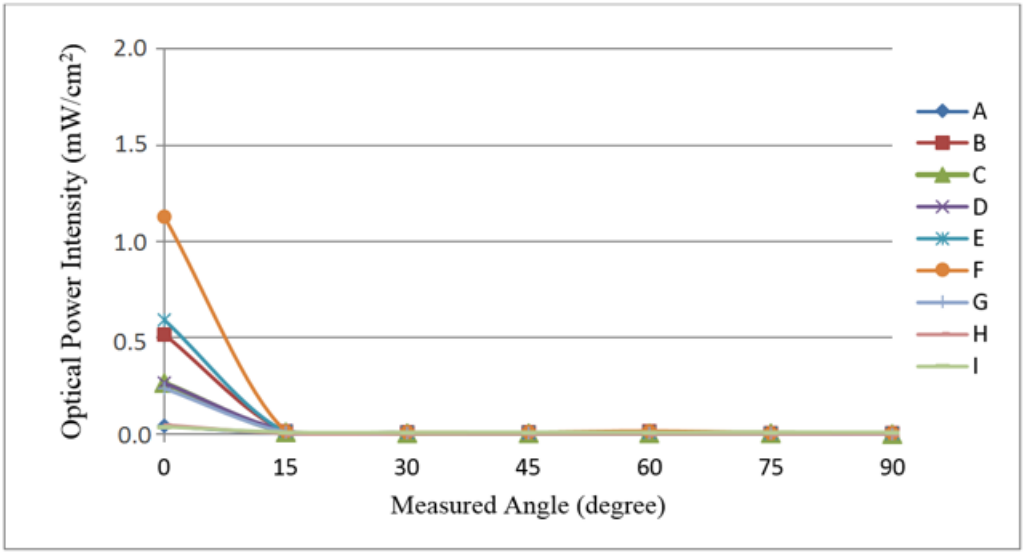

Figure 5-3 Received power at different angles (1 metre distance).

Thus, slight misalignment between the transmitter and the receiver resulted in a considerable loss of optical power. The combination of material property (reflection coefficient) and geometrical property both played a very important role in determining

the detected optical intensity at the receiving end.

If the received optical power density is $P_{d_{rec}}$, and the measured angle is θ, then

$$P_{d_{rec}} \approx A.e^{-k^{\theta}} \text{ watts/cm}^2 \quad (5\text{-}4)$$

where the constants A and k can be determined for the case of each material and each geometry (the geometry to include the length of tube and the tube diameter).

5.5.2 Path loss

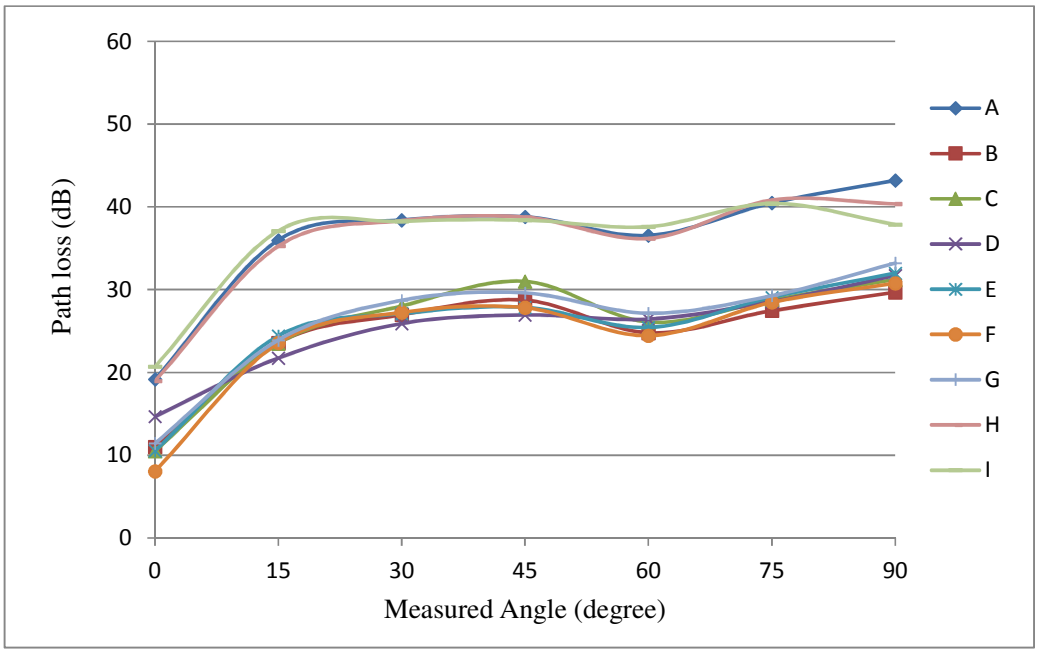

Figure 5-4 Path loss at different angle (0.5 metre distance).

The path loss curves for a 0.5 metre distance shows that cardboard tube (A) and mild steel tube (H) have the highest path loss, as the diameters of these tubes are large. The smaller aluminium tube (F) has the lowest path loss, even though the reflection coefficient is low. This closely agrees with the optical power received discussed in

Section 5.4, the lowest power detected at the receiving end with the highest path loss, and vice versa.

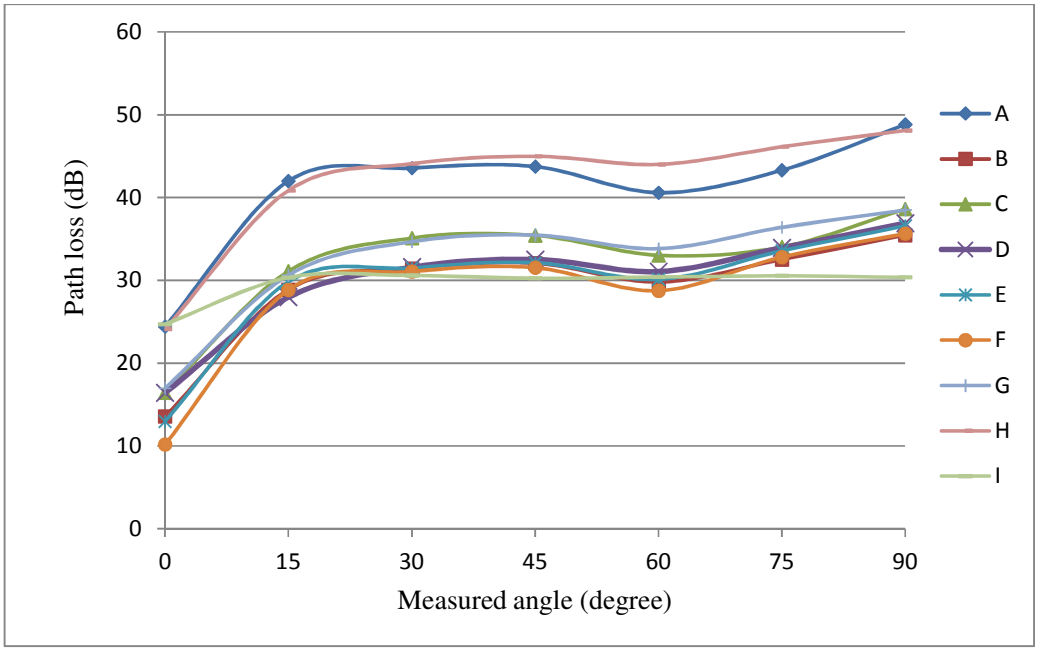

Figure 5-5 Path loss at different angle (1 metre distance).

At a 1 metre separation distance, the path losses were plotted, as in Figure 5-5. The path loss for the 0.5 metre and the 1 metre separation distances have very similar curves. The path loss increased drastically as the transmitter/receiver angle increased up to 15° angles. After this angle, there is a slight increase to the path loss according to the increase in the separation distances.

The investigation on the straight tube demonstrated that the transmission demonstrates a considerable susceptibility to the direction/degree of rotation of the transmitter/receiver. Substantial variety between power received and path loss detected within the tubes, at orientation between 0° right up to 15° angles, was identified. The transmission at an orientation of more than 15° was almost non-

existent, and thus not suitable at all for optical wireless communications.

5.6 Bend tube measurements

Measuring the received power for the bent test tube using existing circuitry resulted in low optical power detected at the receiving end. A considerate amount of received power was detected when using a shorter bent tube. The power required to test bent tubes was found to be high. Thus, the modulator circuit discussed in Chapter 3 was modified, where the transistors, Q1 and Q2, were changed to the high output power transistor, type SC5707 and the IrLED was parallel to gain more power from the transmitter. Four IrLEDs were used to provide enough power for receiving a measurable signal at the other end of the system.

The modified circuit was as shown in Figure 5-8, and the IrLED arrangement was as in Figure 5-6. Resistors R1 – R9, IrLEDs LED2 – LED4, and capacitors C5 –C7, were added to the previous circuit. The total number and the arrangement of IrLEDs were chosen, as in the figure, so that they fitted into the smallest tube opening (20mm square and circular aluminium tubes). The array of four IrLEDs produced 54.48 mW of radiometric output power, or 44.58mW/cm^2 of photometric output power. There was a discrepancy of about 2% between the output calculated for one IrLED (13.34 mW) multiplied four times, and the actual power output of the array of four IrLEDs (54.48 mW).

Figure 5-7 illustrates the frequency response of the transmitter based on the array of four IrLEDs. There is a slight reduction in the bandwidth, but it is always a compromise in between the power and the bandwidth, the latter having reduced to 6 MHz.

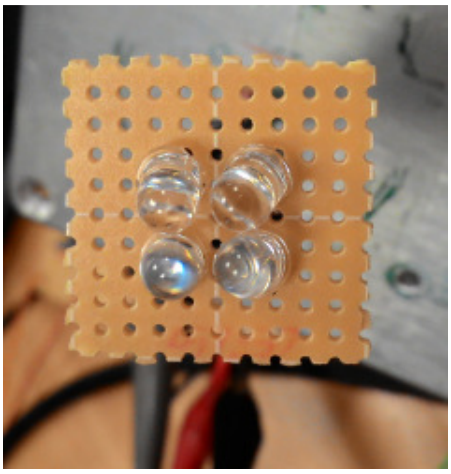

Figure 5-6 Array of four IrLEDs arrangement.

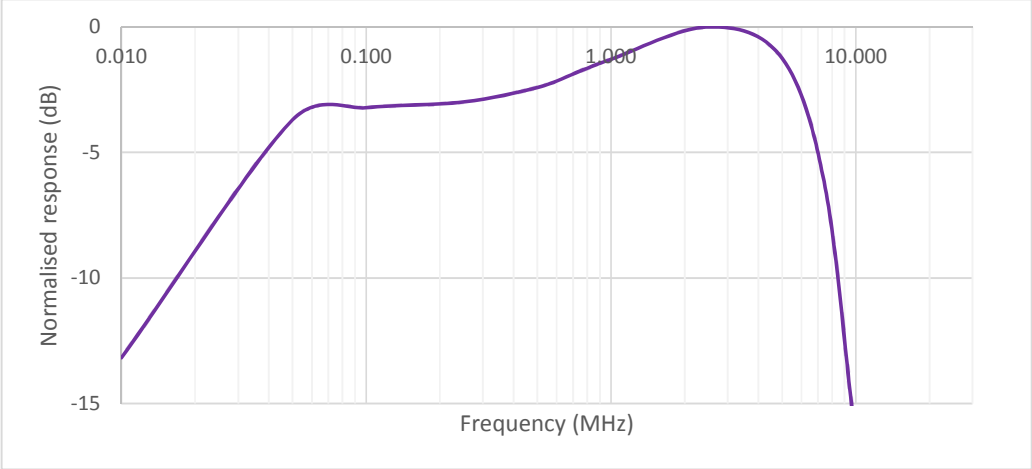

Figure 5-7 Frequency response of array IrLEDs transmitter

The study on the transmission in the bend tubes was performed in two categories, (1) plastic tubes, and (2) metal tubes. The study of the transmission in these media is discussed in detail, in the following section.

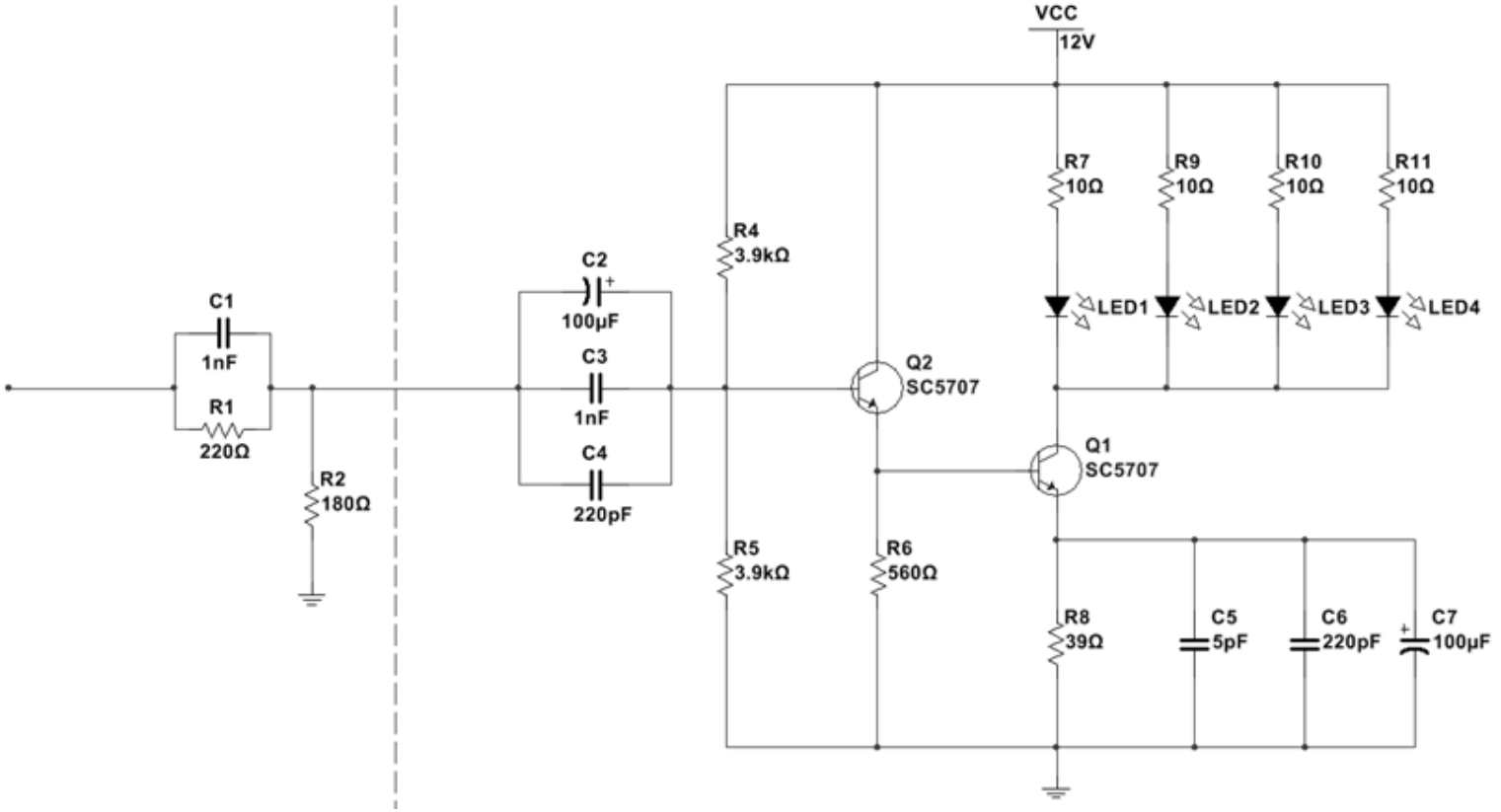

Figure 5-8 Array of four IrLEDs transmitter circuit

5.6.1 Plastic tubes

Investigation on plastic tubes concentrated only on four bending shapes, as in Figure 5-9. The tubes had the same inner diameter, which was 35 mm, but they were of different lengths and bend angles.

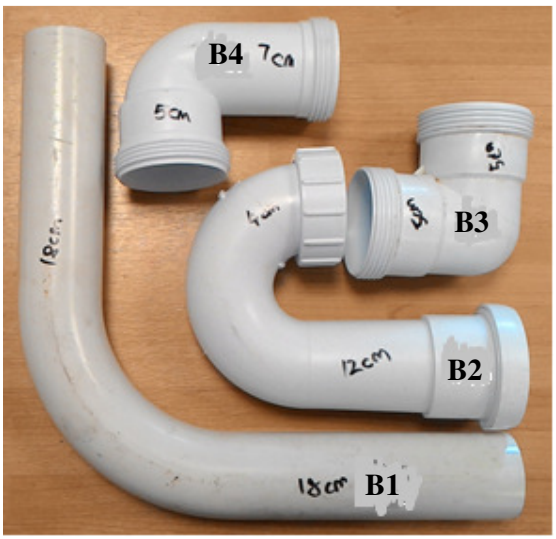

Figure 5-9 Experimental materials bent through different angles – Plastic.

5.6.1.1 Frequency response

Figure 5-10 shows the normalised response of bent plastic tubes. The response for B1 was unable to be measured, as the noise level was high for the measured bandwidth. Furthermore, light rays are diffusely reflected by light coloured objects. Most of the transmitted light will also be reflected backwards when the bending angle is 90°. Figure 5-11(a – d) to Figure 5-14(a – d) show the captured waveforms for B1 – B4 at various modulation frequencies from 100 kHz up to 5 MHz. The waveforms show the transmitted and the received signals at different frequencies. It is clearly seen that the output/received waveform still could be detected at higher frequencies, including B1,

although the noise level is considered high. A clean waveform could be obtained by increasing the transmitted power. However, the transmitted power should comply with eye safety regulations.

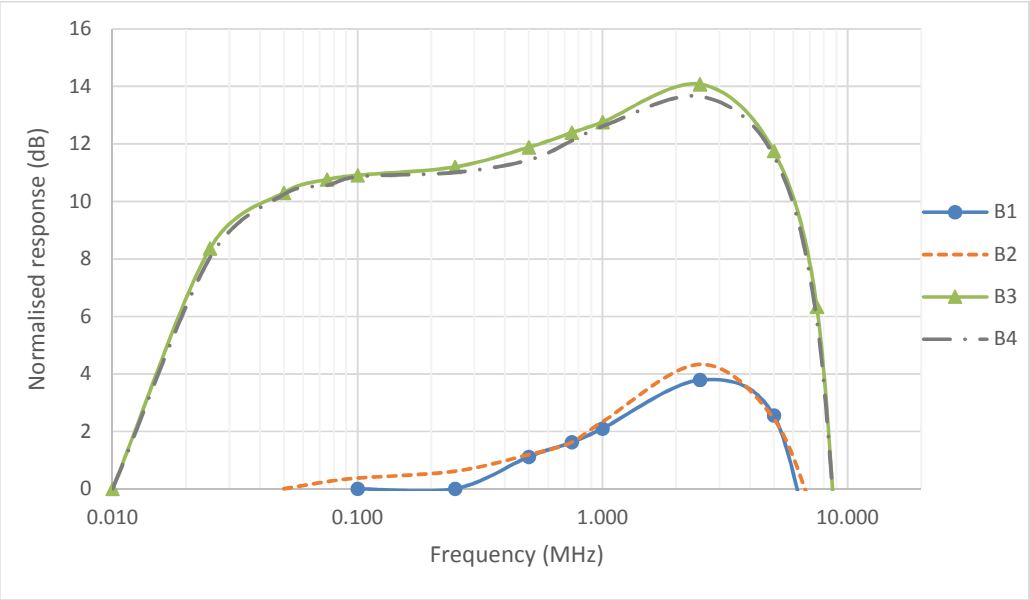

Figure 5-10 Normalised response of plastic tube.

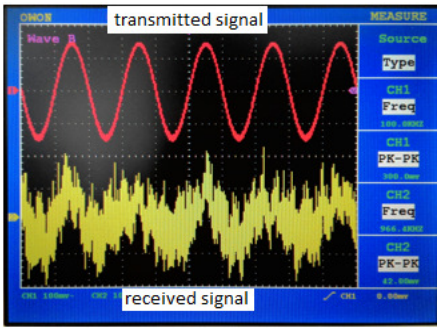

(a) 100 kHz

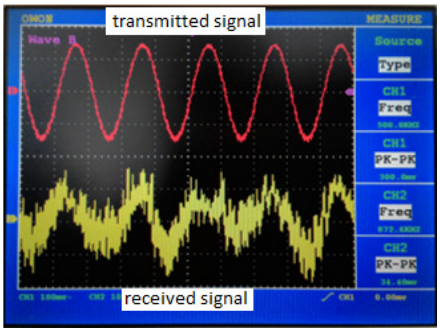

(b) 500 kHz

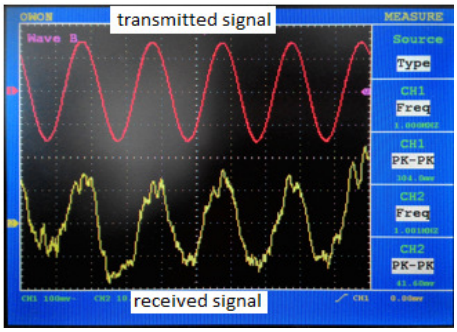

(c) 1 MHz

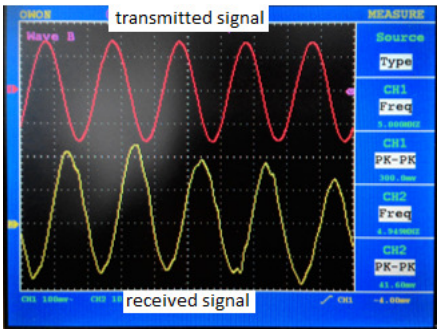

(d) 5 MHz

Figure 5-11 Waveforms of B1

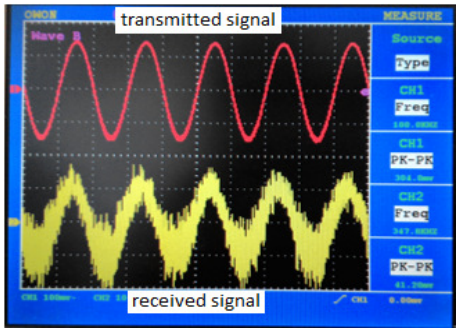

(a) 100 kHz

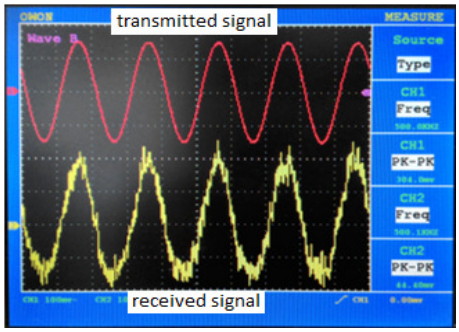

(b) 500 kHz

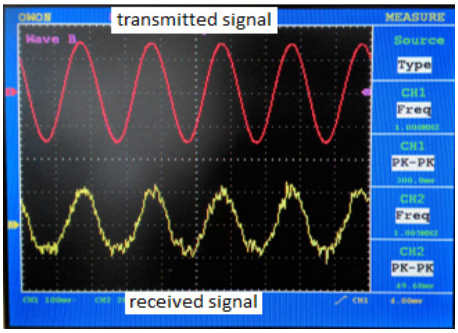

(c) 1 MHz

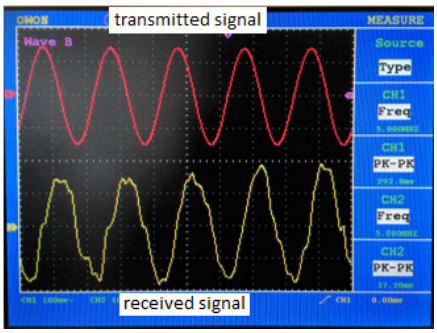

(d) 5 MHz

Figure 5-12 Waveforms of B2.

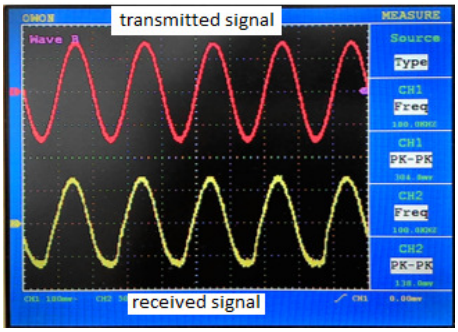

(a) 100 kHz

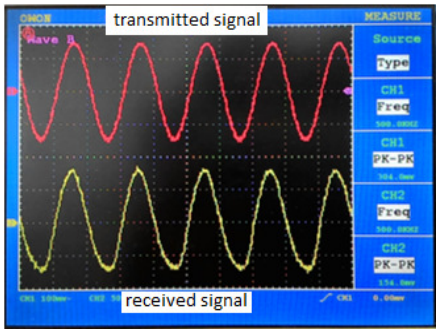

(b) 500 kHz

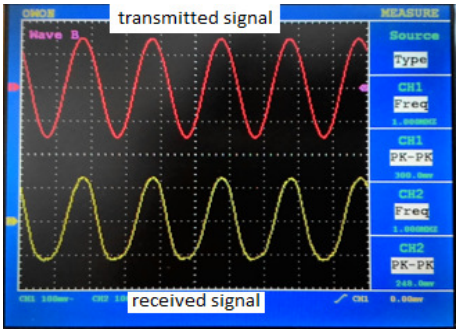

(c) 1 MHz

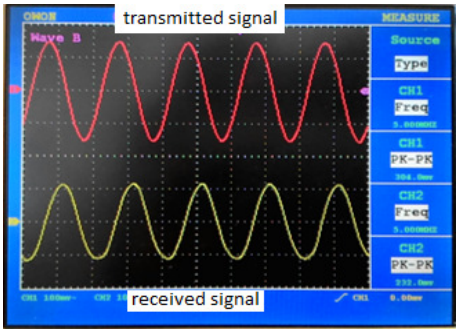

(d) 5 MHz

Figure 5-13 Waveforms of B3.

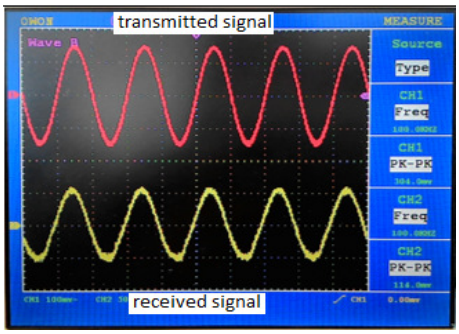

(a) 100 kHz

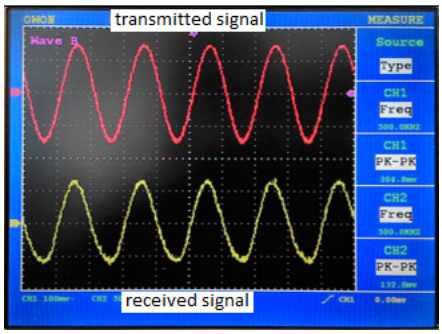

(b) 500 kHz

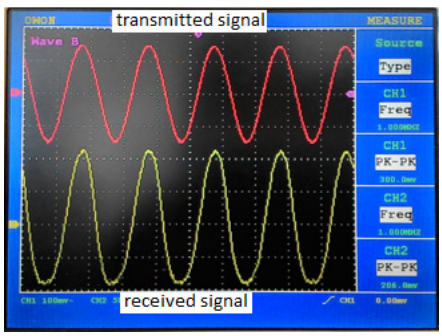

(c) 1 MHz

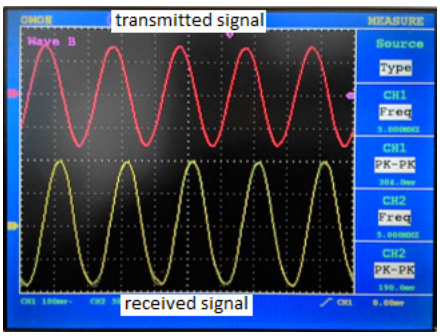

(d) 5 MHz

Figure 5-14 Waveforms of B4.

5.6.1.2 Optical power received and Path loss

Table 5-1 shows the optical power measured at the receiving end, whereas Table 5-2 shows the path loss in the plastic tubes derived from these measurements. B3 received a high optical power, followed by B4, B2 and B1. As the received optical power is inversely related to the path loss, then B1 has the highest loss, followed by B2, B4 and B3. The trend shows that the longer the length the higher the loss, as might be expected. The optical signal-to-noise ratio (SNR) can then be calculated based on the measured data and recorded in Table 5-1. The SNR was calculated, based on the ratio of signal power to the noise power detected by the photo/power meter. The noise power measurements at the receiver were taken when the transmitter was turned OFF.

Table 5-1 Received optical power for plastic tubes.

Frequency (MHz)	B1	B2	B3	B4
Transmitter off	9.80E-06	8.10E-06	8.70E-06	6.40E-06
0.500	1.60E-05	2.63E-05	1.30E-04	1.12E-04
1.000	1.56E-05	2.64E-05	1.34E-04	1.11E-04
5.000	1.56E-05	2.56E-05	1.34E-04	1.11E-04
10.000	1.61E-05	2.60E-05	1.32E-04	1.12E-04
SNR (dB)	**1.61**	**3.21**	**1.52**	**1.74**

Table 5-2 Consequent path loss for plastic tubes.

	B1	B2	B3	B4
Path loss (dB)	28.77	26.60	19.53	20.29

The tube B3 had the lowest SNR (1.52 dB) followed by B4 (1.74 dB), B1 (1.61dB)

and B2 (3.21dB). This shows that the increasing angle will increased the SNR level. B3 and B4 have a low SNR compared to B1, as the length of the tubes is shorter for the same bending angle (90° bend). The path loss in Table 5-2 shows that the shorter tube length has a low path loss compared to the longer tube.

5.6.2 Metal tubes

Extra attention was paid to the metal tubes, as the interest of this study focused on aluminium and steel tubes, to imitate a real vehicle chassis. A simple experiment, prior to the angle selection stage, was undertaken to establish likely parameters, especially angles and choice of particular materials. The experimental setup of the physical arrangement is as shown in Figure 5-15.

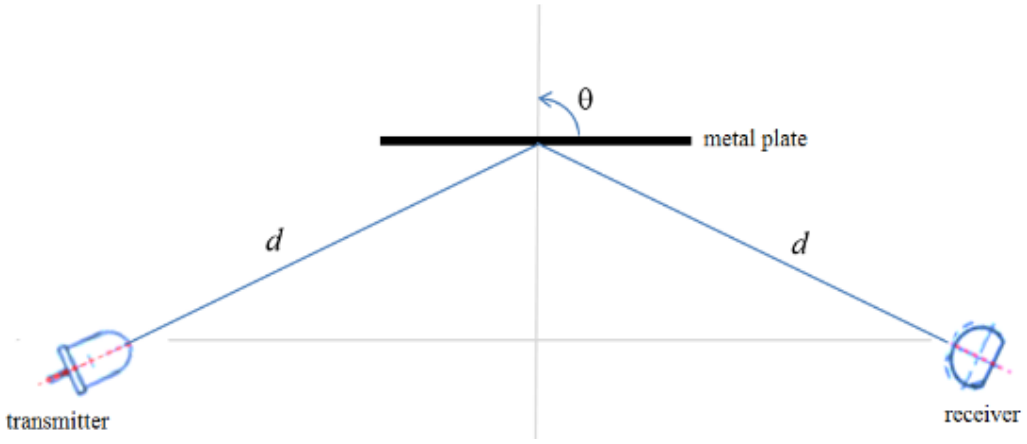

Figure 5-15 Experimental setup for identifying best angle selection.

The transmitter was pointed at a metal plate at certain angle, and the received signal power was captured at the other end. The distance, *d*, between the transmitter and the reflecting metal was the same as the distance between the reflecting metal and the receiver. The metal plate used was an aluminium plate as the reflection coefficient was good compared to that of any other metal in hand. The captured waveforms at

different angles were as in Figure 5-16 (a – e).

Based on the results, three tube configurations, with 30^0, 45^0 and 60^0 bending angles, were selected and fabricated, as in

Table 5-3. The total length of the tube is 1 metre, with a bend to a specific angle at the centre point. The tubes were actually cut and welded in order to get a precise bending angle.

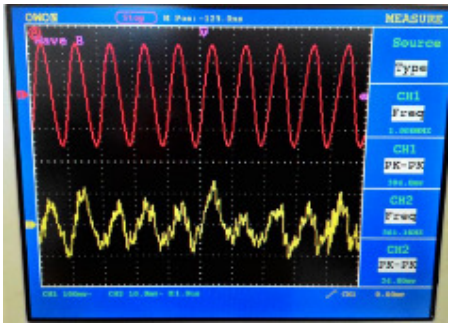

(a) 15° bend

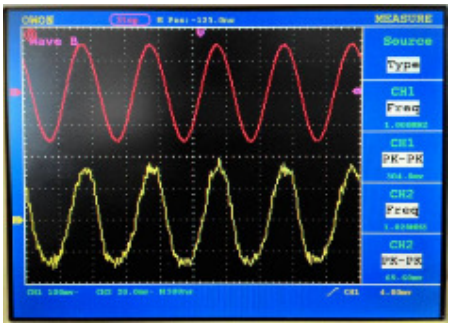

(b) 30° bend

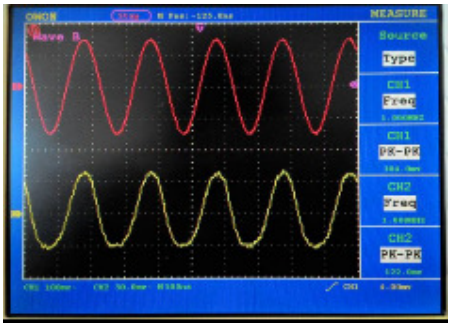

(c) 45° bend

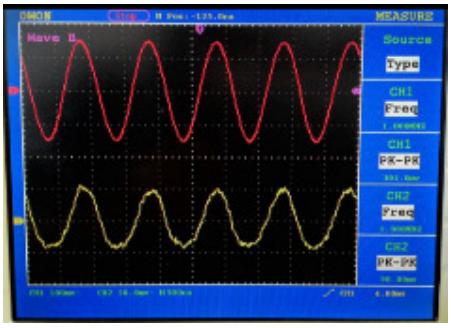

(d) 60° bend

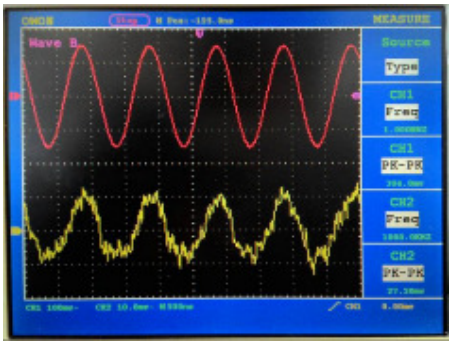

(e) 75° bend

Figure 5-16 Waveforms of best angle selection.

Table 5-3 Experimental metal tube bends

Items	Materials	Items	Materials
C	 Circular mild steel tube	**F**	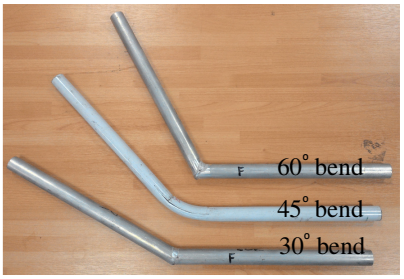 Circular aluminium tube
D	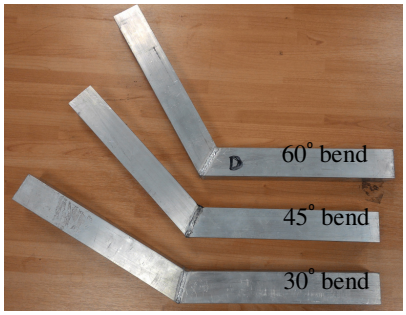 Square aluminium 6082 tube	**G**	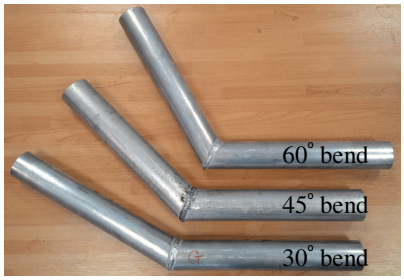 Circular galvanised aluminium tube
E	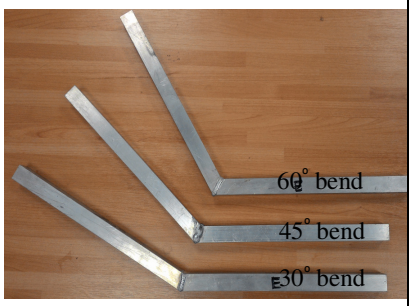 Square aluminium 6082 tube	**H**	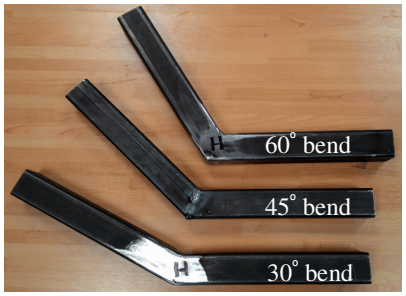 Square mild steel tube

5.6.2.1 Number of reflections

The estimation of the number of reflections within 20 mm and 40mm tubes is made in accordance with Figure 5-17. The drawing is not to scale.

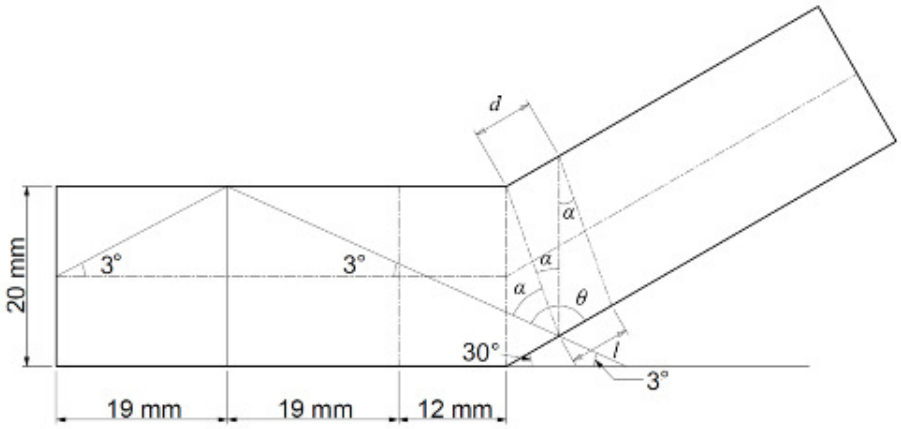

Figure 5-17 Determination of the number of reflections in 20 mm bent tube.

Table 5-4 lists the estimated number of reflections in each tube. The calculations were based on the geometrical shape of the tubes and Snell's law. Appendix C shows their details.

Table 5-4 Estimation number of reflections in bent tubes

	30° bend	45° bend	60° bend
20 mm tube	8	14	25
35 mm tube	5	8	14
40 mm tube	4	7	12

5.6.2.2 Frequency response and waveforms

Based on the improved transmitter circuit and new optical output power produced, only the signal transmitted through square aluminium ((20mm (E) and 40mm (D)), circular aluminium ((20mm (F)) and circular galvanised aluminium (G) tubes were manageable to measure the frequency responses. For other metal tubes, at the receiver, the noise level was higher than the signal detected, and almost no signal was detected

in some of the tubes, although, with the help of lenses more signal could be received, as shown in Figure 5-18. The waveform captured is the example from the circular mild steel tube at 30° bend.

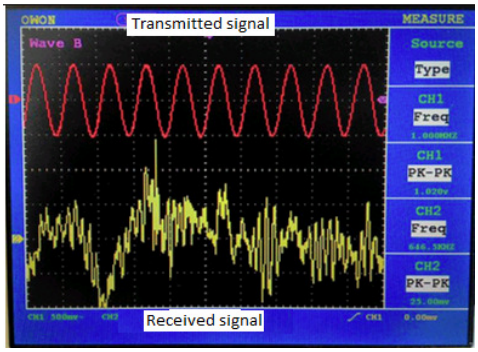

Figure 5-18 Circular mild steel tube captured waveform at 30° bend

Table 5-5 to Table 5-8 show the measured normalised responses and waveforms for the above-mentioned metals, with and without the aid of a lens. It is clearly seen that the use of the lens is not helpful at all. The measured values between with and without lens does not have any significant improvement.

The bandwidth for 30° bend maintained approximately at 6 MHz for all the tubes, unfortunately with different power level. The bandwidth reduced drastically as the bending degrees increases. No signals were detected at 60° bending except for in the circular galvanised aluminium tube. The transmission through 20mm square aluminium tube is the worst at bending angle should not exceed 30° or else no signal were being detected.

Table 5-5 Square aluminium tube normalised response and waveforms

D. Square aluminium tube normalised response

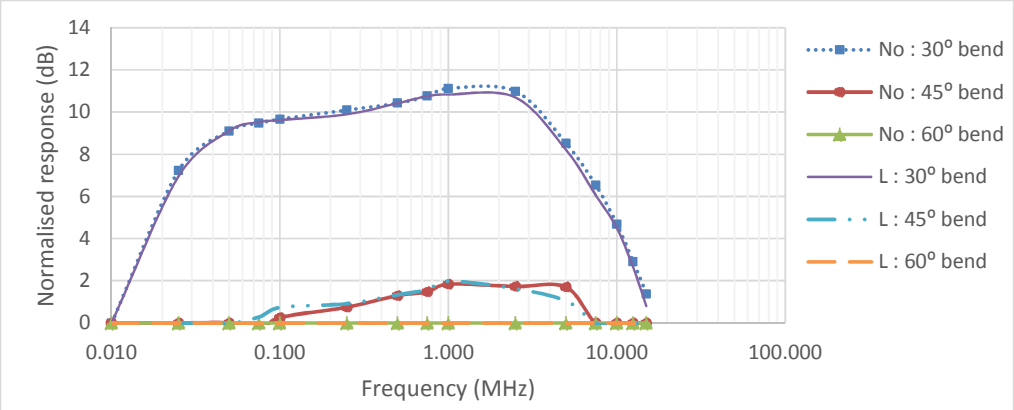

at 30° bend

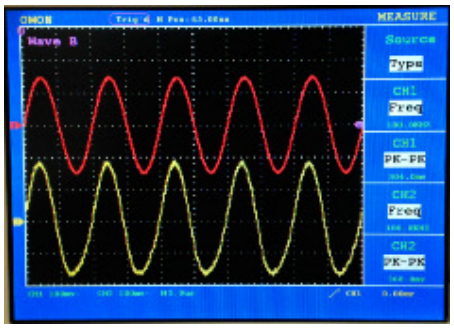

(a) 100 kHz

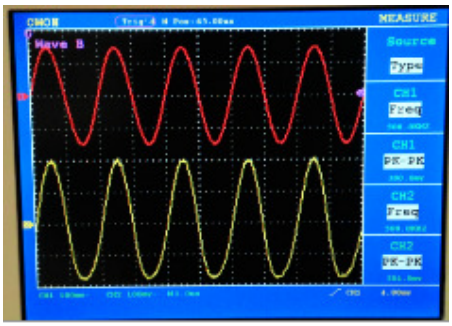

(b) 500 kHz

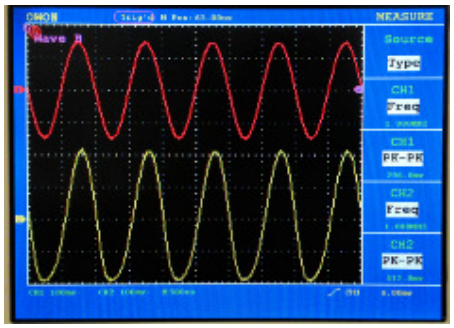

(c) 1 MHz

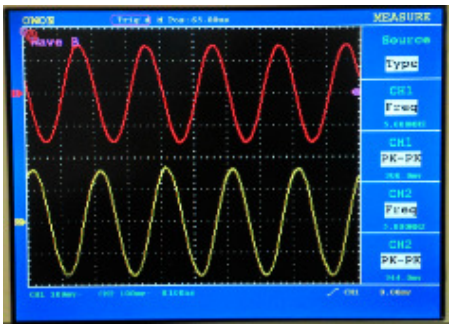

(d) 5 MHz

at 45° bend	
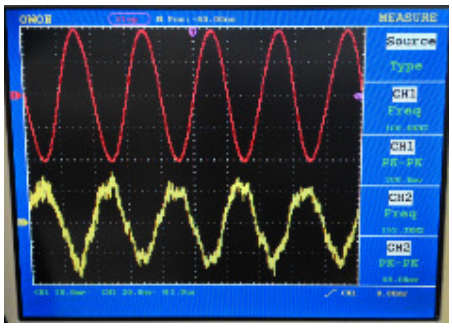	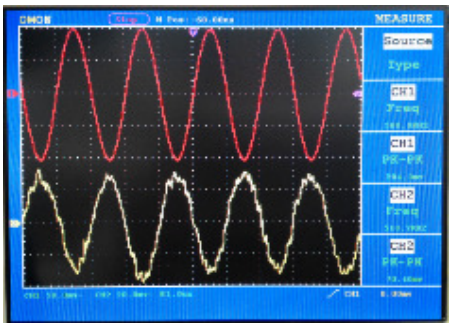
(a) 100 kHz	(b) 500 kHz
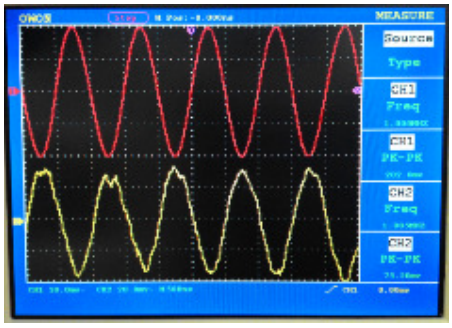	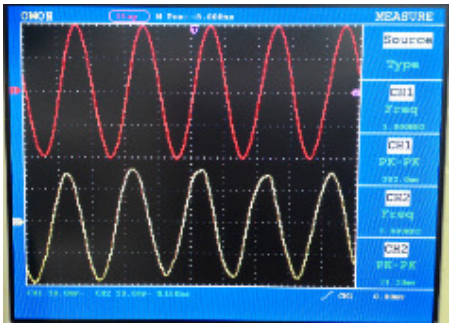
(c) 1 MHz	(d) 5 MHz
at 60° bend	
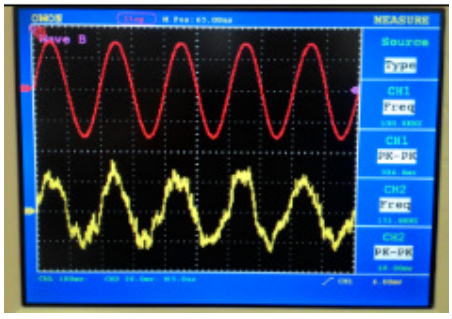	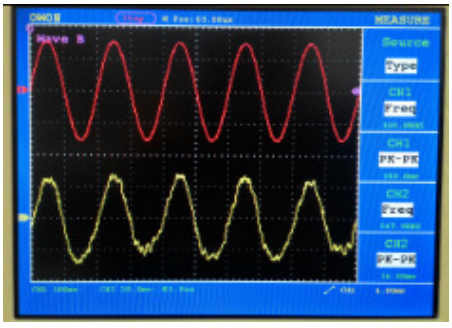
(a) 100 kHz	(b) 500 kHz
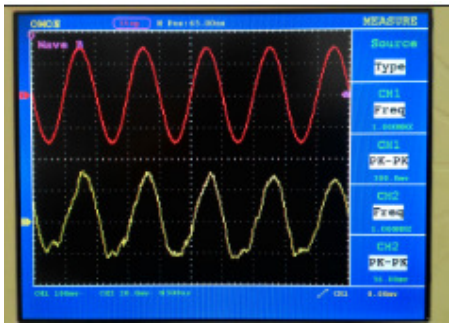	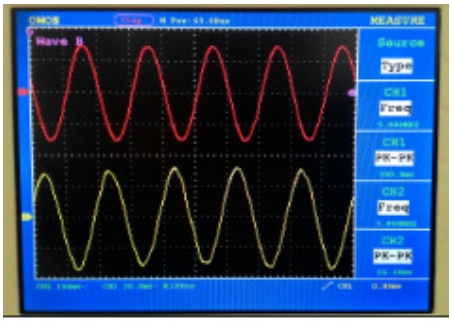
(c) 1 MHz	(d) 5 MHz

Table 5-6 Square aluminium tube normalised response and waveforms

E. Square aluminium normalised response

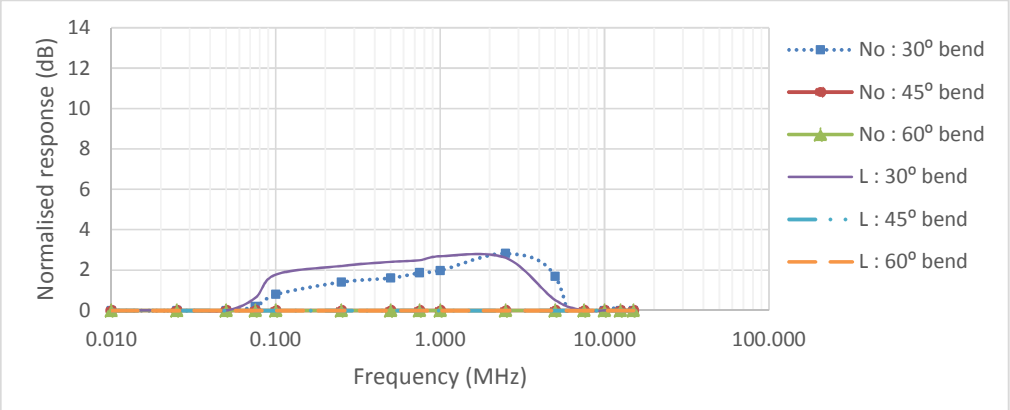

at 30° bend

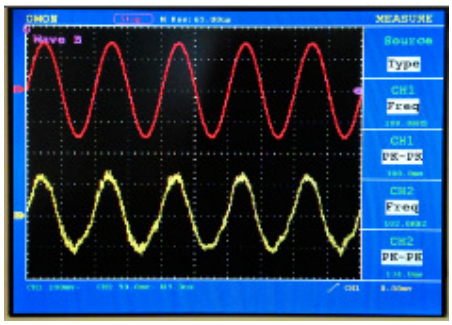

(a) 100 kHz

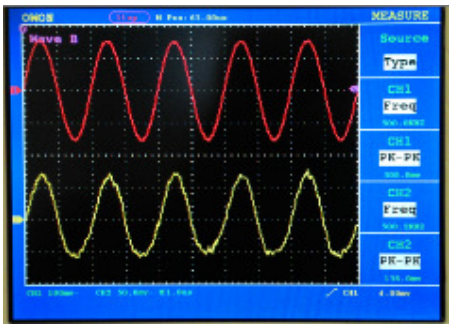

(b) 500 kHz

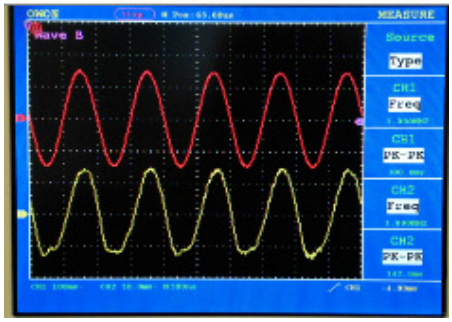

(c) 1 MHz

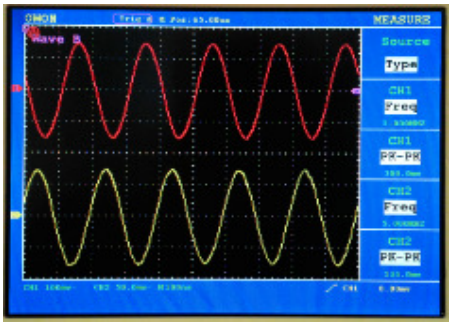

(d) 5 MHz

at 45° bend
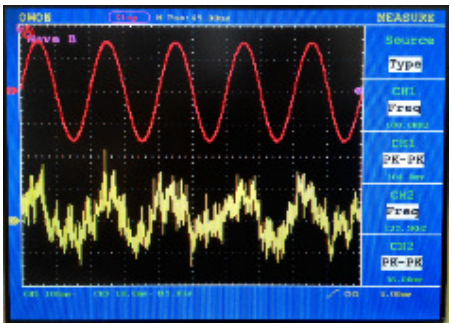
(a) 100 kHz
at 60° bend
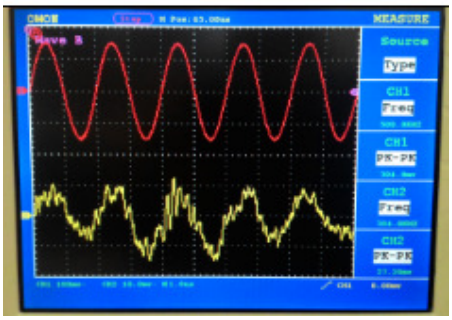
(a) 500 kHz

Table 5-7 Circular aluminium tube normalised response and waveforms

F. Circular aluminium tube normalised response

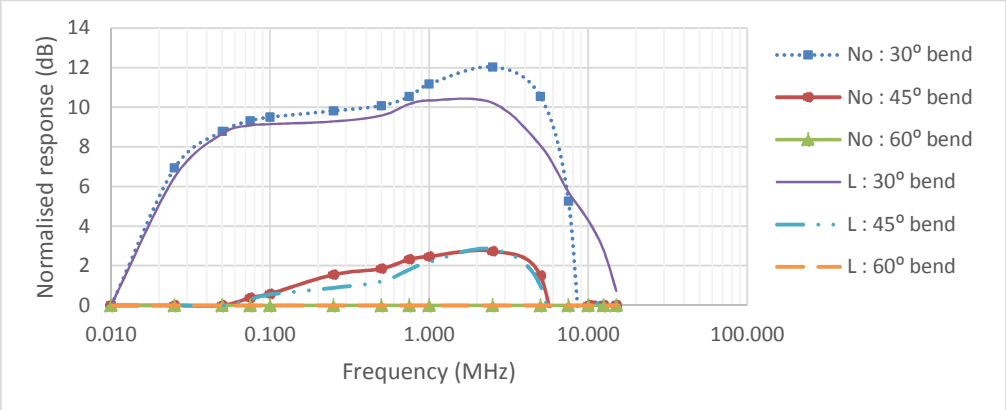

at 30° bend

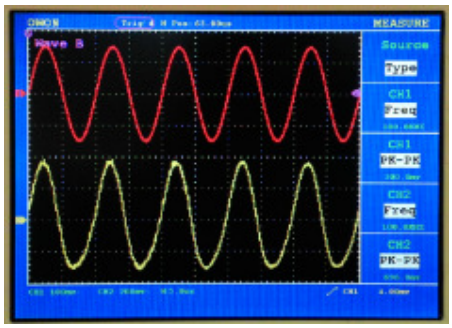

(a) 100 kHz

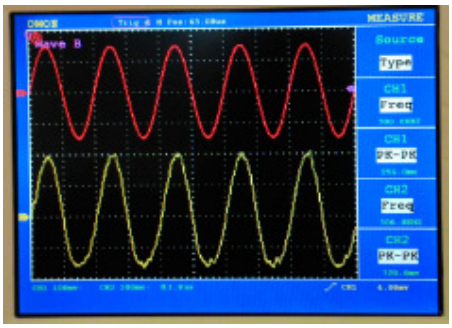

(b) 500 kHz

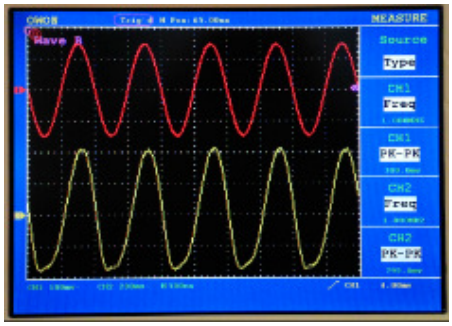

(c) 1 MHz

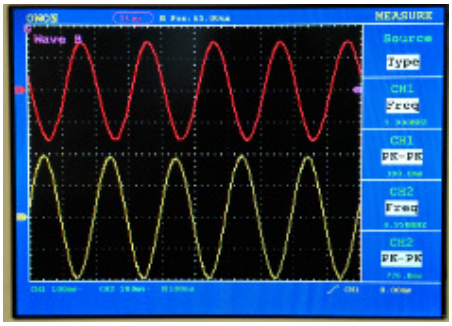

(d) 5 MHz

at 45° bend	
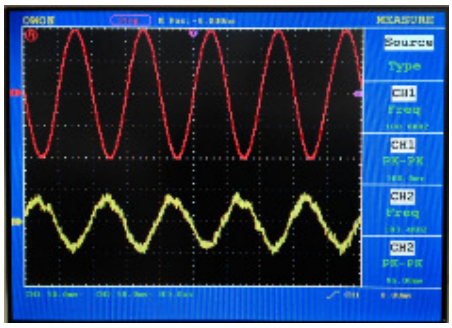	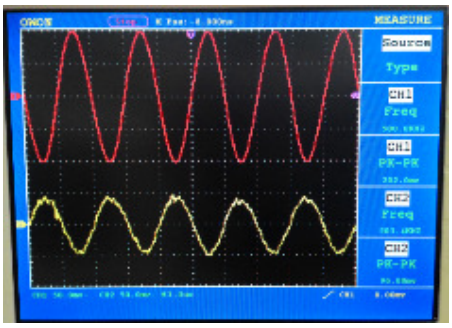
(a) 100 kHz	(b) 500 kHz
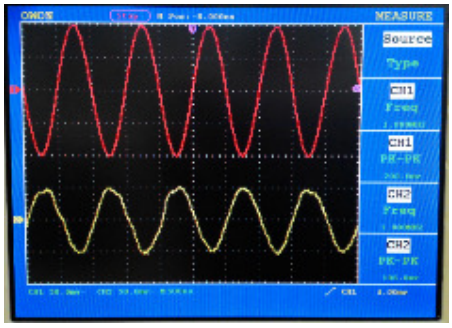	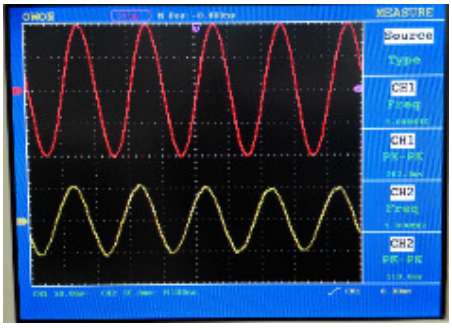
(c) 1 MHz	(d) 5 MHz
at 60° bend	
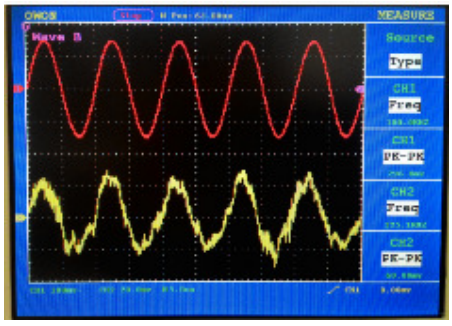	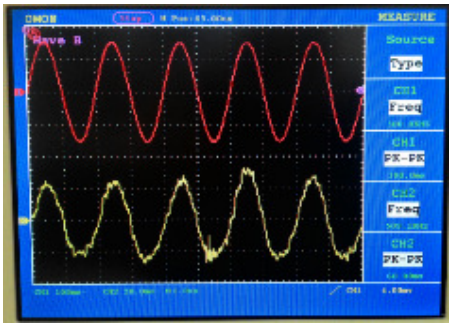
(a) 100 kHz	(b) 500 kHz
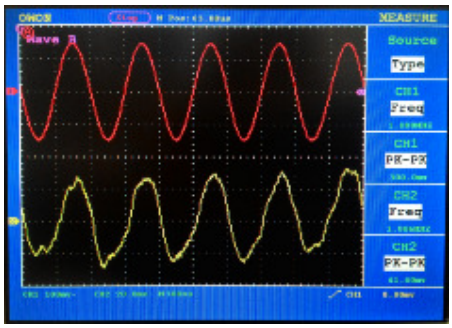	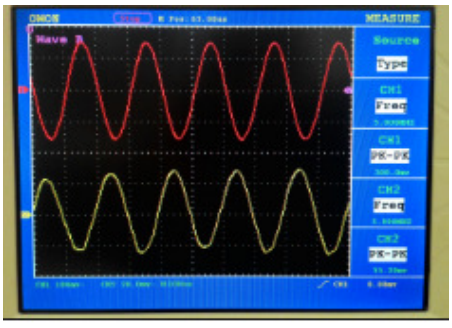
(c) 1 MHz	(d) 5 MHz

Table 5-8 Circular galvanised aluminium normalised response and waveforms

G. Circular galvanised aluminium tube normalised response

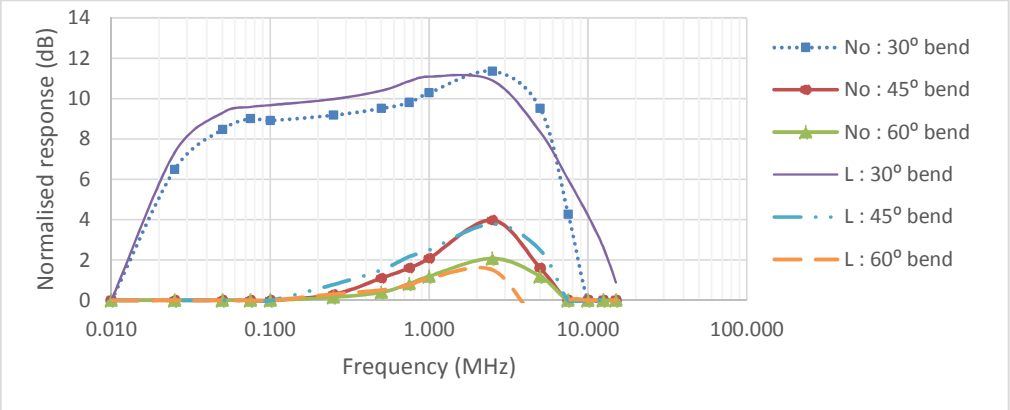

at 30° bend

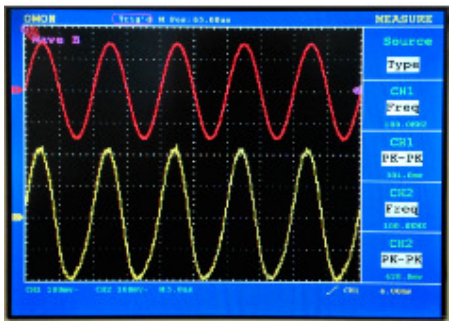

(a) 100 kHz

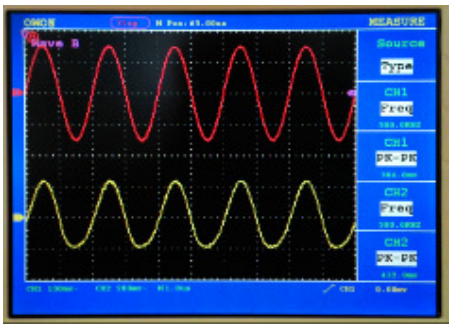

(b) 500 kHz

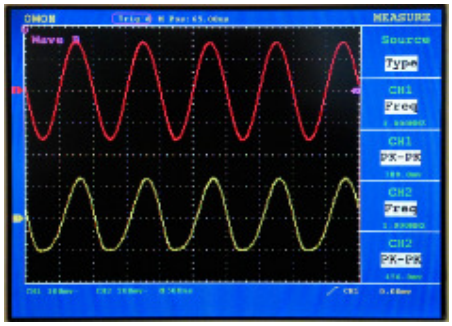

(c) 1 MHz

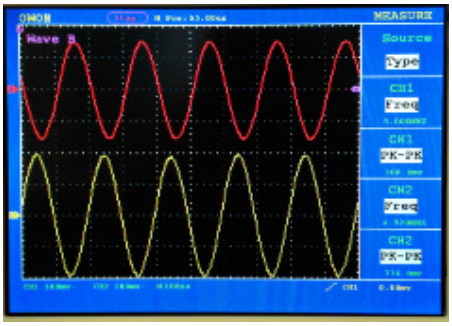

(d) 5 MHz

at 45° bend	
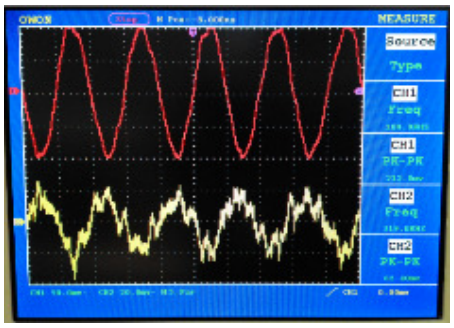	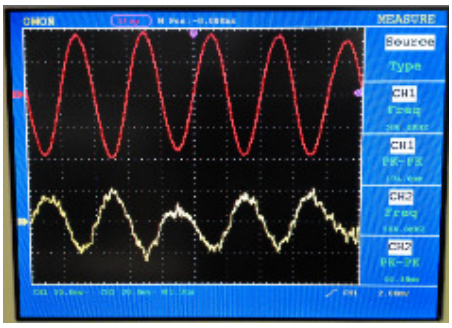
(a) 100 kHz	(b) 500 kHz
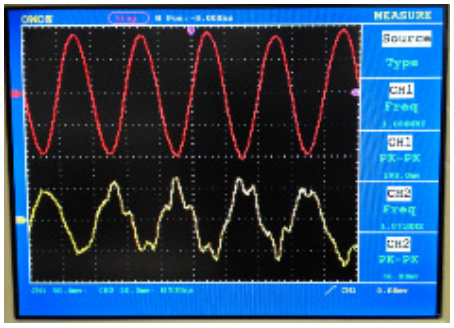	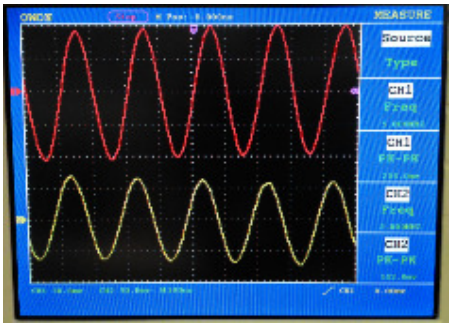
(c) 1 MHz	(d) 5 MHz
at 60° bend	
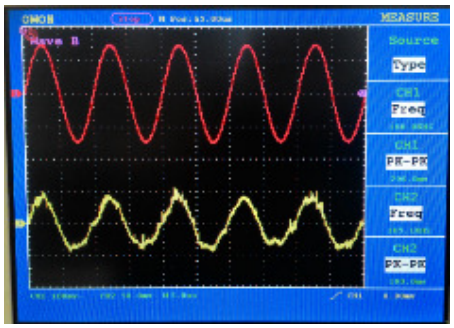	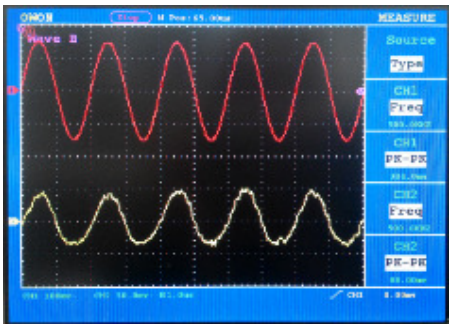
(a) 100 kHz	(b) 500 kHz
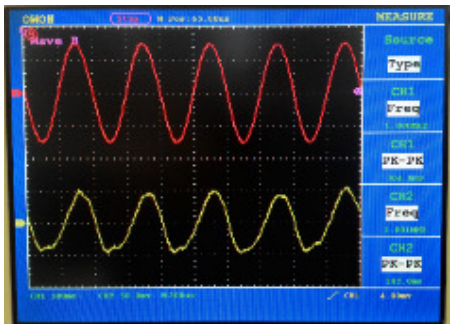	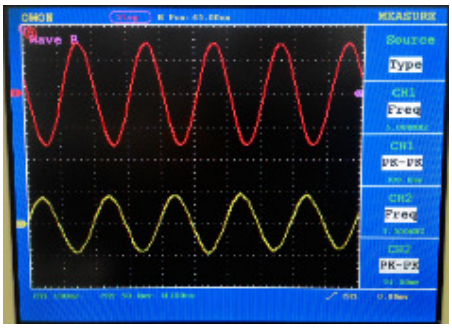
(c) 1 MHz	(d) 5 MHz

5.6.2.3 Optical power received and pass loss

Figure 5-19 tabulates the received optical signal against the number of reflections within the tubes. It is clearly seen that, as the number of reflections increased, the received optical power reduced. The highest optical power received is within the 20 mm circular aluminium tube at 45° bend. The optical power received was at the lowest value within the 60° bend tubes.

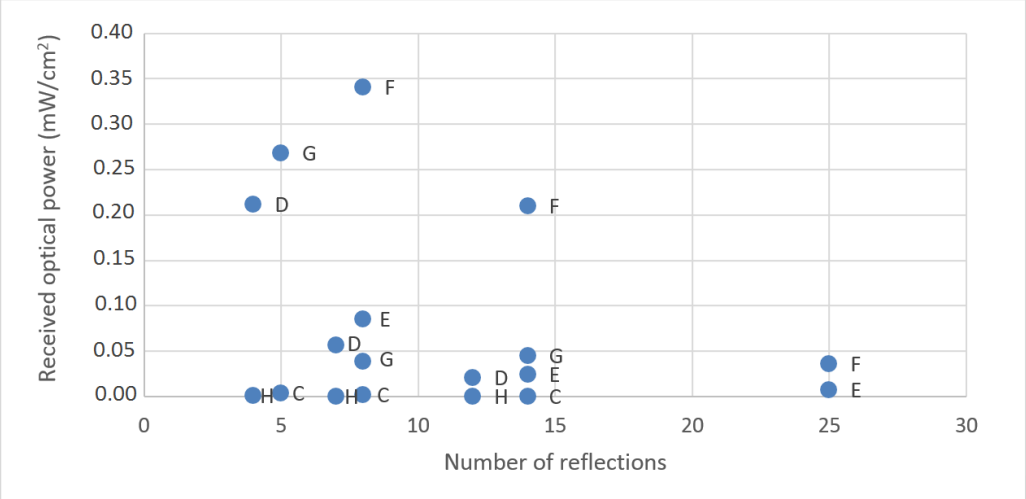

Figure 5-19 Received optical power plotted against number of reflections.

Figure 5-20 and Figure 5-21 tabulate the received optical power at 30°, 40° and 60° bends using the power meter and the photometer respectively. Figure 5-22 and Figure 5-23 plots the path loss at 30°, 40° and 60° bends. The measurement demonstrates that the path loss increases as the transmission angle increases. The lowest path loss is for the 20mm circular aluminium tube, but, unfortunately, the received power is too low. The highest received optical power is the 40mm square aluminium (D), 20mm circular aluminium (F) and 35mm circular galvanised aluminium (G) at almost the same level. Further, the path loss is the lowest in the 20mm circular aluminium (F)

(13.71dB), followed by that in the 35mm circular galvanised aluminium (G) (16.16dB) and 40mm square aluminium (D) (16.64dB) . The path loss increased as the bending angle increased. This proves that the path loss depends not only upon the size and the geometry of the tubes but also upon the reflection coefficient properties, as discussed previously.

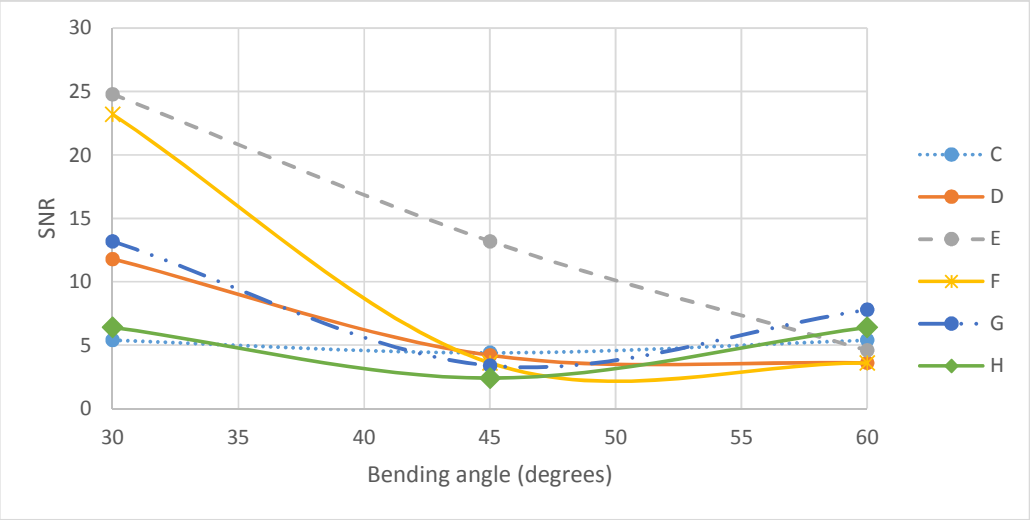

Figure 5-20 Signal to noise ratio (measured using power meter).

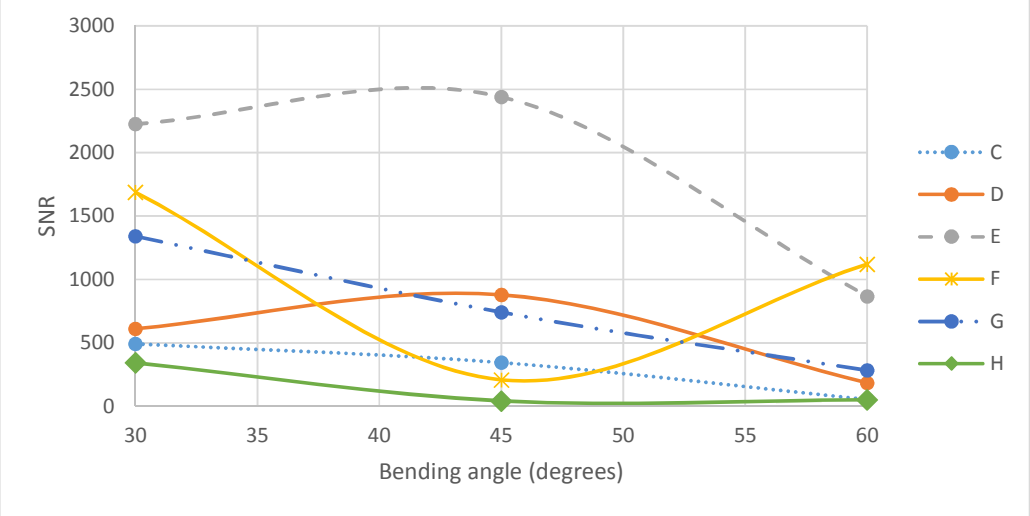

Figure 5-21 Signal to noise ratio (measured using photo meter).

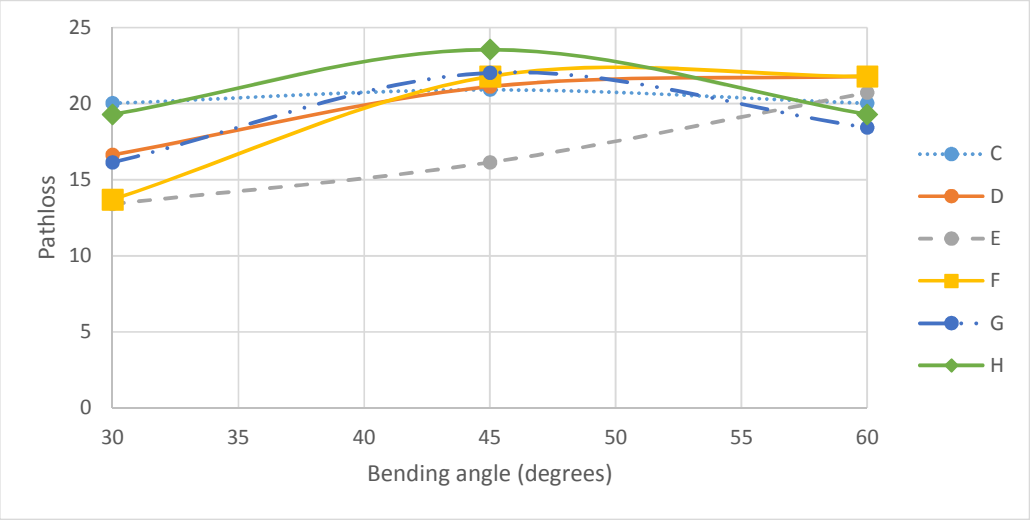

Figure 5-22 Calculated path loss (based on measurement using power meter)

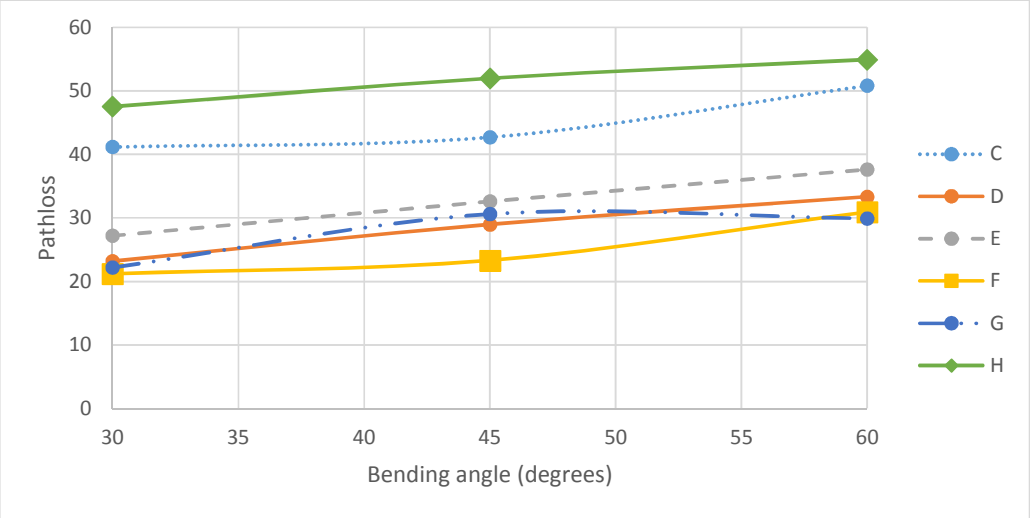

Figure 5-23 Calculated path loss (based on measurement using photo meter)

5.7 Conclusions

This chapter has provided analyses of the channel properties of the NLOS demonstration system concentrating on the transmission angles in straight tubes and bending tubes. The parameters examined in detail included the frequency response, optical power received and the path loss.

The study shows that good transmission is likely to occur within the tubes with transmitter or receiver orientation angle less than 15^{o}. By means of the orientation angle increases, the signal power detected at the receiving end decreases. As expected, the detected signal power is high for 20 mm square aluminium tube and 20 mm circular aluminium tube. This shows that the smaller tube size in addition to high reflection coefficient properties will have lowest path loss. Path loss is higher at 45 ^{o} and 90 ^{o} orientation angles.

For the investigation of bent tubes, high transmit power was required as no signal were being detected at the receiving end using the existing system. Thus, the circuit was modified by adding arrays of 4 IrLEDs in order to improve the transmitter output power. A configuration of 4 IrLEDs was selected as this is the maximum number of IrLEDs that could be fitted inside the smallest tube opening of 20 mm square and circular tubes. This array of IrLEDs produced 54.48 mW or 44.58 mW/cm^2 output power and was sufficient to be detected at the receiving end of bend tubes. The 3 dB cut-off frequency was reduced to 6 MHz, as this is the compromise between the power and bandwidth of the system.

Investigation for the plastic tubes was carried out in 35 mm bent tubes with different lengths and bending angles. Overall performance showed that the transmitted signals were barely detected at the receiving end, as the plastic was not a good reflector.

Moreover, the light rays were diffusely reflected by light coloured objects such as these pipes. At higher frequencies, weak receiving signals could be seen at the receiving end but the noise level was very high, especially for large bending angles. The SNR was extremely low, between 1.52 dB to 3.21 dB

The findings are that the channel is very dynamic, with a great degree of sensitivity to the orientation and degree of rotation of the transmitter and receiver. There is a great variation between the optical received at different transmission angles in straight tubes and bent tubes. The same is true for the frequency responses and path losses in both testing environments. The frequency response reduced drastically as the transmission angle increased and the path loss increased as the bending angle increased.

This chapter has demonstrated that the channel properties do not solely depend on the size and geometry of the tubes, but also the reflection coefficient properties. As the number of reflection increases at larger bending angles, the received power is reduced although the tube diameter is small. Small size tube and small bending angle results in higher detected optical power. But then again, bending angle plays the most important factor in this context. Combining the right tubes geometries with optimised reflection coefficients will boost the optical wireless transmission performance in those tubes.

Chapter 6: Digital System Transmission – a prototype

6.1 Introduction

The main points of interest in optical wireless are the potential of vast transmission capacity due to the unregulated spectrum, the property of the optical wireless network to be restricted to the physical confines of the environment, and its immunity to electromagnetic wave propagation, all of which are well known. These properties are also tremendously valuable to the application of optical wireless within a vehicle, especially as the medium for the transmission of control signals around the vehicle. Furthermore, the benefit of using this technology within the chassis of the vehicle reduces eye safety issues if high power emitters are required.

The work by other researchers in the use of optical wireless within the vehicle is limited to the use in the cabin of the vehicle, and focus on the distribution of entertainment data, which was proposed as early as 1998 [12]. There are no technical developments, or ongoing research developments currently concerning the

transmission of signal in small confined spaces, such as in tubes, being studied by others, as far as can be determined by the author, which motivated the further investigation of the performance of optical wireless in tubes.

In the previous chapters, transmission based on a sinusoidal wave was investigated in LOS and NLOS environments. A generally good performance in an LOS environment is undeniable. In contrast, experiments conducted in an NLOS environment similarly show a reasonable performance of optical wireless communication through metal tubes. A further investigation, based on pulse signal transmission, is required to emulate a real environment.

In general, an optical wireless transmission system is utilized to transmit random messages from a computerized data source to a digital information sink, fundamentally a bit stream, in a reliable and efficient way. This chapter focuses on transmitting a square wave signal, so as to study the system performance in the NLOS environment. Even though this approach may not be the best method to study the performance of a real system, nevertheless, this could be the best way to initiate more studies, based on the results obtained.

As was previously mentioned, this part of the study has concentrated on metal tubes only. In order to explore the possibility of using OW system within a vehicle, the eye pattern of the transmission through each tube has been analysed.

6.2 Methodology

In this chapter, the most straightforward method, (short pulse techniques) were adopted in the measurements, to characterize a real system of diffuse channels. A very short test waveform (pulse) was transmitted to probe a channel directly. A similar

system diagram, as given in Chapter 5 was used in the procedures. The system parameter is as listed:

Input power	:	54.48 mW or 44.58 mW/cm^2
Bandwidth	:	6 MHz
Target BER	:	10^{-4} – 10^{-6}

Although a proper digital transmission setup was not used in the prototype system, the obtained results still can be used to estimate the digital performance of the demonstrator system designed.

A 5V peak-to-peak input signal was generated using a simple 50% duty-cycle oscillator circuit for low frequencies, and a pulse generator for higher frequencies. The resulting eye-diagram was obtained directly at the oscilloscope. The pulse waveform at the input and output of the oscillator are as shown in Figure 6-1.

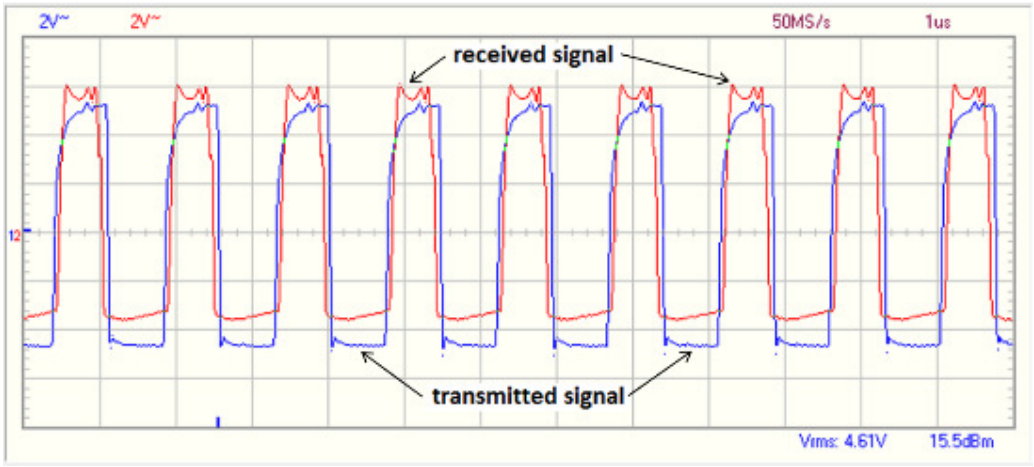

Figure 6-1 Pulse waveform at the oscillator input, and the system output.

It may clearly be seen that a substantial amount of ringing/overshoot at the rising and falling edge of the received signal was present. A few methods were applied to reduce

the overshoot, such as adding a capacitor across the supply rail for improved power suppling decoupling, properly termination of the circuit stages, ensuring that the oscilloscope was in DC-coupled mode, and ensuring that all the components leads were short. Unfortunately, the appearance of the ringing was still significant. The reason why the signal exhibits ringing on the rising and falling edge was undetermined and further analysis need to be done.

When the oscillator circuit was connected to the transmitter, and the output pulses were measured at the receiver, the waveform as in Figure 6-2 was obtained. The overshoot at the falling edge was increased.

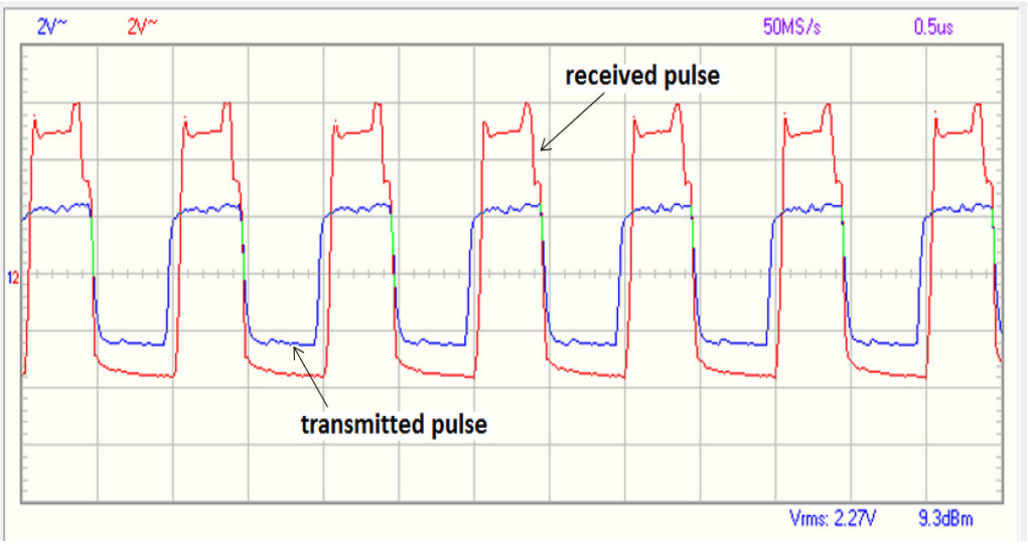

Figure 6-2 Pulse waveform at the receiver output.

As the ringing and overshoot problems were not a major concerned at this stage, the remainder of the experiment was adapted to cope with it. Thus, the duty cycle of the signal will not be the concern from this point forward. The most important parameter to be concentrated on was the eye opening of the received signal.

Table 6-1show the transmitted and received pulse, including the eye diagram at three different frequencies. The measurements were done under free space within back-to-back environment.

At 500 kHz, the input signal is almost a perfect square pulse. The duty cycle of the received signal is 30% and an overshoot occurs at the rising and falling edge of the received signal. The overshoot at the falling edge is more obvious compared to the rising edge with 1.13V high measured from the top flat line. An eye high of 7.26V was measured for the eye pattern. At 1 MHz, the input signal exhibit ringing and the duty cycle of the received signal at 1 MHz is about 41.4%. 1.13V overshoot was measured at the falling edge. The eye opening measured was 7.38V. At 5 MHz, the transmitted and received signals are unable to be measured. Further, the eye diagram was completely closed.

Table 6-1 Transmitted and received pulse with eye pattern at different frequency

Transmitted and received pulse	Eye pattern
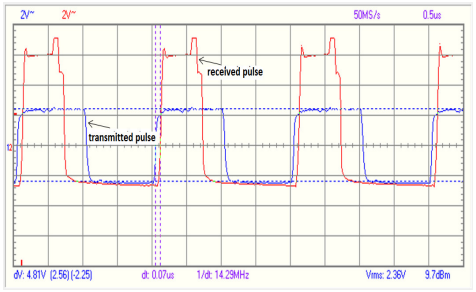	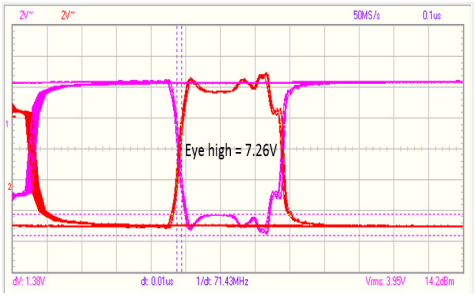

(a) Test waveform at 500 kHz

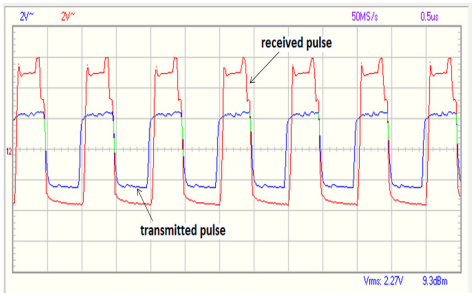	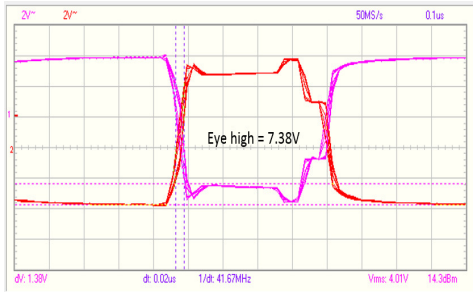

(b) Test waveform at 1 MHz

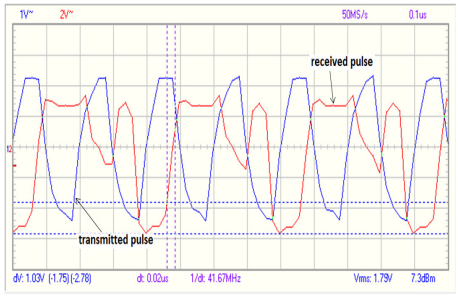	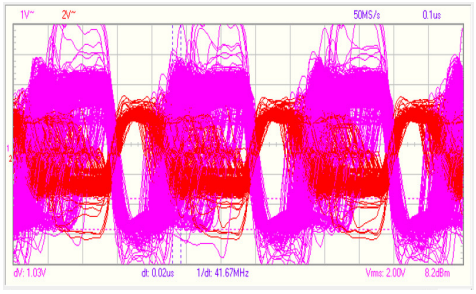

(c) Test waveform at 5 MHz

6.3 Eye pattern

The eye diagram is the most suitable method used for assessing the data transmitting and receiving capabilities. The eye diagrams were obtained from an oscilloscope by superimposing the pulses on top of each other. An eye pattern shows a relative performance of the detected signal. In an eye diagram determination, the clarity of a preferred process between a logical "0" and "1" is resolved as the "openness" of the eye. Generally, a clear and open eye was observed, demonstrating the ability of the receiver to detect a logical "0" and "1" correctly.

The free space transmission measurements were done prior to the experiment through the metal tubes. The measurement were done at back-to-back and at 1 metre distances.

Table 6-2 and Table 6-3 shows the transmitted and received test waveforms, as well as the eye diagram for free space transmission. For 500 kHz and 1 MHz frequencies, the eye diagram is clear as expected at both distances. Unfortunately, for 5 MHz frequency, the eye diagram is completely closed.

The overshoot as explain in Section 6.2, are clearly present at the falling edge of the back-to-back received pulses. The disturbances were also clearly seen on the eye diagram. The overshoot could not be detected at longer distance, but as the distance increased, the duty-cycle worsened.

Table 6-2 Free space transmission: back-to-back - transmitted and received pulse with eye pattern at different frequency

Transmitted and received pulse	Eye pattern
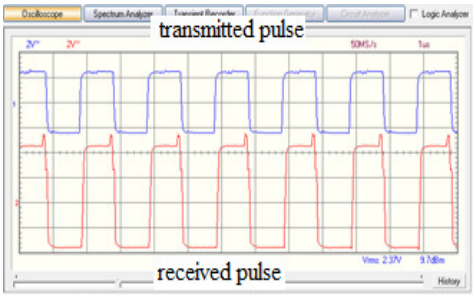	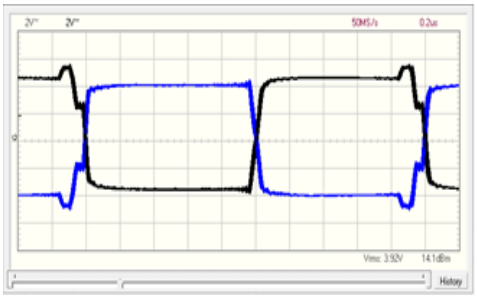

(a) Test waveform at 500 kHz

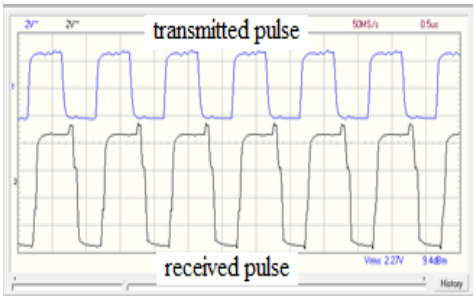	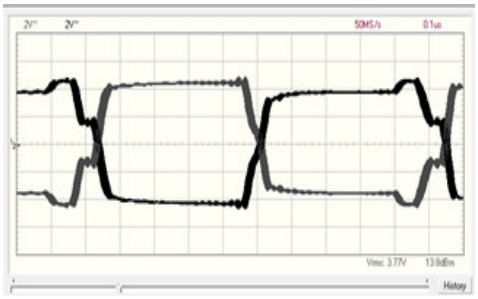

(b) Test waveform at 1 MHz

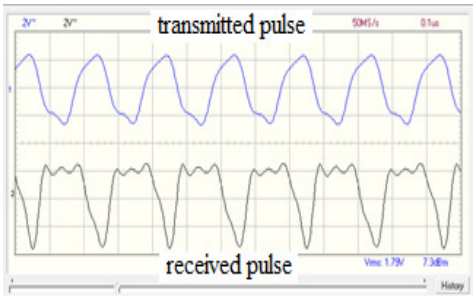	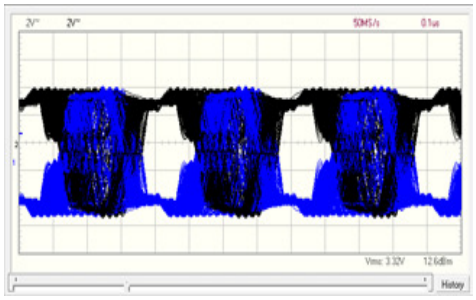

(c) Test waveform at 5 MHz

Table 6-3 Free space transmission: 1 metre distance - transmitted and received pulse with eye pattern at different frequency

Transmitted and received pulse	Eye pattern
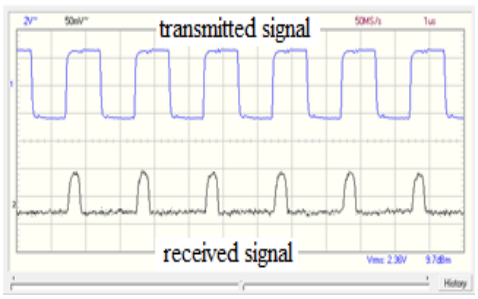	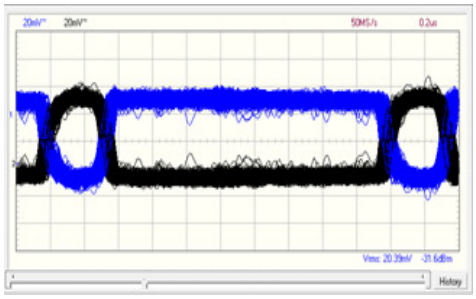

(a) Test waveform at 500 kHz

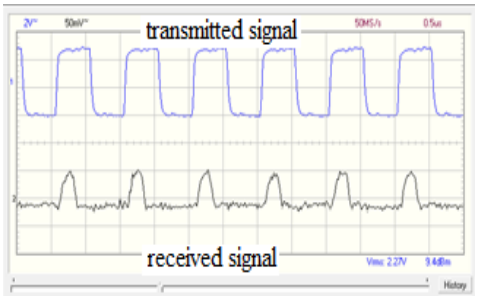	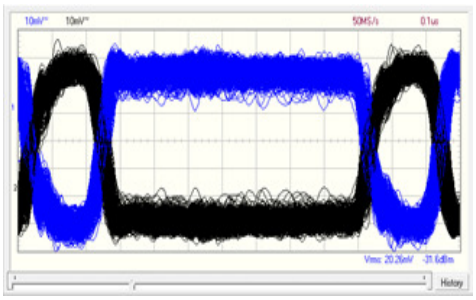

(b) Test waveform at 1 MHz

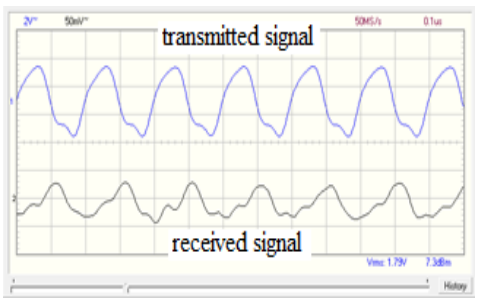	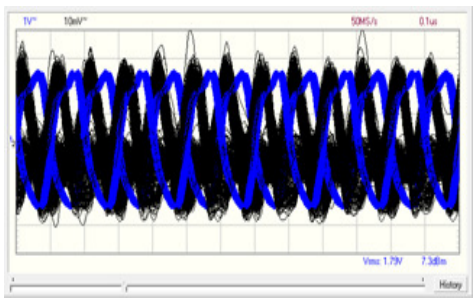

(c) Test waveform at 5 MHz

The eye diagram of the test waveform through different materials at different bending angles is shown in Table 6-4 through to Table 6-21. It clearly seen that the transmission in the circular and square mild steel tube (C and H respectively) is very impractical as the eye pattern are completely closed. There is no detectable signal observable at the receiving end, and thus no possibility for an eye diagram to be present for all test conditions. Thus, this system is totally unusable as it is impossible to recover data.

Transmission through a 20 mm square aluminium tube (E) was good at a 30° bend, but the received signal degraded as the bending angle increased. For a 45° bend, the noise was proportionally greater, but the eye remained open. The eye diagram for a 60° bend was considered to be completely closed.

Overall, a clear and wide opening of eye width for 500 kHz and 1 MHz pulse signals shows the possibility of error-free transmission of data for 40 mm square aluminium tube, 20 mm circular aluminium tune and 35 mm circular galvanised aluminium tube. For the 5 MHz pulse signal, the eye is almost closed. This reveals that the received signal for the high-frequency case is not acceptable with the system as designed. Transmission at a higher frequency reduces the signal quality, and any enhancement techniques would have to be considered to overcome for this effect.

Based on this finding, the remainder of the investigation will only focuses on 40 mm square aluminium tube, 20 mm circular aluminium tube and 35 mm circular galvanised aluminium tube, concentrated on the SNR, Q-factor and BER.

Table 6-4 Transmission within 35mm circular mild steel tube at 30° bend - transmitted and received pulse with eye pattern at different frequency

Transmitted and received pulse	Eye pattern
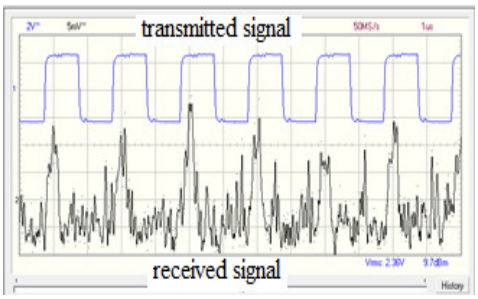	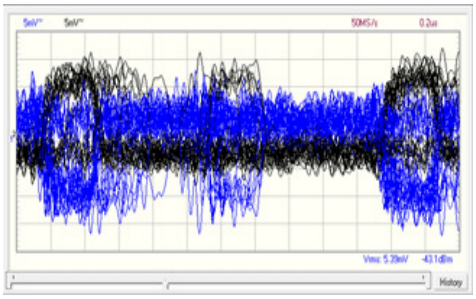

(a) Test waveform at 500 kHz

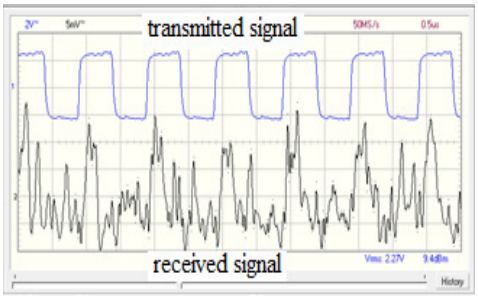	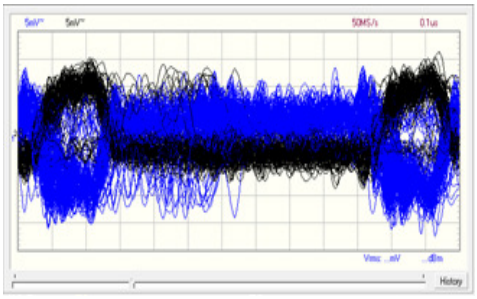

(b) Test waveform at 1 MHz

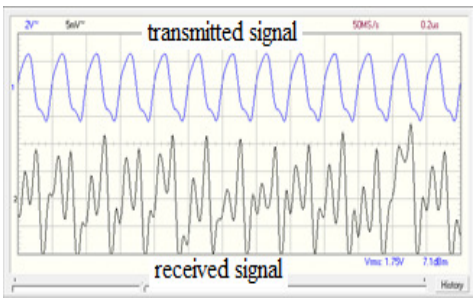	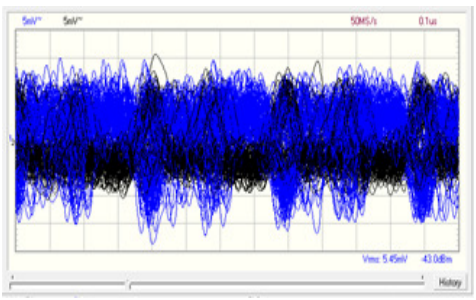

(c) Test waveform at 5 MHz

Table 6-5 Transmission within 35mm circular mild steel tube at 45° bend - transmitted and received pulse with eye pattern at different frequency

Transmitted and received pulse	Eye pattern
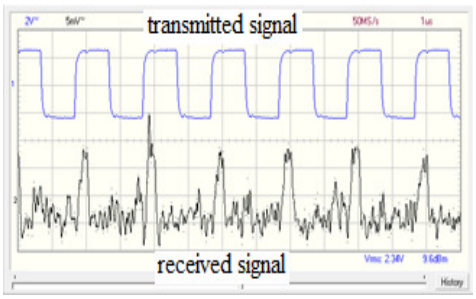	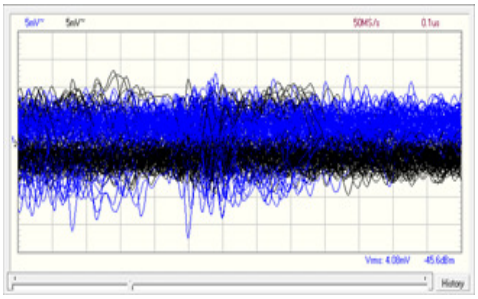

(a) Test waveform at 500 kHz

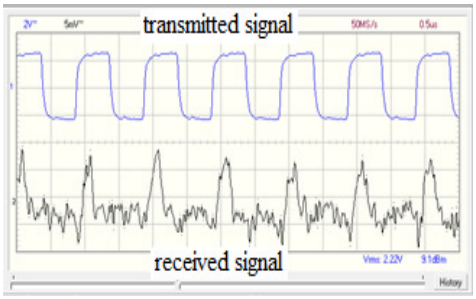	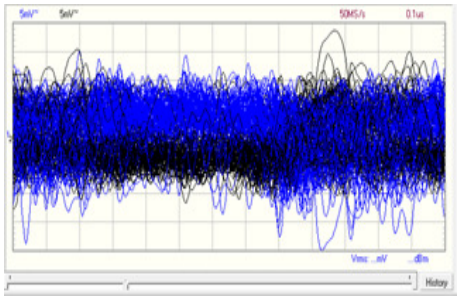

(b) Test waveform at 1 MHz

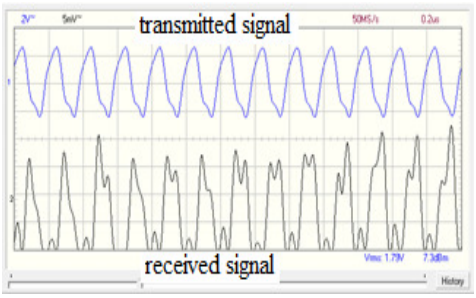	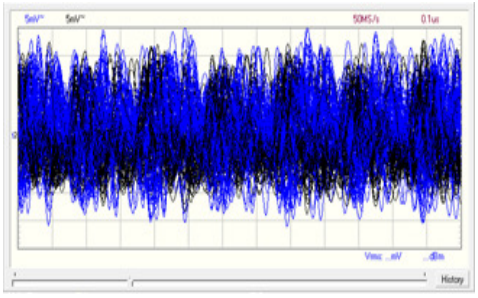

(c) Test waveform at 5 MHz

Table 6-6 Transmission within 35mm circular mild steel tube at 60° bend - transmitted and received pulse with eye pattern at different frequency

Transmitted and received pulse	Eye pattern
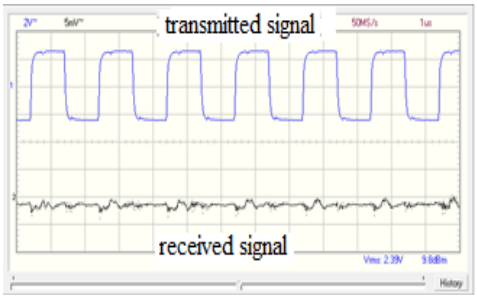	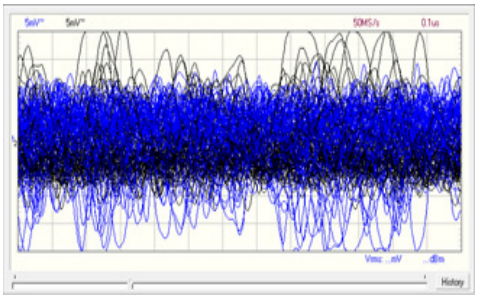

(a) Test waveform at 500 kHz

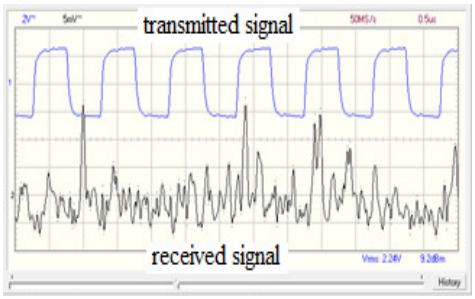	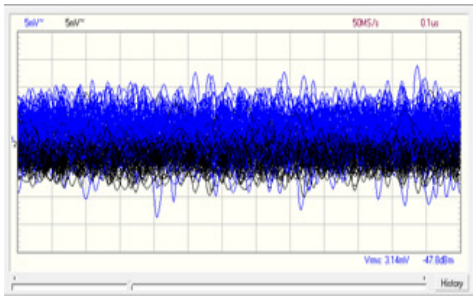

(b) Test waveform at 1 MHz

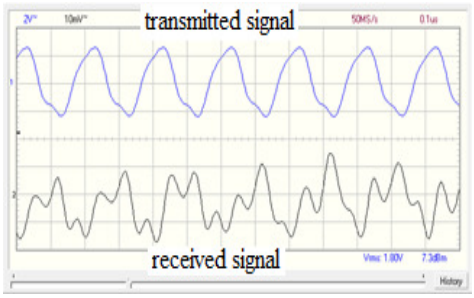	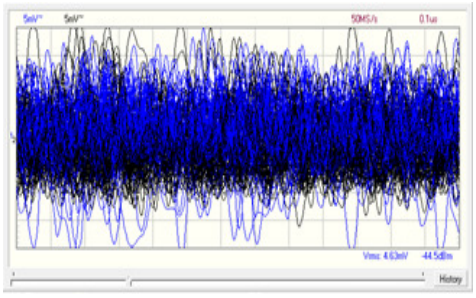

(c) Test waveform at 5 MHz

Table 6-7 Transmission within 40 mm square aluminium tube at 30° bend - transmitted and received pulse with eye pattern at different frequency

Transmitted and received pulse	Eye pattern
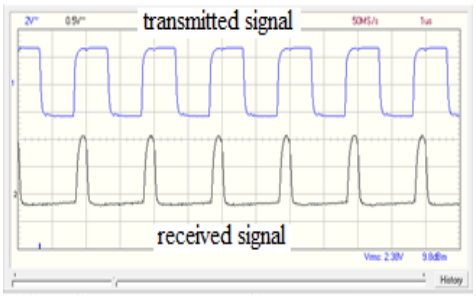	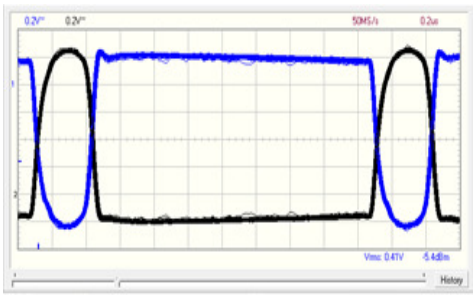

(a) Test waveform at 500 kHz

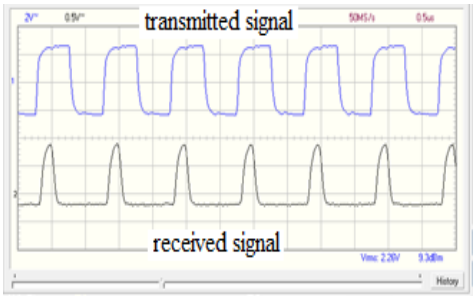	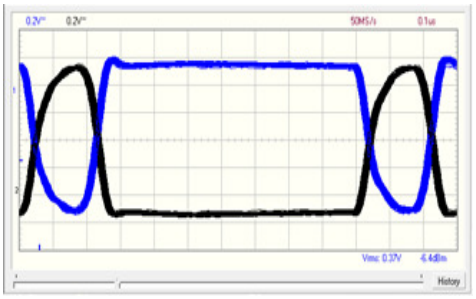

(b) Test waveform at 1 MHz

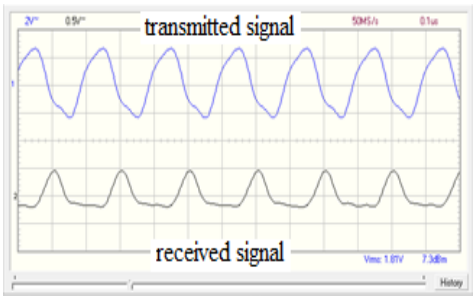	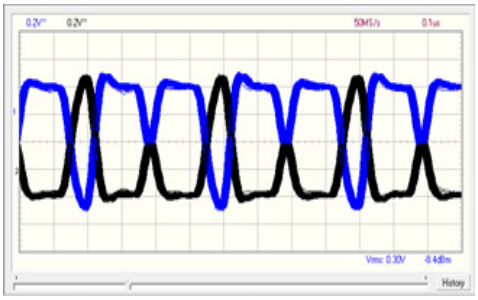

(c) Test waveform at 5 MHz

Table 6-8 Transmission within 40 mm square aluminium tube at 45° bend - transmitted and received pulse with eye pattern at different frequency

Transmitted and received pulse	Eye pattern
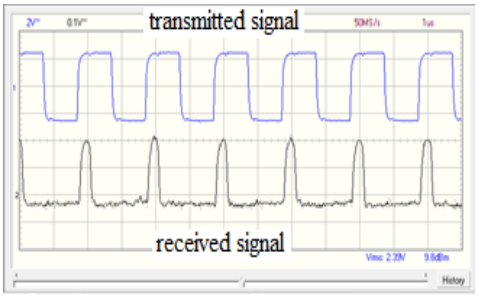	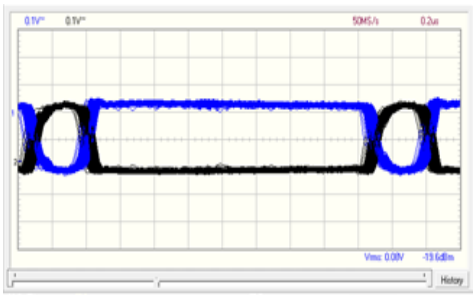

(a) Test waveform at 500 kHz

	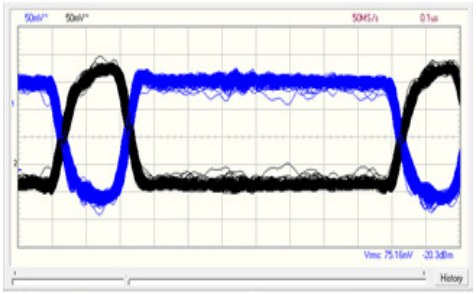

(b) Test waveform at 1 MHz

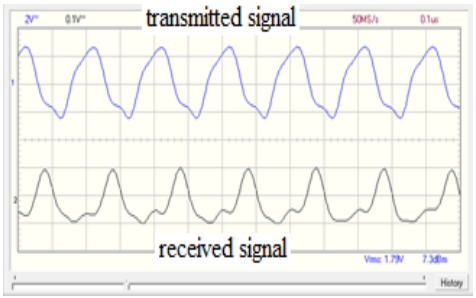	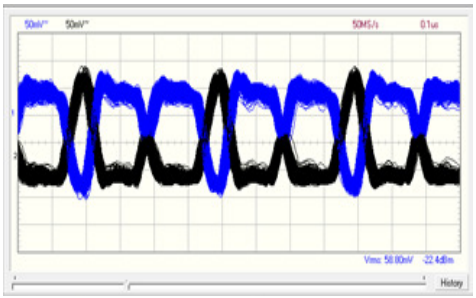

(c) Test waveform at 5 MHz

Table 6-9 Transmission within 40 mm square aluminium tube at 60° bend - transmitted and received pulse with eye pattern at different frequency

Transmitted and received pulse	Eye pattern
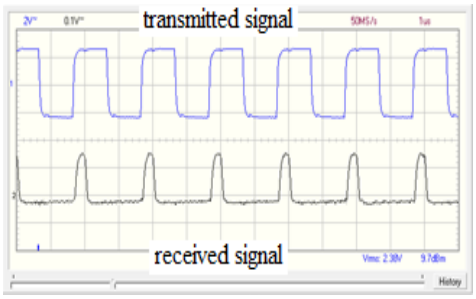	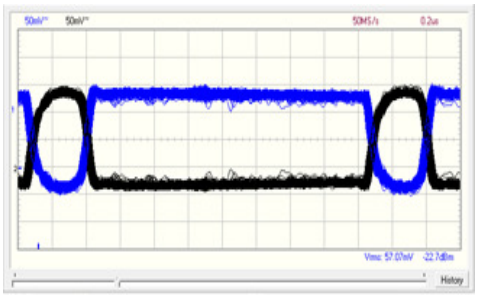

(a) Test waveform at 500 kHz

	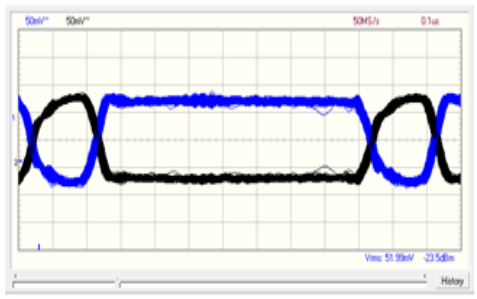

(b) Test waveform at 1 MHz

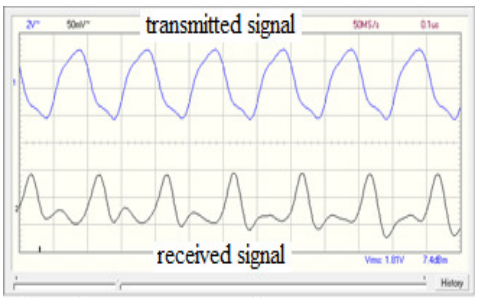	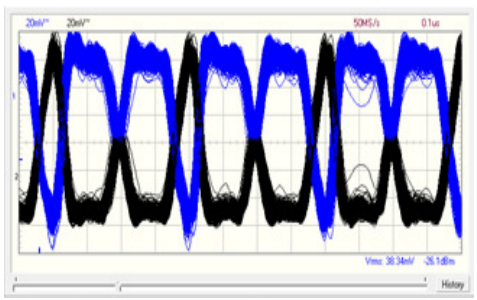

(c) Test waveform at 5 MHz

Table 6-10 Transmission within 20 mm square aluminium tube at 30° bend - transmitted and received pulse with eye pattern at different frequency

Transmitted and received pulse	Eye pattern
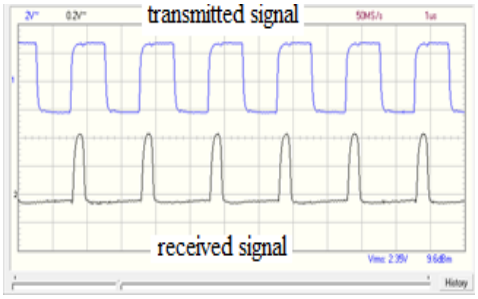	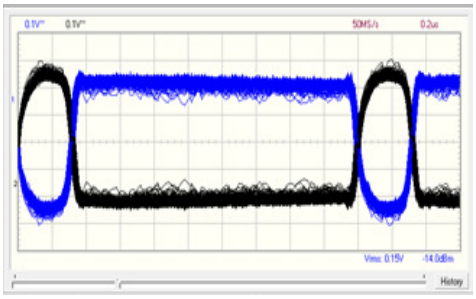

(a) Test waveform at 500 kHz

	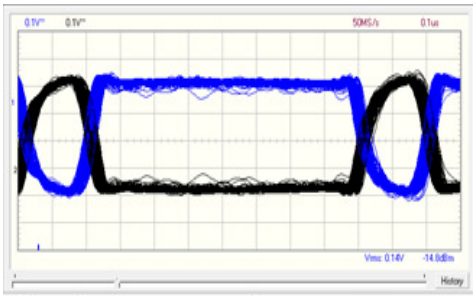

(b) Test waveform at 1 MHz

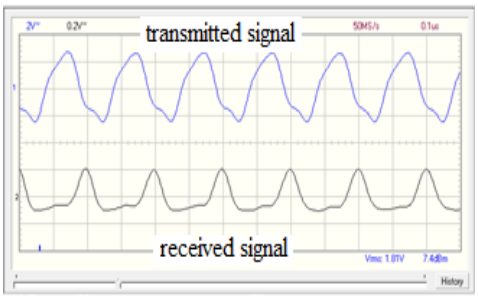	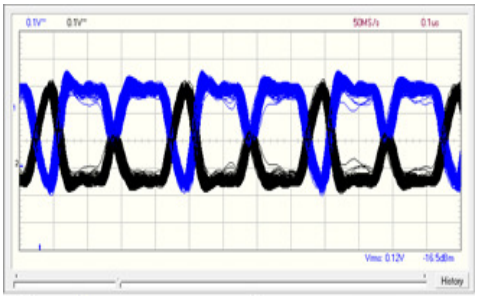

(c) Test waveform at 5 MHz

Table 6-11 Transmission within 20 mm square aluminium tube at 45° bend - transmitted and received pulse with eye pattern at different frequency

Transmitted and received pulse	Eye pattern
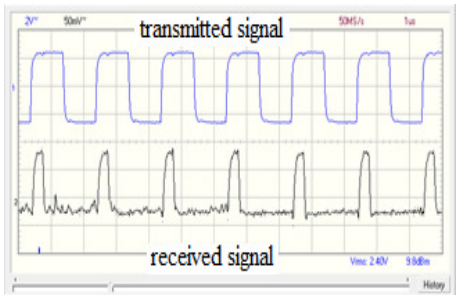	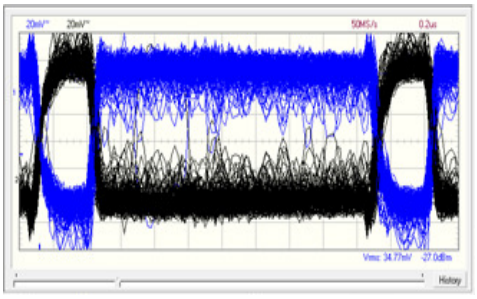

(a) Test waveform at 500 kHz

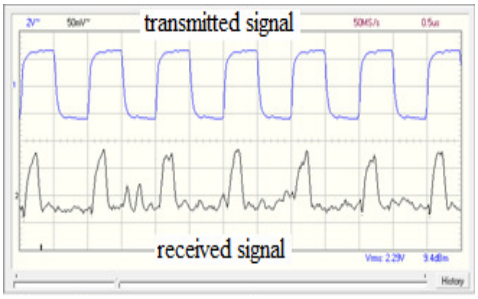	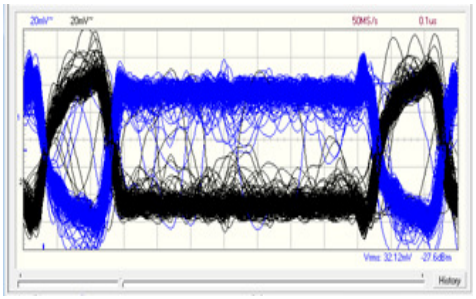

(b) Test waveform at 1 MHz

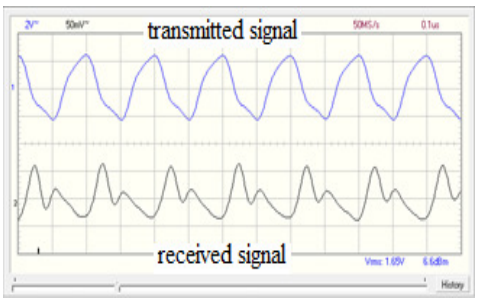	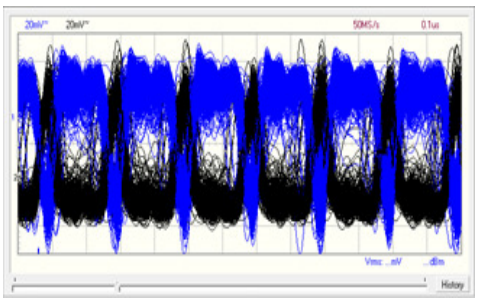

(c) Test waveform at 5 MHz

Table 6-12 Transmission within 20 mm square aluminium tube at 60° bend - transmitted and received pulse with eye pattern at different frequency

Transmitted and received pulse	Eye pattern
	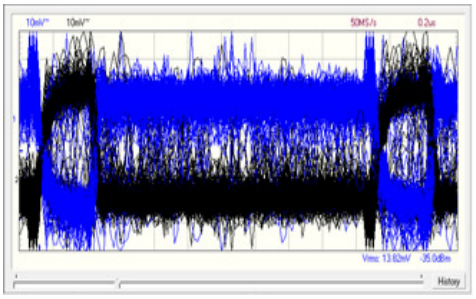

(a) Test waveform at 500 kHz

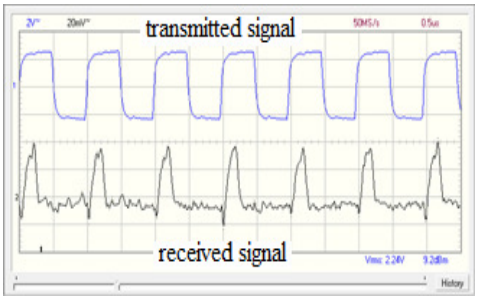	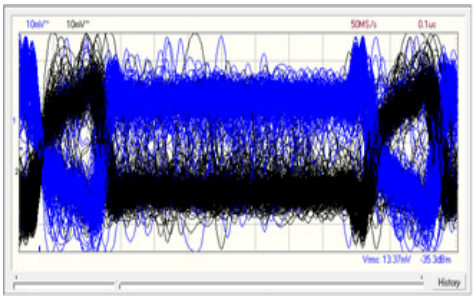

(b) Test waveform at 1 MHz

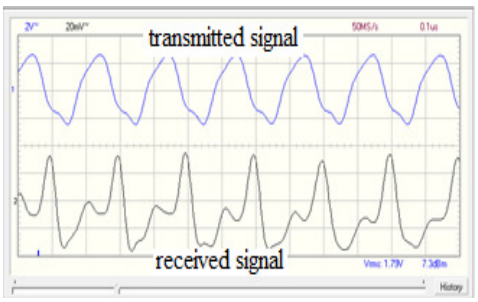	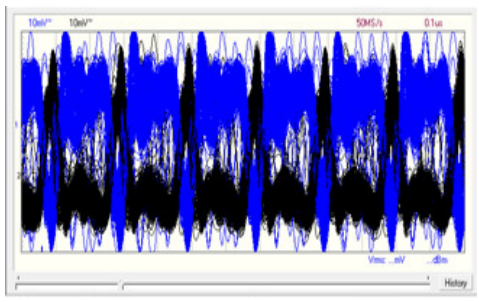

(c) Test waveform at 5 MHz

Table 6-13 Transmission within 20 mm circular aluminium tube at 30° bend - transmitted and received pulse with eye pattern at different frequency

Transmitted and received pulse	Eye pattern
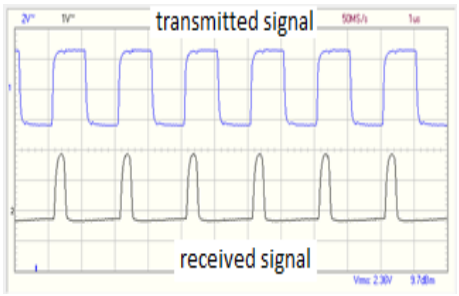	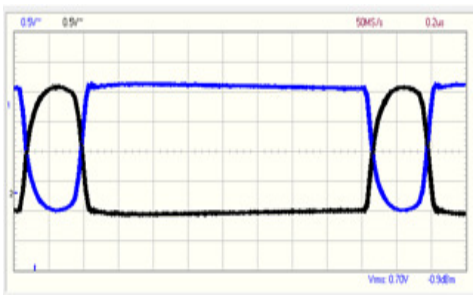

(a) Test waveform at 500 kHz

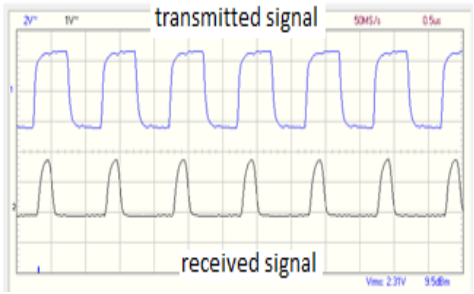	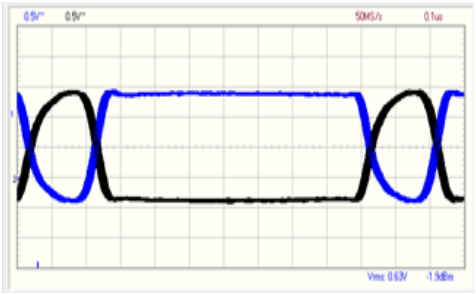

(b) Test waveform at 1 MHz

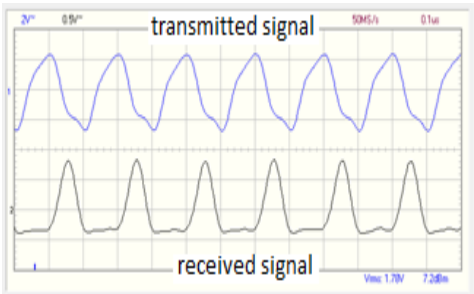	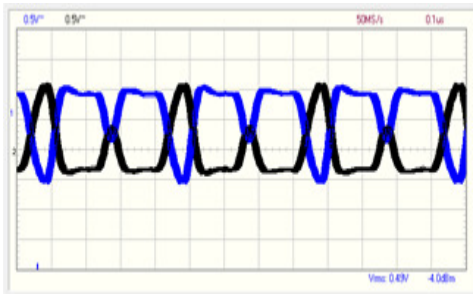

(c) Test waveform at 5 MHz

Table 6-14 Transmission within 20 mm circular aluminium tube at 45° bend - transmitted and received pulse with eye pattern at different frequency

Transmitted and received pulse	Eye pattern
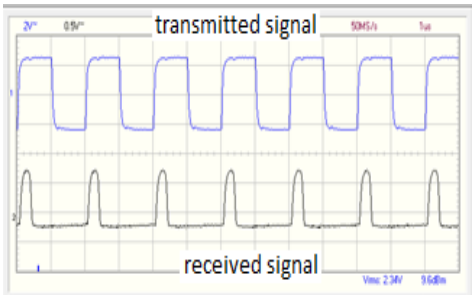	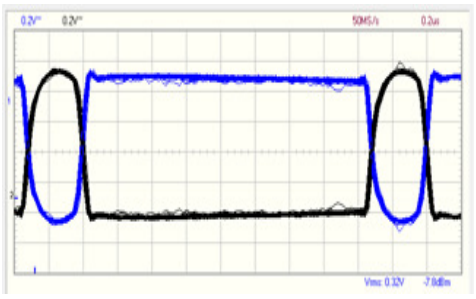

(a) Test waveform at 500 kHz

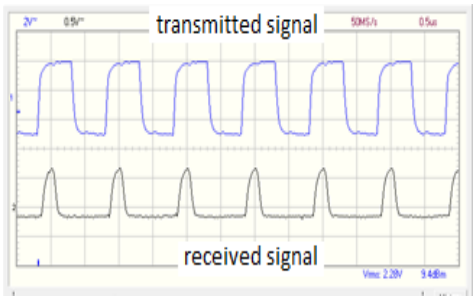	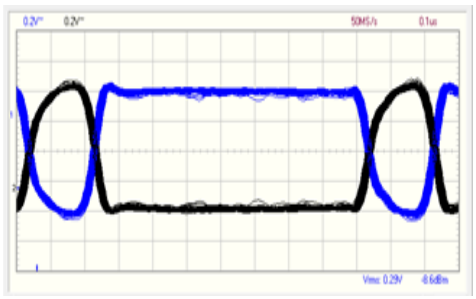

(b) Test waveform at 1 MHz

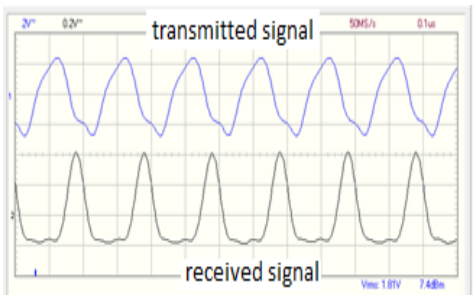	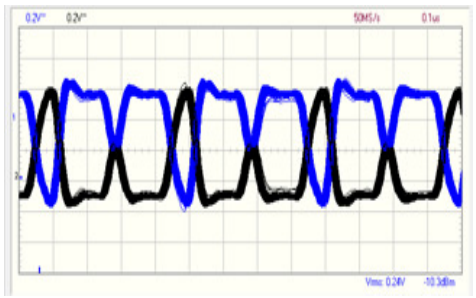

(c) Test waveform at 5 MHz

Table 6-15 Transmission within 20 mm circular aluminium tube at 60° bend - transmitted and received pulse with eye pattern at different frequency

Transmitted and received pulse	Eye pattern
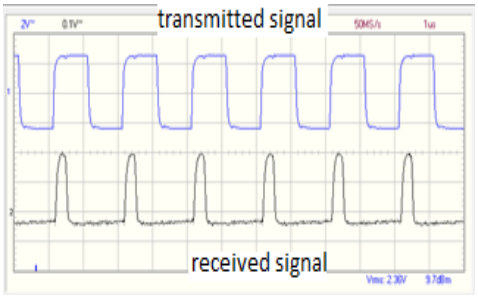	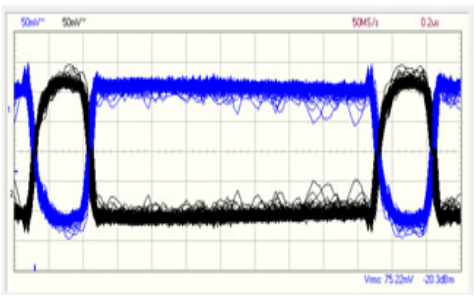

(a) Test waveform at 500 kHz

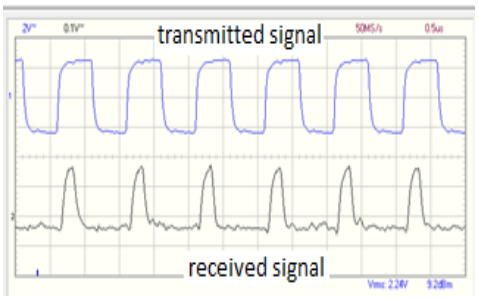	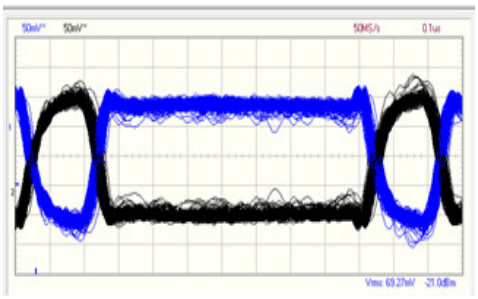

(b) Test waveform at 1 MHz

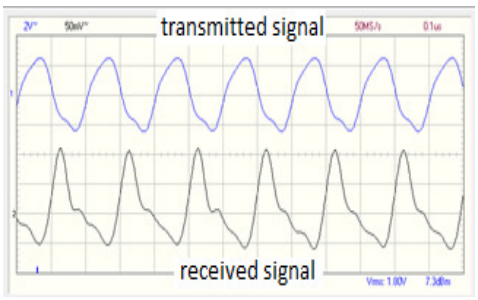	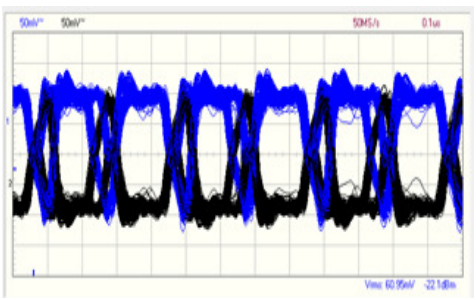

(c) Test waveform at 5 MHz

Table 6-16 Transmission within 35 mm circular galvanised aluminium tube

at 30° bend - transmitted and received pulse with eye pattern at different frequency

Transmitted and received pulse	Eye pattern
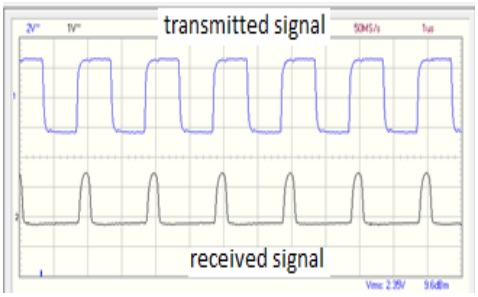	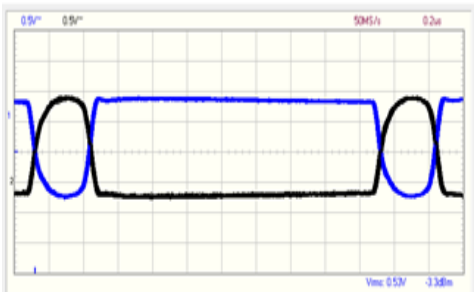

(a) Test waveform at 500 kHz

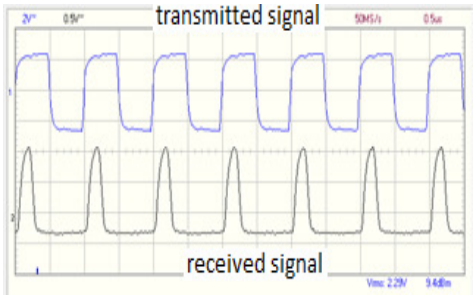	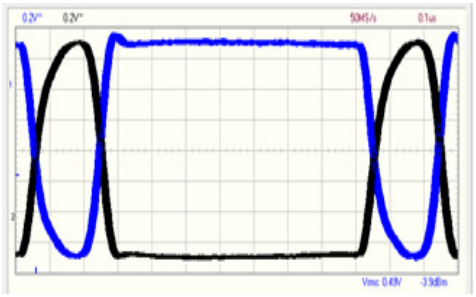

(b) Test waveform at 1 MHz

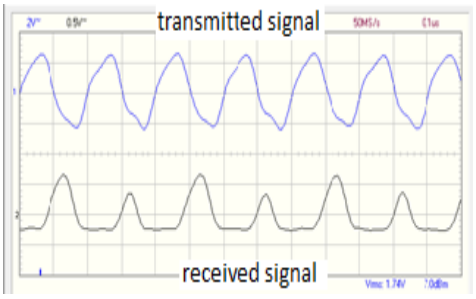	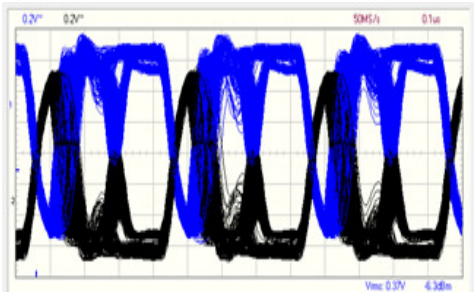

(c) Test waveform at 5 MHz

Table 6-17 Transmission within 35 mm circular galvanised aluminium tube

at 45° bend - transmitted and received pulse with eye pattern at different frequency

Transmitted and received pulse	Eye pattern
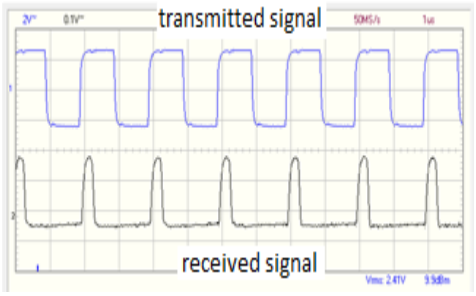	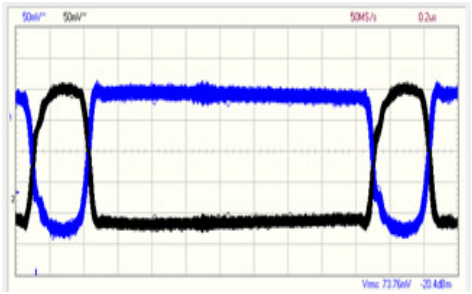

(a) Test waveform at 500 kHz

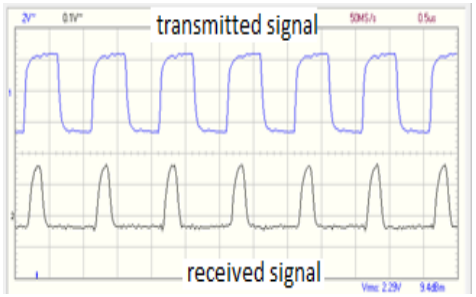	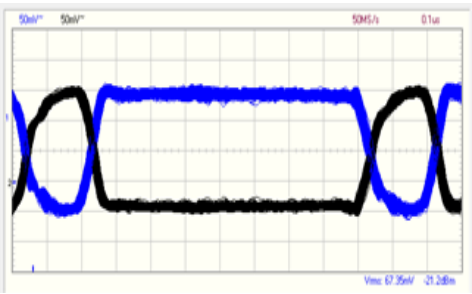

(b) Test waveform at 1 MHz

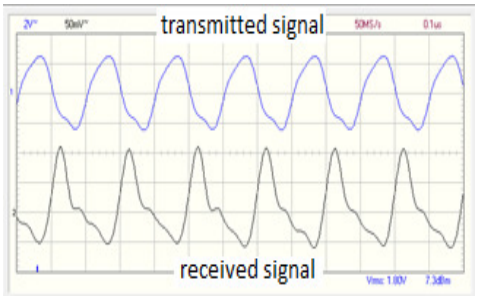	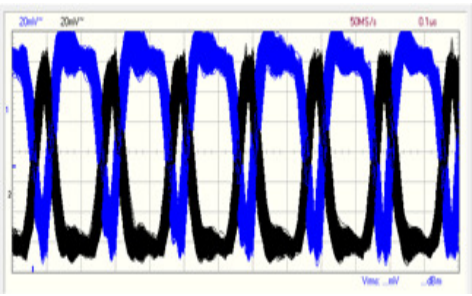

(c) Test waveform at 5 MHz

Table 6-18 Transmission within 35 mm circular galvanised aluminium tube

at 60° bend - transmitted and received pulse with eye pattern at different frequency

Transmitted and received pulse	Eye pattern
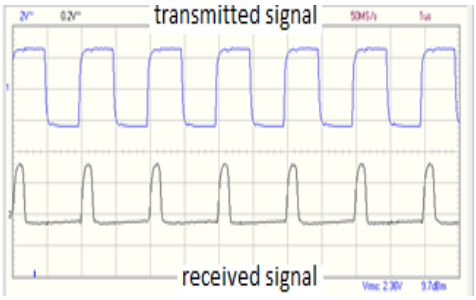	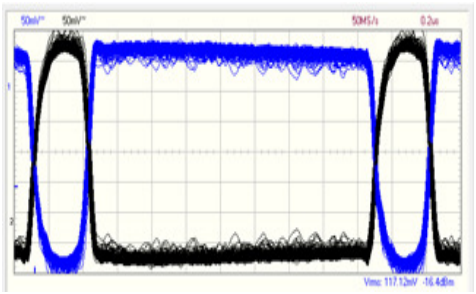

(a) Test waveform at 500 kHz

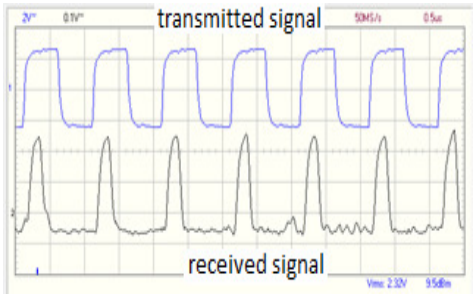	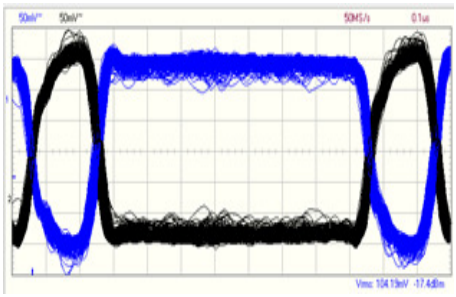

(b) Test waveform at 1 MHz

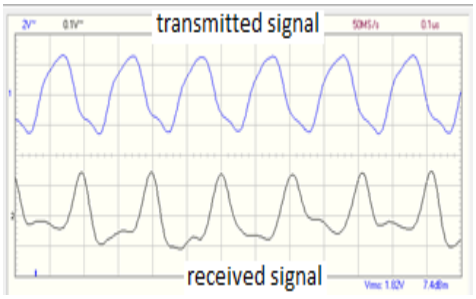	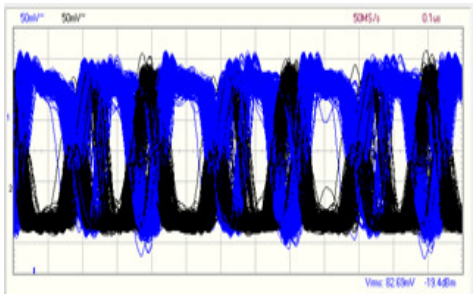

(c) Test waveform at 5 MHz

Table 6-19 Transmission within 40 mm square mild steel tube

at 30° bend - transmitted and received pulse with eye pattern at different frequency

Transmitted and received pulse	Eye pattern
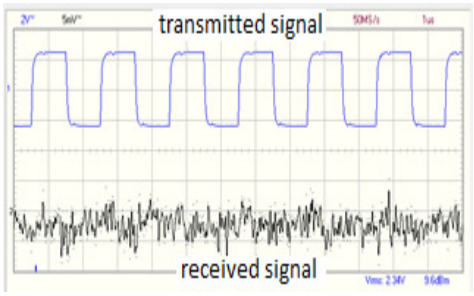	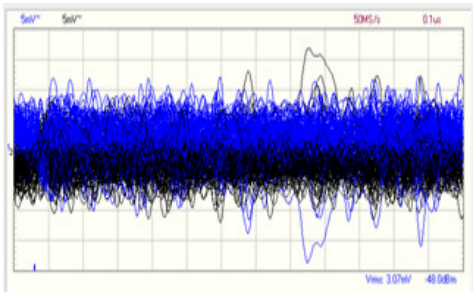

(a) Test waveform at 500 kHz

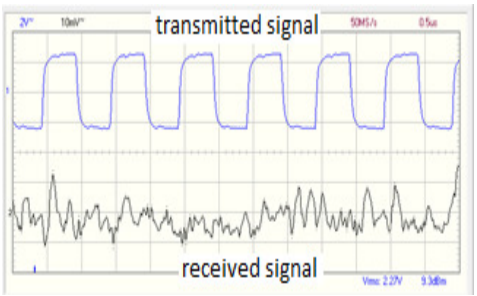	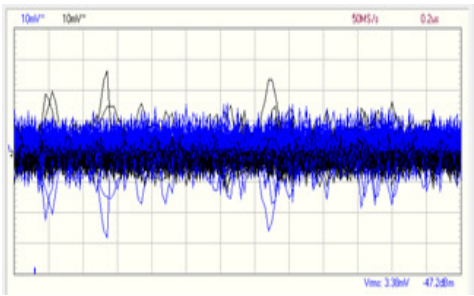

(b) Test waveform at 1 MHz

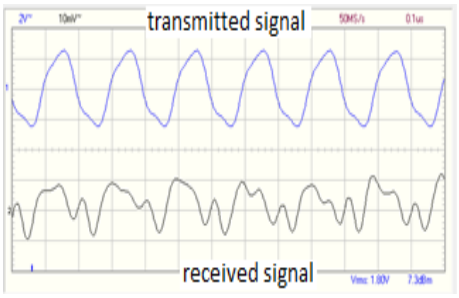	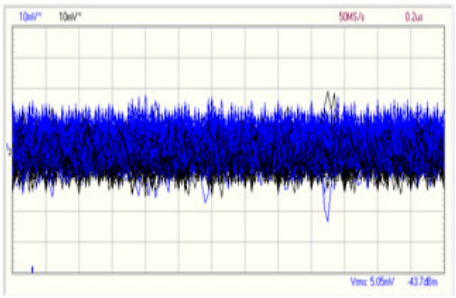

(c) Test waveform at 5 MHz

Table 6-20 Transmission within 40 mm square mild steel tube

at 45° bend - transmitted and received pulse with eye pattern at different frequency

Transmitted and received pulse	Eye pattern
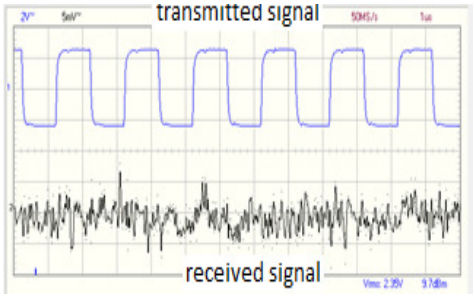	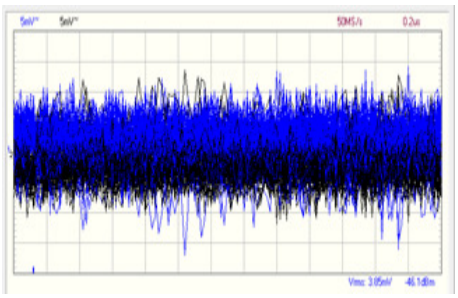

(a) Test waveform at 500 kHz

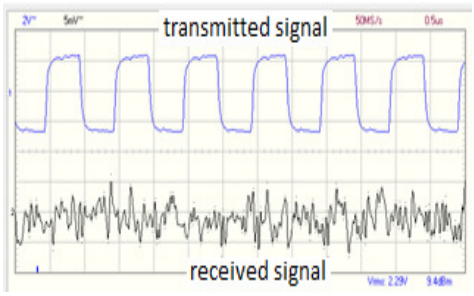	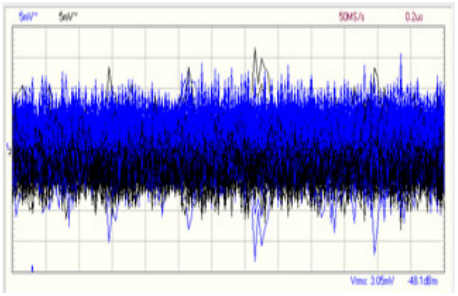

(b) Test waveform at 1 MHz

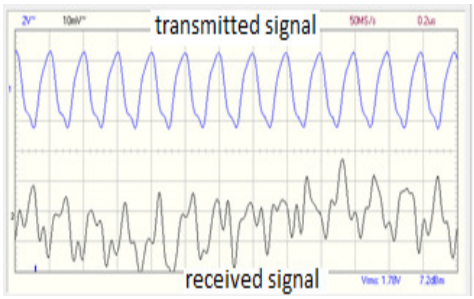	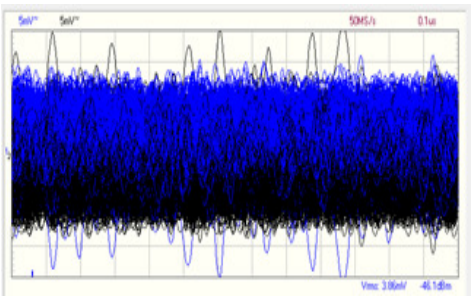

(c) Test waveform at 5 MHz

Table 6-21 Transmission within 40 mm square mild steel tube

at 60° bend - transmitted and received pulse with eye pattern at different frequency

Transmitted and received pulse	Eye pattern
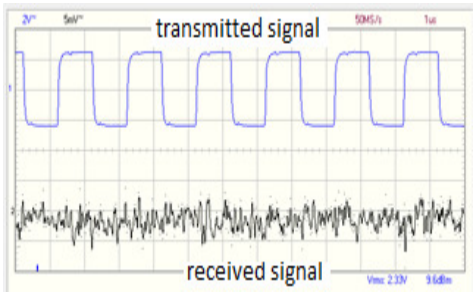	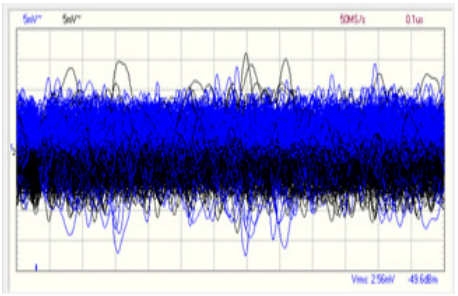

(a) Test waveform at 500 kHz

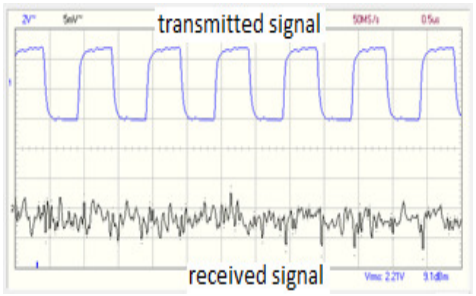	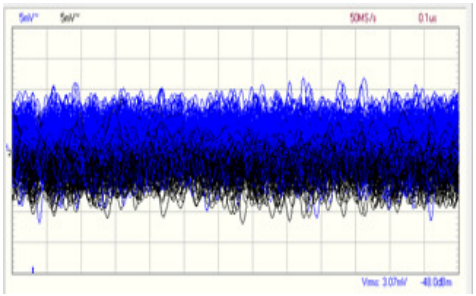

(b) Test waveform at 1 MHz

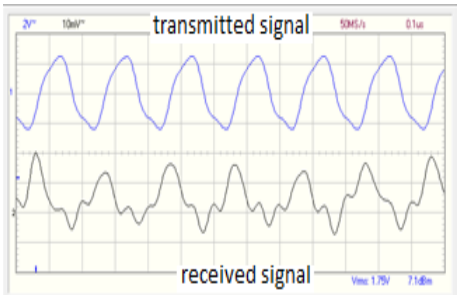	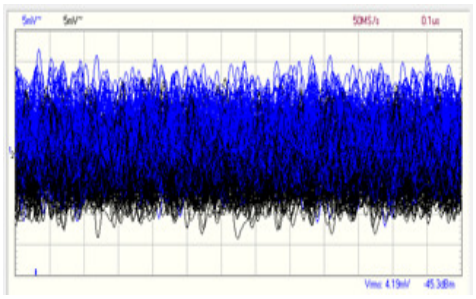

(c) Test waveform at 5 MHz

Three fundamental performance measures of the system are discussed as follows:

6.3.1 SNR

As the 35 mm circular mild steel tube and 40mm square mild steel tube having badly distorted eye pattern, the remainder of the investigation will omit these two sample. Furthermore badly distorted eye pattern indicated that the system totally could not be used. Figure 6-3 indicates the measured SNR at the receiver at 500 kHz, 1 MHz and 5 MHz. This measurement was critical, as the BER characteristics of each detected signal were dependent on it. Detected signals having a high SNR were given more weight than detected signals with a low SNR.

Higher SNR value were measured at 30^{o} bend in circular galvanised aluminium tube, measured at 30.6 dB. Followed by 20 mm circular aluminium tube at 29.8 dB. The SNR value keep decreasing with the increase of bending angle. As the eye pattern are badly distorted at 45^{o} and 60^{o} bend, the SNR was unable to be detected for 20mm square aluminium tube. The finding also proved that the SNR value above 15.6 dB discussed in Chapter 3, gives poor eye opening, which will lead to unacceptable BER and therefore are not suitable to be applied.

Overall, the amount of distortion measured increased as the bending angle and transmission frequency increased. More errors were presented in the transmission at higher wavelengths and over greater distances. This was due to the path loss, which is increased as the transmission distance increased. Furthermore, the transmission quality also degraded as the bending angle increased. The other reason for errors in the transmission was the extension of the pulse, where a single “0” pulse appeared to be approximately triple a standard one, in its length. The basis of the pulse extension was unknown, and requires further investigation.

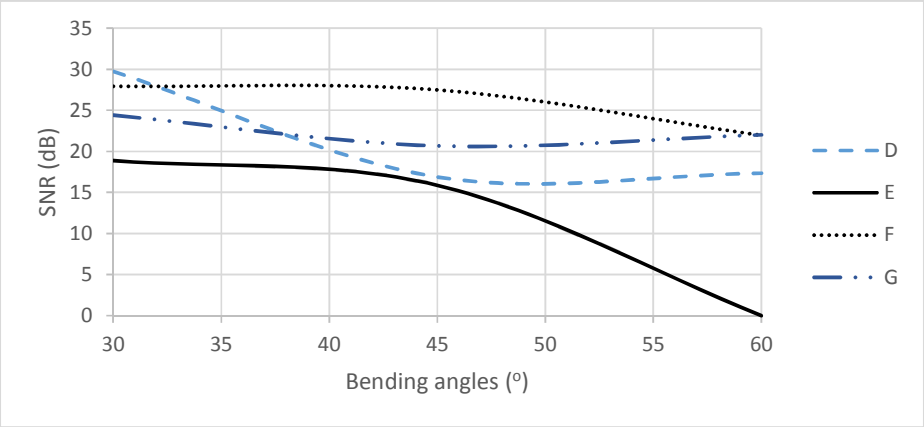

(a) 500 kHz

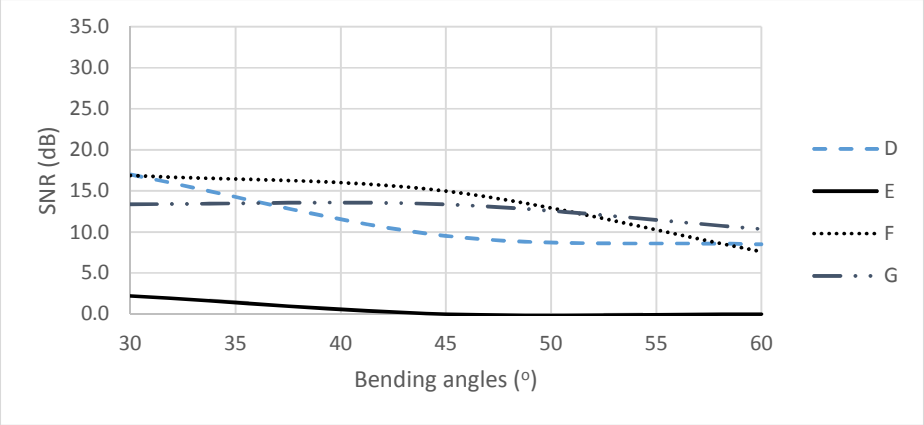

(b) 1 MHz

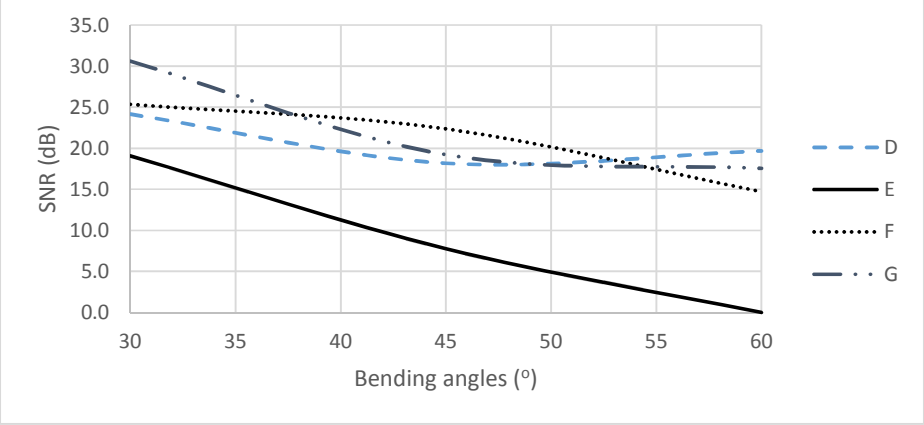

(c) 5 MHz

Figure 6-3 SNR at the receiver at different frequency.

6.3.2 Relationship between SNR, Q-factor and BER

Based on the SNR measured, the value of Q-factor and BER are estimated by using the Equation 6-1 and 6-2 [54][101][102]

$$Q_{dB} = SNR + 10\log\frac{B_o}{B_c} \tag{6-1}$$

$$BER = \frac{1}{2}\, erfc\left(\frac{Q}{\sqrt{2}}\right) \tag{6-2}$$

where B_o is the bandwidth of the photodetector, 17.5 MHz for this research and B_c is the bandwidth of the receiver, which is 6 MHz.

The relationship between SNR, Q-factor and BER are graphically illustrated as in Figure 6-4 and Figure 6-5. The graph illustrated the BER under different SNR and Q-factor for different bending angles, which is 30^o, 45^o and 60^o bend for this case.

As stated in Chapter 3, the expected BER for the system is between 10^{-4} up to 10^{-6}, chosen based on the expected BER for the indoor environment. Unfortunately, based on the estimated value, only the signal transmitted through 20 mm square aluminium tube could achieve the desired BER. The study also shows that, for the diffuse channel, it is required to have less than 2 dB SNR, in order to achieve an acceptable bit error rate of 10^{-4}. For other tubes, the BER is between 10^{-18} up to 10^{-137} for SNR of 7.6 dB and 13.4 dB respectively. The SNR is extremely large to produce a satisfactory BER set for the system.

The minimum value of Q-factor calculated is 4.6 in 20 mm square aluminium tube at 45^o and 60^o bend. While the maximum value for Q-factor is 35.3 in circular galvanised aluminium at 30^o bend. Unfortunately, in practical, the least value of Q-factor that will allow an error-free system (BER of 10^{-9}) is 6. As expected, a higher values of Q-

factor has been obtained from the designed system.

To obtain more accurate BER, the use of a bit error rate tester is advisable because it is a specific device used to measures the BER for a system. The value obtained in this section is just an approximation based on the measured SNR.

Generally, in this study, it could be observed that the three performance measures of SNR, Q-factor and BER is difficult to relate with each other and not uniquely related in terms of geometrical shapes and material of the tubes. Thus, more accurate model needed in order to relate the SNR to the Q-factor and to the BER accurately.

Table 6-22 summarizes the performance of the free space transmission and within the bent tubes. Transmission at 500 kHz and 1 MHz showed error-free optical wireless communication in all the measurements, except for the transmission through both the circular and square mild steel tubes. The transmission system using a frequency of 5 MHz produces errors, even at the shortest distances (free space back-to-back transmission).

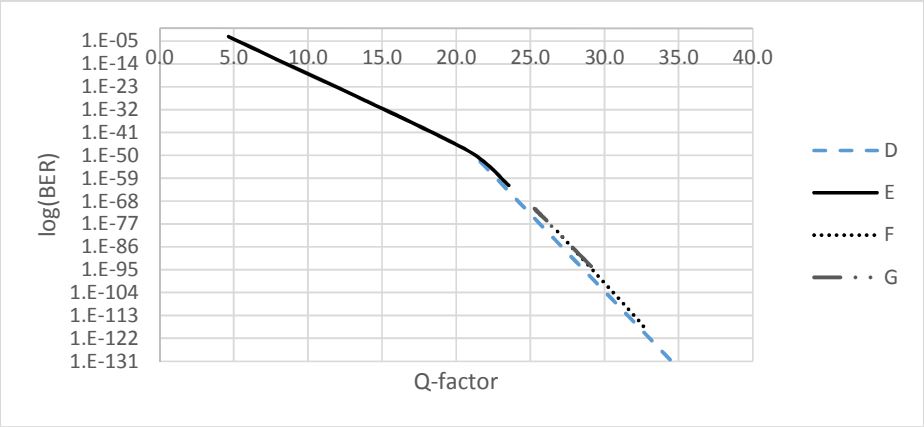

(a) 500 kHz

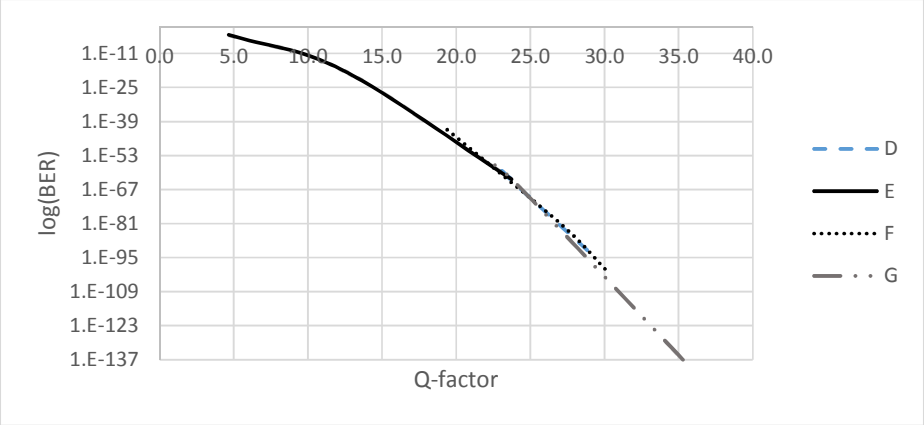

(b) 1 MHz

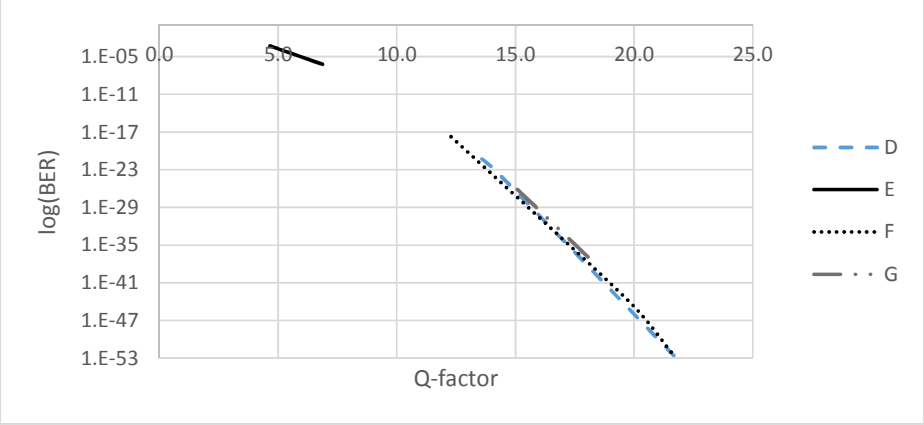

(c) 5 MHz

Figure 6-4 relationship between BER and Q-factor.

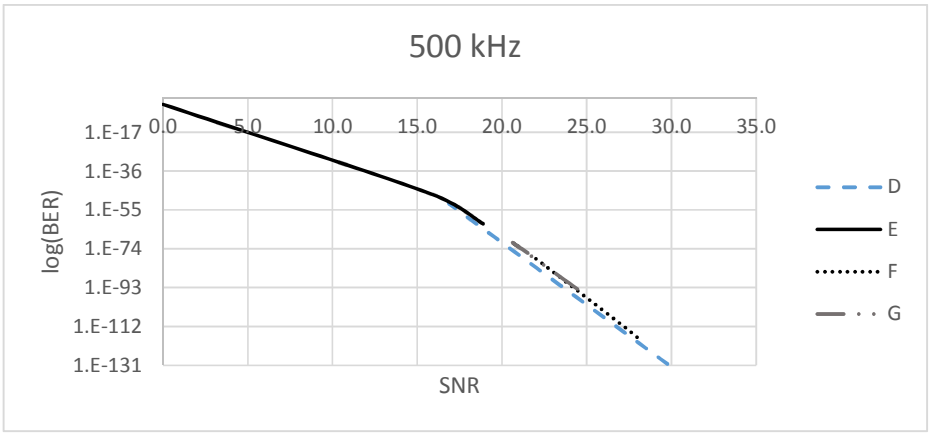

(a) 500 kHz

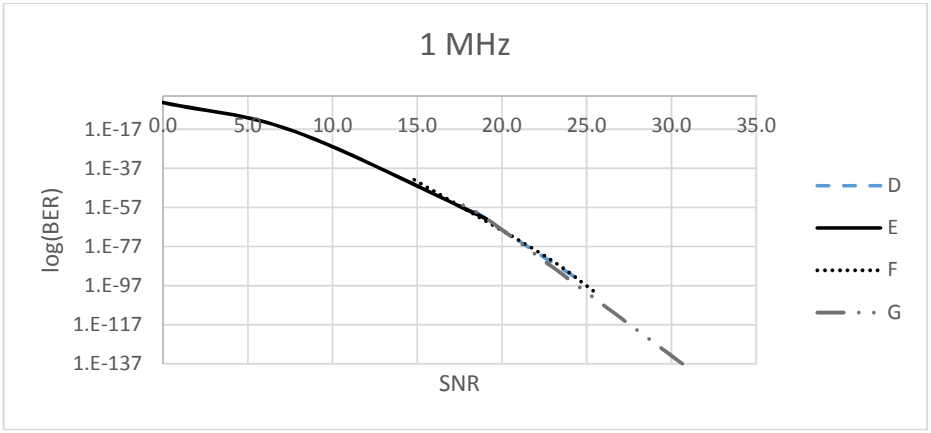

(b) 1 MHz

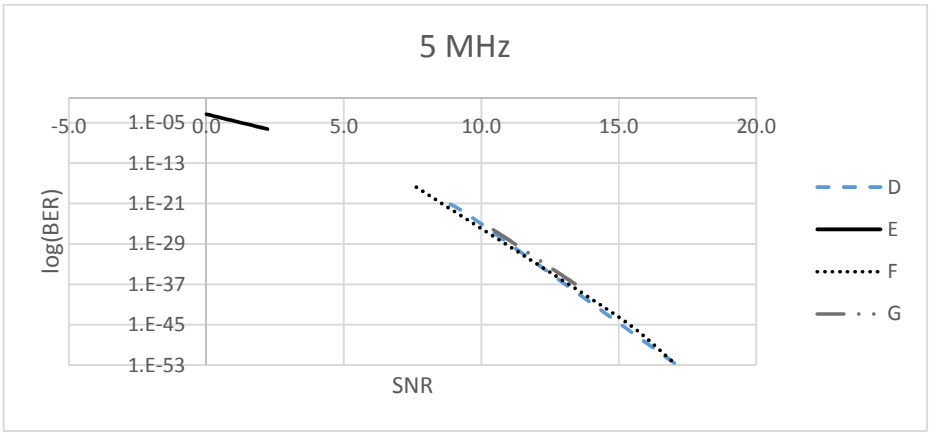

(c) 5 MHz

Figure 6-5 relationship between BER and SNR.

Table 6-22 performance summary

	30^0 bend	45^0 bend	60^0 bend	500 kHz	1 MHz	5 MHz	comments
FREE SPACE							
Line-of-sight transmission at • Back-to-back • 1 meter distance				√ √	√ √	X X	Distortion occur at 1 meter distance, but still acceptable.
STEEL TUBE							
C. Circular mild steel tube (35mm Diameter)	X	X	X	X	X	X	
D. Square aluminium tube (40mm X 40mm)	√	√	√	√	√	X	
E. Square aluminium tube (20mm X 20mm)	√	√	√	√	√	X	Received signal get worst as the bending angle increased.
F. Circular aluminium tube (20mm Diameter)	√	√	√	√	√	X	At 45^0 and 60^0 bend, distortion was detected but still considered as good receiving signal. Better than E.
G. Circular galvanised aluminium tube (35mm Diameter)	√	√	√	√	√	X	Received signal get worst as the bending angle increased. At 45^0 and 60^0 bend, distortion is detected but still consider as good receiving signal
H. Square mild steel tube (40mm X 40mm)	X	X	X	X	X	X	

PLASTIC TUBE							
B1				√	√	X	
B2				√	√	X	
B3				√	√	X	
B4				√	√	X	

6.4 Conclusion

In this chapter, the performance of the NLOS detected pulse signal characteristics under different tubes geometries have been presented based on the eye diagram analysis. Typically, principle operational functionality of the optical wireless for employment within a vehicular environment using a very short pulse has been successfully demonstrated, based on the 6 MHz system. The pulse waveform received at the receiving end displays a ringing on the rising and falling edge, but the signals is still considered as a good receiving signal. As this is not a concerned at this stage, the remainder of the study was adapted to cope with the ringing issue. The opening of the eye pattern is the most concerned factor in this phase.

Generally, a clear and wide opening of eye width for 500 kHz and 1 MHz pulse signals shows the possibility of error-free transmission of data for 40 mm square aluminium tube, 20 mm circular aluminium tune and 35 mm circular galvanised aluminium tube. Unfortunately, the eye pattern is almost closed for the 5 MHz pulse signal. This shows that the transmission at a higher frequency reduces the signal quality, and other enhancement techniques should be considered in order to overcome this effect.

Investigation on the SNR, Q-factor and BER focuses on 40 mm square aluminium tube, 20 mm circular aluminium tune and 35 mm circular galvanised aluminium tube. Higher SNR value were measured at 30^{o} bend in circular galvanised aluminium tube and at 60^{o} bend, most eye pattern are badly distorted. The target BER parameter set for the study (10^{-4} to 10^{-6}) were not successfully achieved for the transmission within the tubes except for the 20 mm square aluminium tube at smaller bending angle. Nevertheless, further improvement on the receiver sensitivity and proper BER measurement techniques are believed could improve the performance.

Thus, in order to keep the BER at below the expected value, a highly sensitive receiver need to be design. Besides, a proper modulation scheme were required in order to improve the quality of the transmitted signal in terms of SNR and BER.

Through observation of the eye pattern, the system works best in 20 mm square aluminium tube and acceptable for the galvanised aluminium tube. An extremely high SNR detected for all other tubes, which yield to very small BER.

In addition, the received signal quality got poorer when the bending angle, the distance/length and transmission frequency increased. This was true for both plastic and metal tubes. Furthermore, the link performance were also is limited by the capability of the designed system. The obtained results could be used to obtain some estimate of the digital performance of the system.

Chapter 7: Conclusions and future work

7.1 Summary of the work

Nearly exponential development of in-vehicle, embedded electronic frameworks has been seen all through the previous few decades. The design, employment, organisation, and integration of such complex distributed systems bring new challenges for the intra-vehicular sector. With this foundation, it is important to develop new procedures for capturing this necessity.

Optical wireless communication offers attractive benefits over the wired and the RF wireless channel. Thus, optical wireless communication can became a significant complement for the other communication systems. It is still in the initial staged of exploration within the vehicular environment, but its application prospects are very attractive.

This chapter concludes the thesis with main findings from the previous chapter considerations, and discussions. The main task of the work described in this thesis was

to study the optical wireless characterization for employment within a vehicular environment, aiming for the usage within the vehicle chassis in particular.

Chapter 2 covers an optical wireless communication system and automotive network, which concentrates on the wired and wireless intra-vehicular networks that build up current passive and active interaction of vehicle domains. The efficiency of those networks were also covered. Research developments in optical wireless for vehicular applications also were discussed. Based on an intensive literature review presented in ***Chapter 2***, the prospective of implementing optical wireless systems within the vehicular environment was identified.

Chapter 3 discussed in detail the hardware implementation that specifically designed for this project application, based on commercial off-the-shelf components. The requirement sets were based on the intra-vehicular network bandwidth requirement and indoor optical wireless minimum requirement. Based on the design system, 13 MHz system with 15.6 dB SNR were obtained, achieving the estimated objective. Noise analysis that affects the system sensitivity of the circuit developed was also discussed.

In ***Chapter 4***, channel characteristics for LOS configurations within different kinds of environment were studied in detail. The studies were focussed on the frequency response, the optical power and the path loss. Wise alignment of the emitter and the receiver will ensure that LOS communications are able to support high transmission speeds. The experimental results proved that the transmission was affected by the size, geometry and the reflection coefficient of the materials, in addition to other limiting factors such as the optoelectronic devices at the transmit end, and at the receiver itself. Hence, this part suggested that transmission using optical wireless communication technology within smaller in size and high reflection coefficient material are promising

in straight tubes, in addition to good transmitter and high sensitivity receiver. While, the diffuse link with angled transmitter and/or receiver orientation, and bent tubes at different angles depends greatly on signal reflections on the inner surface of the tubes. This implies limits for the achievable data rate, and requires higher transmission power. In detailed exploration in ***Chapter 5***, it was certain that, in order to support angle transmission for NLOS configurations, a high power transmitter was required. Depending upon this power requirement, the circuits were further improved, by using an array of four IRLEDs, which produces 54.48 mW or 44.58 mW/cm^2 output power. The findings shows that the channel characteristics have a great degree of sensitivity to the orientation and degree of rotation of the transmitter and receiver. Good transmission is likely to occur within the tubes with transmitter or receiver orientation angle less than 15^{o}and within a smaller diameter tube, in addition to high reflective coefficient tube properties. There is a pronounced discrepancy between the frequency responses, optical received and path losses at different transmission angles in straight tubes and bent tubes. The frequency response reduced drastically as the transmission angle increased, and the path loss increased as the bending angle increased. The transmission within plastic tube are not as good as in metal tube as the plastic is not a good reflector and light rays are diffusely reflected in plastic. The chapter also suggested that transmission within bend tube should use large inner diameter tube, as less number of reflection occurs in the tube, in addition to minimum bend angle. Thus less / low SNR produces. Finally, the most suitable material for the transmission is the circular galvanised aluminium or any material with high reflective coefficient properties.

In ***Chapter 6,*** an interesting feature of this project was presented. This chapter studied the eye pattern of the received signals within the metal tubes. Generally, the

operational functionality of digital system has been successfully demonstrated based on 6 MHz system, although the targeted BER of 10^{-4} to 10^{-6} were not positively realised. A clear and wide opening of eye width for 500 kHz and 1 MHz pulse signals shows the possibility of error-free transmission of data for 40 mm square aluminium tube, 20 mm circular aluminium tune and 35 mm circular galvanised aluminium tube. The received signal was good with the right combination between the size, geometry, bending angle and transmitter/receiver orientation. The results also show that the transmission within smaller size metallic tubes gives promising outcomes. In addition, transmission at 500 kHz and 1 MHz shows a feasible, error-free optical wireless communication.

In conclusion, it is hoped these results have provided useful initial insights into the viability of implementing an OWC system in intra-vehicle applications. Using IRLED within the tubes, the system demonstrates suitable channel characteristics for OW system deployment, not only for LOS configuration but also for NLOS configuration with the proper parameter combinations. The experimental results presented in this thesis indicate that transmitting a signal wave within a tube is feasible. A highly sensitive receiver design were improved to keep the BER below the expected value, and a proper modulation scheme is also required in order to improve the quality of the transmitted signal in terms of SNR and BER. The ideas, of course, do not end here. The results presented so far only incorporate the channel frequency response, power density and path loss.

7.2 Improvements and suggestions for further work

The principle expectation of this research was to investigate the prospect for the transmission of automotive control signals utilising optical wireless channels and to study the characteristics of the transmitted signal through the confined spaces. Overall, the various aspects of this research were addressed; and open up more opportunities for further work within each area discussed in this thesis. Some of the feasible extent for future work is concisely described here.

Firstly, the extent of feasible modifications to transceiver required to improve the power and bandwidth limitations of the designed prototype are discussed. This could be realised by using a detector with a wider FOV for better signal detection as well as using of optics aids (lens and concentrator). Increasing the power by adding more IrLEDs in parallel could be one of the methods, but need to comply with the eye-safety requirement. Further technical investigation needs to take place, in terms of hardware enhancement, in order to reduce the ringing/overshoot at the rising and falling edge of the received signal, and the duty cycle problems mentioned in Chapter 6.

Secondly, in this thesis, relatively fundamental mathematical models have been evaluated, which covers the surface level only, based on the experimental results. It could be better if the theoretical and simulation models could be considered as a comparison method for empirical results, and a better system model could be derived. Using these theoretical and simulation models, the accuracy of empirical models could be entirely evaluated.

Another area for future research is evaluation by using real modulated signal manipulation in the digital domain for higher transmission capacity. This will emulate a real environment.

Future work should also aim to conduct similar procedures in other forms of open and

enclosed environments. Thus, other experimental environments such as background noise, transmission within EMI environments, MIMO and so on, where more complicate impact factors are considered for the numerical and empirical analysis, could also be considered. Empirical studies within more than one bent tube would also be useful.

Lastly, a useful expansion is to explore, compare and contrast the various types of modulation schemes and transmission protocols, appropriate for real time applications.

References

[1] N. Navet, Y. Song, F. Simonot-Lion, and C. Wilwert, "Trends in automotive communication systems," in *Proceedings of the IEEE*, 2005, vol. 93, no. 6, pp. 1204–1223.

[2] G. Leen, D. Heffernan, and A. Dunne, "Digital networks in the automotive vehicle," *Computing and Control Engineering Journal*, vol. 10, no. 6, pp. 257–66, 1999.

[3] A. Shrinath and A. Emadi, "Electronic control units for automotive electrical power systems: communication and networks," *Proceedings of the Institution of Mechanical Engineers, Part D: Journal of Automobile Engineering*, vol. 218, no. 11, pp. 1217–1230, 2004.

[4] R. Pratt, F. Tuffner, and K. Gowri, "Electric Vehicle Communication Standards Testing and Validation Phase I: SAE J2847/1," 2011.

[5] "What do SAE Standards Offer the Automotive Electronics Industry?" [Online]. Available: http://www.sae.org/smartgrid/p90475.pdf. [Accessed: 25–08-2016].

[6] T. Nolte, H. Hansson, and L. L. Bello, "Wireless automotive communications," in *Euromicro Conference on Real-Time Systems, Palma de Mayorca*, 2005, vol. 6, no. 8, pp. 35–38.

[7] U. Keskin, "In-vehicle communication networks: a literature survey," *Computer Science Report*, vol. 10, 2009.

[8] G. S. Bickel, "Inter/intra-vehicle wireless communication," 2008. [Online]. Available: http://www1. cse. wustl. edu/\~ jain/cse574-06/ftp/vehicular_wireless/,. [Accessed: Apr-2015].

[9] R. J. Green, "Optical wireless with application in automotives," in *Proceedings of 12th International Conference on Transparent Optical Networks*, 2010, pp. 1–4.

[10] G. Leen and D. Heffernan, “Vehicles without wires,” *Computing & Control Engineering Journal*, vol. 12, no. 5, pp. 205–211, 2001.

[11] A. Lim and D. Bevly, *U29: Commercial Vehicle Secure Network for Safety and Mobility Applications Final Report*. National Transportation Research Center, Incorporated, University Transportation Center, 2011.

[12] I. Arruego, H. Guerrero, S. Rodriguez, J. Martinez-Oter, J. Jimenez, J. Dominguez, A. Martin-Ortega, J. de Mingo, J. Rivas, V. Apéstigue, and others, “OWLS: a ten-year history in optical wireless links for intra-satellite communications,” *IEEE Journal on Selected Areas in Communications*, vol. 27, no. 9, pp. 1599–1611, 2009.

[13] F. R. Gfeller and U. Bapst, “Wireless in-house data communication via diffuse infrared radiation,” *Proceedings of the IEEE*, vol. 67, no. 11, pp. 1474–1486, 1979.

[14] S. Miller, “Waveguide as a communication medium,” *The Bell System Technical Journal*, vol. 33, no. 6, pp. 1209–1265, 1954.

[15] P. V. Nikitin, D. D. Stancil, A. G. Cepni, O. K. Tonguz, A. E. Xhafa, and D. Brodtkorb, “Propagation model for the HVAC duct as a communication channel,” *IEEE Transactions on Antennas and Propagation*, vol. 51, no. 5, pp. 945–951, 2003.

[16] D. D. Stancil, O. K. Tonguz, A. Xhafa, A. Cepni, P. Nikitin, and D. Brodtkorb, “High-speed internet access via HVAC ducts: a new approach,” in *Proceedings of the Global Telecommunications Conference*, 2001, vol. 6, pp. 3604–3607.

[17] R. Ohlmann, P. Richards, and M. Tinkham, “Far infrared transmission through metal light pipes,” *JOSA*, vol. 48, no. 8, pp. 531–532, 1958.

[18] K. E. Peiponen and T. Tsuboi, “Metal surface roughness and optical reflectance,” *Optics & Laser Technology*, vol. 22, no. 2, pp. 127–130, 1990.

[19] C. R. Lomba, R. T. Valadas, and A. de O. Duarte, “Experimental characterisation and modelling of the reflection of infrared signals on indoor surfaces,” in *Proceedings of the IEE Optoelectronics*, 1998, vol. 145, no. 3, pp. 191–197.

[20] V. Pohl, V. Jungnickel, and C. von Helmolt, “A channel model for wireless infrared communication,” in *The 11th IEEE International Symposium on Personal, Indoor and Mobile Radio Communications*, 2000, vol. 1, pp. 297–303.

[21] V. Jungnickel, V. Pohl, S. Nonnig, and C. von Helmolt, “A physical model of the wireless infrared communication channel,” *IEEE Journal on Selected Areas in Communications*, vol. 20, no. 3, pp. 631–640, 2002.

[22] N. Hayasaka and T. Ito, “Channel modeling of nondirected wireless infrared indoor diffuse link,” *Electronics and Communications in Japan (Part I: Communications)*, vol. 90, no. 6, pp. 9–19, 2007.

[23] M. D. Higgins, “Genetic algorithm optimisation methods applied to the indoor optical wireless communications channel,” 2009.

[24] D. Ding and X. Ke, “A new indoor VLC channel model based on reflection,” *Optoelectronics Letters*, vol. 6, pp. 295–298, 2010.

[25] H. Yang and C. Lu, “Infrared wireless LAN using multiple optical sources,” in *IEE Proceedings on Optoelectronics*, 2000, vol. 147, no. 4, pp. 301–307.

[26] F. Miramirkhani and M. Uysal, “Channel Modeling and Characterization for Visible Light Communications,” *IEEE Photonics Journal*, vol. 7, no. 6, pp. 1–16, 2015.

[27] J. M. Kahn, W. J. Krause, and J. B. Carruthers, “Experimental characterization of non-directed indoor infrared channels,” *IEEE Transactions on Communications*, vol. 43, no. 234, pp. 1613–1623, 1995.

[28] M. Pakravan, M. Kavehrad, and H. Hashemi, “Measurement of rotation effects in an indoor infrared channel,” in *Proceeding of 48th IEEE Vehicular Technology Conference*, 1998, vol. 3, pp. 2100–2103.

[29] H. Hashemi, G. Yun, M. Kavehrad, F. Behbahani, and P. A. Galko, “Indoor propagation measurements at infrared frequencies for wireless local area networks applications,” *IEEE Transactions on Vehicular Technology* , vol. 43, no. 3, pp. 562–576, 1994.

[30] D. Wu, Z. Ghassemlooy, S. Rajbhandari, and H. Le Minh, “Channel Characteristics Analysis and Experimental Demonstration of a Diffuse Cellular Indoor Visible Light Communication System,” *The Mediterranean Journal of Electronics and Communications*, 2012.

[31] G. W. Marsh and J. M. Kahn, “Performance evaluation of experimental 50-Mb/s diffuse infrared wireless link using on-off keying with decision-feedback equalization,” *IEEE Transactions on Communications*, vol. 44, no. 11, pp. 1496–1504, 1996.

[32] A. Sivabalan and J. John, “Modeling and simulation of indoor optical wireless channels: a review,” in *Proceedings of the Conference on Convergent Technologies for Asia-Pacific Region* , 2003, vol. 3, pp. 1082–1085.

[33] J. R. Barry, J. M. Kahn, W. J. Krause, E. A. Lee, and D. G. Messerschmitt, “Simulation of multipath impulse response for indoor wireless optical channels,” *IEEE Journal on Selected Areas in Communications*, vol. 11, no. 3, pp. 367–379, 1993.

[34] R. Perez-Jimenez, J. Berges, and M. Betancor, “Statistical model for the impulse response on infrared indoor diffuse channels,” *IET Electronics Letters*, vol. 33, no. 15, pp. 1298–1300, 1997.

[35] F. Lopez-Hernandez and M. Betancor, “DUSTIN: algorithm for calculation of impulse response on IR wireless indoor channels,” *IET Electronics Letters*, vol. 33, no. 21, pp. 1804–1806, 1997.

[36] F. Lopez-Hernandez, R. Perez-Jimeniz, and A. Santamaria, “Monte Carlo calculation of impulse response on diffuse IR wireless indoor channels,” *IET Electronics Letters*, vol. 34, no. 12, pp. 1260–1262, 1998.

[37] J. Lopez-Hernandez, R. Perez-Jimenez, and A. Santamaria, “Modified Monte Carlo scheme for high-efficiency simulation of the impulse response on diffuse IR wireless indoor channels,” *IET Electronics Letters*, vol. 34, no. 19, pp. 1819–1820, 1998.

[38] J. B. Carruthers and P. Kannan, “Iterative site-based modeling for wireless infrared channels,” *IEEE Transactions on Antennas and Propagation*, vol. 50, no. 5, pp. 759–765, 2002.

[39] J. M. Kahn and J. R. Barry, “Wireless infrared communications,” *Proceedings of the IEEE*, vol. 85, no. 2, pp. 265–298, 1997.

[40] N. Schmitt, T. Pistner, C. Vassilopoulos, D. Marinos, A. Boucouvalas, M. Nikolitsa, C. Aidinis, and G. Metaxas, “Diffuse wireless optical link for aircraft intra-cabin passenger communication,” in *Proceedings of 5th International Symposium on Communication Systems, Networks and Digital Signal Processing*, 2006, pp. 625–628.

[41] G. K. Karagiannidis, S. Arnon, J. R. Barry, R. Schober, and M. Uysal, “Optical wireless communications,” *IEEE Journal on Selected Areas in Communications*, vol. 27, no. 9, pp. 1521–1525, 2009.

[42] J. Grubor, O. Jamett, J. Walewski, S. Randel, and K.-D. Langer, “High-speed wireless indoor communication via visible light,” *ITG-Fachbericht-Breitbandversorgung in Deutschland-Vielfalt für alle*, 2007.

[43] H. Elgala, R. Mesleh, and H. Haas, “Impact of LED nonlinearities on optical wireless OFDM systems,” in *Proceedings of the IEEE 21st International Symposium on Personal Indoor and Mobile Radio Communications*, 2010, pp. 634–638.

[44] C. Singh, Y. Singh, J. John, and K. Tripathi, “High-Speed Power-Efficient Indoor Optical Wireless System.”

[45] R. J. Green, “Secure communications: The infrared alternative,” in *Proceedings of ICTON Mediterranean Winter Conference*, 2007, pp. 1–4.

[46] I. Stefan, H. Elgala, R. Mesleh, D. O. Brien, and H. Haas, “Optical wireless OFDM system on FPGA: Study of LED nonlinearity effects,” in *Proceedings of IEEE 73rd Vehicular Technology Conference*, 2011, pp. 1–5.

[47] V. Lalithambika, “Application of VLSI to optical wireless networks,” Department of Engineering, University of Cambridge, Cambridge, UK, 2002.

[48] Y. Zeng, “Adaptive modulation schemes for optical wireless communication systems,” 2010.

[49] H. Elgala, “A Study on the Impact of Nonlinear Characteristics of LEDs on Optical OFDM,” 2010.

[50] U. Sethakaset, “Modulation and coding techniques for infrared wireless local area networks,” 2006.

[51] J. Wang, Z. Xu, and W. Hu, “Improved DPPM modulation for optical wireless communications,” in *Proceedings of SPIE*, 2004, vol. 5281, p. 483.

[52] T. Ohtsuki, “Multiple-subcarrier modulation in optical wireless communications,” *IEEE Communications Magazine*, vol. 41, no. 3, pp. 74–79, 2003.

[53] H. Joshi, R. Green, and M. S. Leeson, “Multiple sub-carrier optical wireless systems,” in *Proceedings of 10th Anniversary International Conference on Transparent Optical Networks*, 2008, vol. 4, pp. 184–188.

[54] H. Elgala, R. Mesleh, and H. Haas, “Indoor optical wireless communication: potential and state-of-the-art,” *IEEE Communications Magazine*, vol. 49, no. 9, pp. 56–62, 2011.

[55] M. Schmid, “Automotive Bus Systems,” *ATMEL Applications Journal*, vol. Winter 2006, no. 6, pp. 29–32, 2006.

[56] G. Leen and D. Heffernan, “Expanding automotive electronic systems,” *Computer*, vol. 35, no. 1, pp. 88–93, 2002.

[57] M. Farsi, K. Ratcliff, and M. Barbosa, “An overview of controller area network,” *Computing and Control Engineering Journal*, vol. 10, no. 3, pp. 113–120, 1999.

[58] W. Tong, C. Tong, and Y. Liu, “A Data Engine for Controller Area Network,” in *Proceedings of International Conference on Computational Intelligence and Security*, 2007, pp. 1015–1019.

[59] H. Othman, Y. Aji, F. Fakhreddin, and A. Al-Ali, “Controller area networks: Evolution and applications,” in *Proceedings of 2nd Information and Communication Technologies*, 2006, vol. 2, pp. 3088–3093.

[60] C. Quigley, P. Jones, R. McMurran, and P. Faithfull, “Design approaches for integrating CAN with emerging time-triggered protocols,” in *Proceedings of IEEE International Conference on Communications*, 2006.

[61] T. Nolte, H. Hansson, and L. L. Bello, “Automotive communications-past, current and future,” in *Proceedings of 10th IEEE Conference on Emerging Technologies and Factory Automation*, 2005, vol. 1, pp. 985–992.

[62] S. S. S. V. K. M. V. Bhalerao, “A Survey of Wireless Communication Using Visible Light,” *International Journal of Advances in Engineering & Technology,*, vol. 5, no. 2, pp. 188–197, 2013.

[63] T. Kibler, S. Poferl, G. Böck, H.-P. Huber, and E. Zeeb, “Optical data buses for automotive applications,” *Journal of Lightwave Technology*, vol. 22, no. 9, pp. 2184–2199, 2004.

[64] F. Sethna, E. Stipidis, and F. Ali, “What lessons can controller area networks learn from FlexRay,” in *Proceedings of IEEE Vehicle Power and Propulsion Conference*, 2006, pp. 1–4.

[65] M. Ahmed, C. U. Saraydar, T. ElBatt, J. Yin, T. Talty, and M. Ames, “Intra-vehicular wireless networks,” in *Proceedings of 2007 IEEE Globecom Workshops*, 2007, pp. 1–9.

[66] M. Lessard, “IDB-1304 automotive reference platform-enabling in-vehicle entertainment,” *Mindready Solutions, Research Triangle Park, NC*, 2003.

[67] J. Zhang, P. V. Orlik, Z. Sahinoglu, A. F. Molisch, and P. Kinney, “UWB systems for wireless sensor networks,” *Proceedings of the IEEE*, vol. 97, no. 2, pp. 313–331, 2009.

[68] M. Heddebaut, V. Deniau, and K. Adouane, “In-vehicle WLAN radio-frequency communication characterization,” *IEEE Transactions on Intelligent Transportation Systems*, vol. 5, no. 2, pp. 114–121, 2004.

[69] N. Baker, “ZigBee and Bluetooth strengths and weaknesses for industrial applications,” *Computing & Control Engineering Journal*, vol. 16, no. 2, pp. 20–25, 2005.

[70] L. Liu, Y. Wang, N. Zhang, and Y. Zhang, “UWB channel measurement and modeling for the intra-vehicle environments,” in *Proceedings of 12th IEEE International Conference on Communication Technology*, 2010, pp. 381–384.

[71] W. Zhuang, X. S. Shen, and Q. Bi, “Ultra-wideband wireless communications,” *Wireless communications and mobile computing*, vol. 3, no. 6, pp. 663–685, 2003.

[72] W. Hong, L. Liu, N. Zhang, C. Yu, H. Zhang, J. Chen, Z. Kuai, and J. Zhou, “Simulation and experiment on in-car channel characteristics,” in *Proceedings of the Asia-Pacific Symposium on Electromagnetic Compatibility* , 2008, pp.

467–469.

[73] D. Porcino and W. Hirt, “Ultra-wideband radio technology: potential and challenges ahead,” *IEEE Communications Magazine*, vol. 41, no. 7, pp. 66–74, 2003.

[74] S. Dissanayake, P. Karunasekara, D. Lakmanaarachchi, A. Rathnayaka, and A. Samarasinghe, “Zigbee Wireless Vehicular Identification and Authentication System,” in *Proceedings of the 4th International Conference on Information and Automation for Sustainability*, 2008, pp. 257–260.

[75] H. M. Tsai, W. Viriyasitavat, O. K. Tonguz, C. Saraydar, T. Talty, and A. MacDonald, “Feasibility of in-car wireless sensor networks: A statistical evaluation,” in *Proceedings of the 4th Annual IEEE Communications Society Conference on Sensor, Mesh and Ad Hoc Communications and Networks*, 2007, pp. 101–111.

[76] O. K. Tonguz, H.-M. Tsai, T. Talty, A. Macdonald, and C. Saraydar, “RFID technology for intra-car communications: A new paradigm,” in *Proceedings of 64th IEEE Vehicular Technology Conference*, 2006, pp. 1–6.

[77] O. Strobel, R. Rejeb, and J. Lubkoll, “Communication in automotive systems: Principles, limits and new trends for vehicles, airplanes and vessels,” in *Proceedings of 12th International Conference on Transparent Optical Networks*, 2010, pp. 1–6.

[78] N. Fujimoto, A. Ishizuka, M. Moriya, and M. Goto, “Low-Cost and Versatile Gigabit PDF Transceivers for Very-Short-Reach Application,” *Research Reports of the Faculty of Engineering, Kinki University*, no. 40, pp. 87–101, 2006.

[79] X. Chen, *Requirements and concepts for future automotive electronic architectures from the view of integrated safety*. Univ.-Verlag, 2008.

[80] E. Kelling, M. Friedewald, T. Leimbach, M. Menzel, P. Säger, H. Seudié, B. Weyl, A. Fuchs, O. Henniger, M. S. Idrees, and others, “Deliverable D2. 1: Specification and evaluation of e-security relevant use cases,” 2009.

[81] M. Higgins, R. Green, and M. Leeson, “Optical Wireless for Intra-Vehicle Communications: A Channel Viability Analysis,” *IEEE Transactions on Vehicular Technology*, no. 99, pp. 123–129, 2012.

[82] K. Cui, G. Chen, Q. He, and Z. Xu, “Indoor optical wireless communication by ultraviolet and visible light,” in *SPIE Optical Engineering and Applications*, 2009, pp. 74640–7464.

[83] G. Pang, C. Chan, H. Liu, and T. Kwan, “Dual use of LEDs: Signaling and communications in ITS,” *Proceedings of 5th World Congr. Intelligent Transport Systems*, pp. 12–16, 1998.

[84] Y. Tanaka, “A Study on Optical Wireless Communication Systems and Their Applications,” Ph.D. thesis, Keio University, 2002.

[85] S. Hranilovic, “Spectrally efficient signalling for wireless optical intensity channels,” Ph.D. thesis, Dept. of Electrical & Computer Eng., University of Toronto, 2003.

[86] D. W. K. Wong, “Diffuse indoor optical wireless local area networks,” Ph.D. thesis, School of Electrical and Electronic Engineering, Nanyang Technological University, Singapore, 2008.

[87] A. Ramli, “Free space optical front-end receiver’s bandwidth enhancement employing micro-electro mechanical systems variable feedback capacitor,” M.Eng. thesis, Faculty of Electrical Engineering, Universiti Teknologi Malaysia, 2010.

[88] M. F. L. Abdullah, “Techniques for signal to noise ratio adaptation in infrared optical wireless for optimisation of receiver performance,” Ph.D. thesis, School of Engineering, University of Warwick, UK, 2006.

[89] F. Perry, “Predicting the performance of a photodetector,” *Boston Electronics Corporation*, vol. 72, 2003.

[90] H. A. Alhagagi, “Theory and optimisation of double conversion heterodyne photoparametric amplifier,” School of Engineering, University of Warwick, UK, 2012.

[91] D. V. Perepelitsa, “Johnson noise and shot noise,” *MIT Department of Physics, Cambridge, MA*, vol. 2, 2006.

[92] S. Jivkova and M. Kavehrad, “Receiver designs and channel characterization for multi-spot high-bit-rate wireless infrared communications,” *Communications, IEEE Transactions on*, vol. 49, no. 12, pp. 2145–2153, 2001.

[93] MISSING:smith1982receiver, “MISSING:smith1982receiver,” 2016.

[94] T. Komine, “Visible light wireless communications and its fundamental study,” 2005.

[95] A. Al-Ghamdi and J. Elmirghani, “Characterization of mobile spot diffusing optical wireless systems with diversity receiver,” in *IEEE International Conference on Communications*, 2004, vol. 1, pp. 133–138.

[96] Z. Ghassemlooy, A. Hayes, and B. Wilson, “Reducing the effects of intersymbol interference in diffuse DPIM optical wireless communications,” in *Optoelectronics, IEE Proceedings-*, 2003, vol. 150, no. 5, pp. 445–452.

[97] S. Dimitrov, R. Mesleh, H. Haas, M. Cappitelli, M. Olbert, and E. Bassow, “Path Loss Simulation of an Infrared Optical Wireless System for Aircrafts,”

in *Proceedings of the IEEE Global Telecommunications Conference*, 2009, pp. 1–6.

[98] S. Arumugam and J. John, "Effect of transmitter positions on received power and bandwidth in diffuse indoor optical wireless systems," *Optical and quantum electronics*, vol. 39, no. 1, pp. 1–14, 2007.

[99] K. Sindhubala and B. Vijayalakshmi, "Design and implementation of visible light communication system in indoor environment," *ARPN Journal of Engineering and Applied Sciences*, vol. 10, no. 7, pp. 2882–2886, 2006.

[100] J. B. Carruthers and J. M. Kahn, "Modeling of nondirected wireless infrared channels," *IEEE Transactions on Communications*, vol. 45, no. 10, pp. 1260–1268, 1997.

Appendices

Appendix A

Apparatus

Boonton Electronics Capacitance meter

Ealing photometer

Thor Labs power meter with S314C sensor

Appendix B

Datasheets

High Speed Infrared Emitting Diode, 850 nm, Surface Emitter Technology

FEATURES

- Package type: leaded
- Package form: T-1¾
- Dimensions (in mm): Ø 5
- Leads with stand-off
- Peak wavelength: λ_p = 850 nm
- High reliability
- High radiant power
- High radiant intensity
- Narrow angle of half intensity: $\varphi = \pm 3°$
- Suitable for high pulse current operation
- Good spectral matching with CMOS cameras
- Material categorization: For definitions of compliance please see www.vishay.com/doc?99912

RoHS COMPLIANT HALOGEN FREE GREEN

DESCRIPTION

As part of the SurfLight™ portfolio, the VSLY5850 is an infrared, 850 nm emitting diode based on GaAlAs surface emitter chip technology with extreme high radiant intensity, high optical power and high speed, molded in a clear, untinted plastic package, with a parabolic lens.

APPLICATIONS

- Infrared radiation source for operation with CMOS cameras
- High speed IR data transmission
- Smoke-automatic fire detectors
- IR Flash

PRODUCT SUMMARY

COMPONENT	I_e (mW/sr)	φ (deg)	λ_p (nm)	t_r (ns)
VSLY5850	600	± 3	850	10

Note
- Test conditions see table "Basic Characteristics"

ORDERING INFORMATION

ORDERING CODE	PACKAGING	REMARKS	PACKAGE FORM
VSLY5850	Bulk	MOQ: 4000 pcs, 4000 pcs/bulk	T-1¾

Note
- MOQ: minimum order quantity

ABSOLUTE MAXIMUM RATINGS (T_{amb} = 25 °C, unless otherwise specified)

PARAMETER	TEST CONDITION	SYMBOL	VALUE	UNIT
Reverse voltage		V_R	5	V
Forward current		I_F	100	mA
Peak forward current	t_p/T = 0.5, t_p = 100 µs	I_{FM}	200	mA
Surge forward current	t_p = 100 µs	I_{FSM}	1	A
Power dissipation		P_V	190	mW
Junction temperature		T_j	100	°C
Operating temperature range		T_{amb}	- 40 to + 85	°C
Storage temperature range		T_{stg}	- 40 to + 100	°C
Soldering temperature	t ≤ 5 s, 2 mm from case	T_{sd}	260	°C
Thermal resistance junction/ambient	J-STD-051, leads 7 mm, soldered on PCB	R_{thJA}	230	K/W

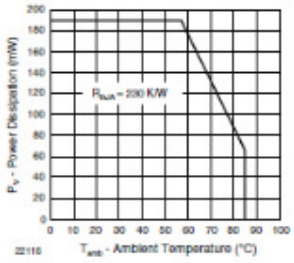

Fig. 1 - Power Dissipation Limit vs. Ambient Temperature

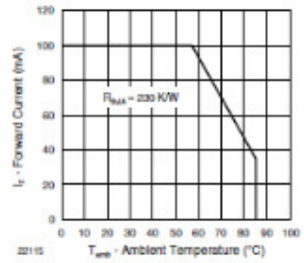

Fig. 2 - Forward Current Limit vs. Ambient Temperature

BASIC CHARACTERISTICS (T_{amb} = 25 °C, unless otherwise specified)

PARAMETER	TEST CONDITION	SYMBOL	MIN.	TYP.	MAX.	UNIT
Forward voltage	I_F = 100 mA, t_p = 20 ms	V_F		1.65	1.9	V
	I_F = 1 A, t_p = 100 µs	V_F		2.9		V
Temperature coefficient of V_F	I_F = 1 mA	TK_{VF}		- 1.45		mV/K
	I_F = 10 mA	TK_{VF}		- 1.25		mV/K
Reverse current		I_R	not designed for reverse operation			µA
Junction capacitance	V_R = 0 V, f = 1 MHz, E = 0	C_j		125		pF
Radiant intensity	I_F = 100 mA, t_p = 20 ms	I_e	300	600	900	mW/sr
	I_F = 1 A, t_p = 100 µs	I_e		5100		mW/sr
Radiant power	I_F = 100 mA, t_p = 20 ms	ϕ_e		55		mW
Temperature coefficient of ϕ_e	I_F = 100 mA	$TK\phi_e$		- 0.35		%/K
Angle of half intensity		φ		± 3		deg
Peak wavelength	I_F = 100 mA	λ_p	840	850	870	nm
Spectral bandwidth	I_F = 100 mA	$\Delta\lambda$		30		nm
Temperature coefficient of λ_p	I_F = 100 mA	$TK\lambda_p$		0.25		nm/K
Rise time	I_F = 100 mA	t_r		10		ns
Fall time	I_F = 100 mA	t_f		10		ns

BASIC CHARACTERISTICS (T_{amb} = 25 °C, unless otherwise specified)

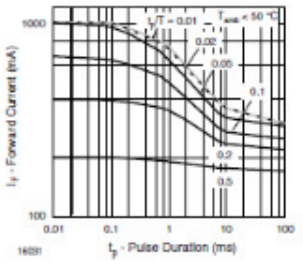

Fig. 3 - Pulse Forward Current vs. Pulse Duration

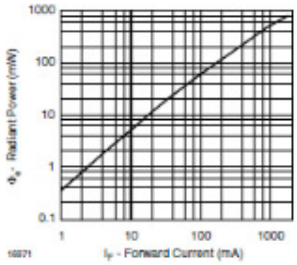

Fig. 6 - Radiant Power vs. Forward Current

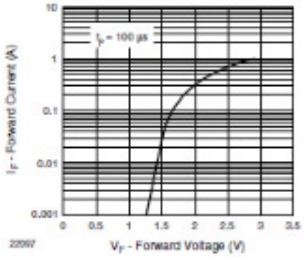

Fig. 4 - Forward Current vs. Forward Voltage

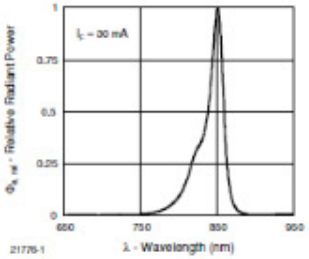

Fig. 7 - Relative Radiant Power vs. Wavelength

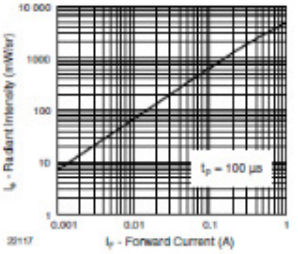

Fig. 5 - Radiant Intensity vs. Forward Current

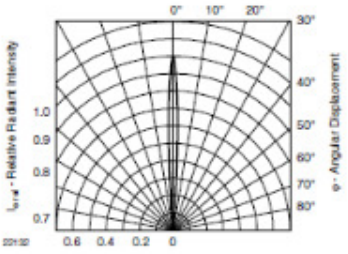

Fig. 8 - Relative Radiant Intensity vs. Angular Displacement

PACKAGE DIMENSIONS in millimeters

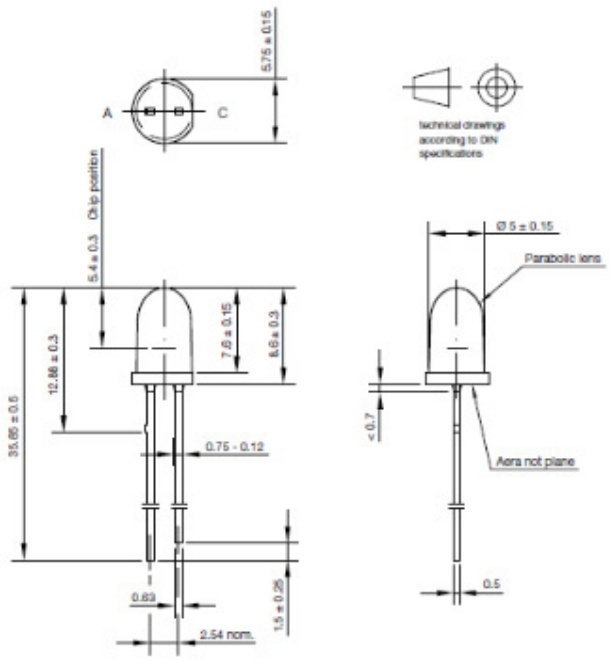

Drawing-No.: 6.544-5385.01-4
Issue: 2; 08.03.10
20531

Not indicated tolerances ± 0.1

Silizium-PIN-Fotodiode mit Tageslichtsperrfilter
Silicon-PIN-Photodiode with Daylight Filter
Lead (Pb) Free Product - RoHS Compliant

SFH 205 F

Wesentliche Merkmale

- Speziell geeignet für Anwendungen bei 950 nm
- Kurze Schaltzeit (typ. 20 ns)
- 5 mm-Plastikbauform im LED-Gehäuse
- Auch gegurtet lieferbar

Features

- Especially suitable for applications of 950 nm
- Short switching time (typ. 20 ns)
- 5 mm LED plastic package
- Also available on tape and reel

Anwendungen

- IR-Fernsteuerung von Fernseh- und Rundfunkgeräten, Videorecordern, Lichtdimmern, Gerätefernsteuerungen
- Lichtschranken für Gleich- und Wechsellichtbetrieb

Applications

- IR-remote control of hi-fi and TV sets, video tape recorders, dimmers, remote control of various equipment
- Photointerrupters

Typ Type	Bestellnummer Ordering Code
SFH 205 F	Q62702P0102

Grenzwerte
Maximum Ratings

Bezeichnung Parameter	Symbol Symbol	Wert Value	Einheit Unit
Betriebs- und Lagertemperatur Operating and storage temperature range	T_{op}; T_{stg}	– 40 … + 100	°C
Sperrspannung Reverse voltage	V_R	32	V
Verlustleistung, T_A = 25 °C Total power dissipation	P_{tot}	150	mW

Kennwerte (T_A = 25 °C, λ = 950 nm)
Characteristics

Bezeichnung Parameter	Symbol Symbol	Wert Value	Einheit Unit
Fotostrom Photocurrent V_R = 5 V, E_e = 1 mW/cm²	I_P	60 (≥ 45)	µA
Wellenlänge der max. Fotoempfindlichkeit Wavelength of max. sensitivity	$\lambda_{S\,max}$	950	nm
Spektraler Bereich der Fotoempfindlichkeit S = 10% von S_{max} Spectral range of sensitivity S = 10% of S_{max}	λ	800 … 1100	nm
Bestrahlungsempfindliche Fläche Radiant sensitive area	A	7.00	mm²
Abmessungen der bestrahlungsempfindlichen Fläche Dimensions of radiant sensitive area	$L \times B$ $L \times W$	2.65 × 2.65	mm × mm
Halbwinkel Half angle	φ	± 60	Grad deg.
Dunkelstrom, V_R = 10 V Dark current	I_R	2 (≤ 30)	nA
Spektrale Fotoempfindlichkeit Spectral sensitivity	S_λ	0.59	A/W
Quantenausbeute Quantum yield	η	0.77	Electrons Photon
Leerlaufspannung, E_e = 0.5 mW/cm² Open-circuit voltage	V_O	330 (≥ 250)	mV

Kennwerte (T_A = 25 °C, λ = 950 nm)
Characteristics (cont'd)

Bezeichnung Parameter	Symbol Symbol	Wert Value	Einheit Unit
Kurzschlußstrom, E_e = 0.5 mW/cm² Short-circuit current	I_{SC}	28	µA
Anstiegs- und Abfallzeit des Fotostromes Rise and fall time of the photocurrent R_L = 50 Ω; V_R = 5 V; λ = 850 nm; I_p = 800 µA	t_r, t_f	20	ns
Durchlaßspannung, I_F = 100 mA, E = 0 Forward voltage	V_F	1.3	V
Kapazität, V_R = 0 V, f = 1 MHz, E = 0 Capacitance	C_0	72	pF
Temperaturkoeffizient von V_O Temperature coefficient of V_O	TC_V	– 2.6	mV/K
Temperaturkoeffizient von I_{SC} Temperature coefficient of I_{SC}	TC_I	0.18	%/K
Rauschäquivalente Strahlungsleistung Noise equivalent power V_R = 10 V	NEP	4.3×10^{-14}	$\frac{W}{\sqrt{Hz}}$
Nachweisgrenze, V_R = 10 V Detection limit	D*	6.2×10^{12}	$\frac{cm \times \sqrt{Hz}}{W}$

Relative Spectral Sensitivity
$S_{rel} = f(\lambda)$

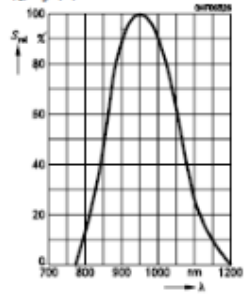

Photocurrent $I_P = f(E_e)$, V_R = 5 V
Open-Circuit Voltage $V_O = f(E_e)$

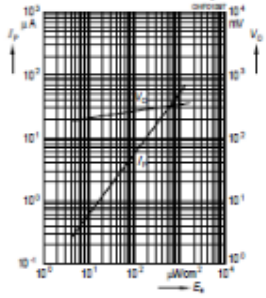

Total Power Dissipation
$P_{tot} = f(T_A)$

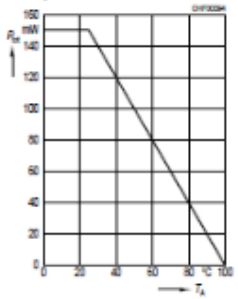

Dark Current
$I_R = f(V_R)$, E = 0

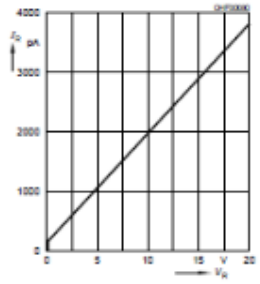

Capacitance
$C = f(V_R)$, f = 1 MHz, E = 0

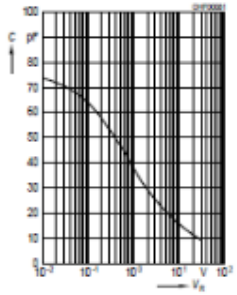

Dark Current
$I_R = f(T_A)$, V_R = 10 V, E = 0

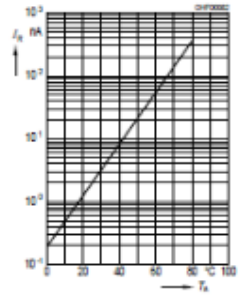

Directional Characteristics
$S_{rel} = f(\varphi)$

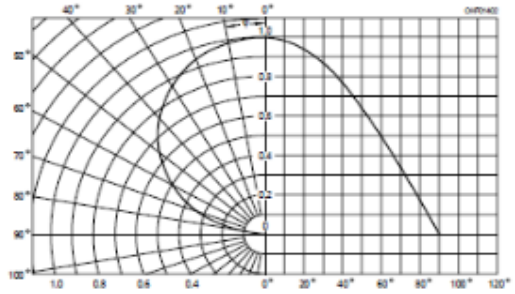

Maßzeichnung
Package Outlines

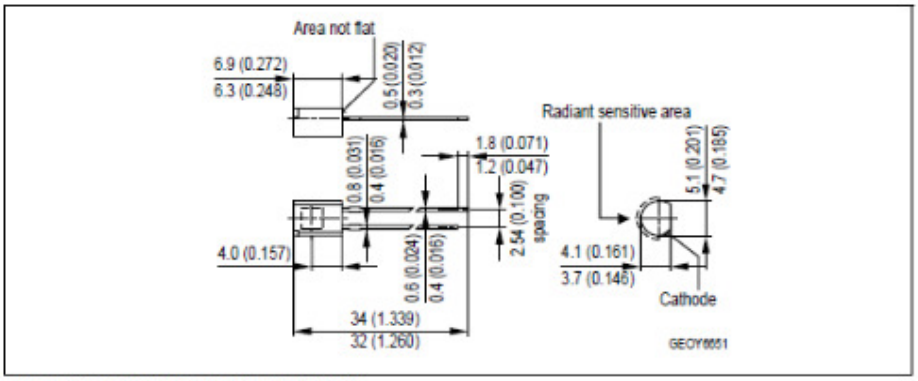

Maße in mm (inch) / Dimensions in mm (inch).

Lötbedingungen
Soldering Conditions
Wellenlöten (TTW) (nach CECC 00802)
TTW Soldering (acc. to CECC 00802

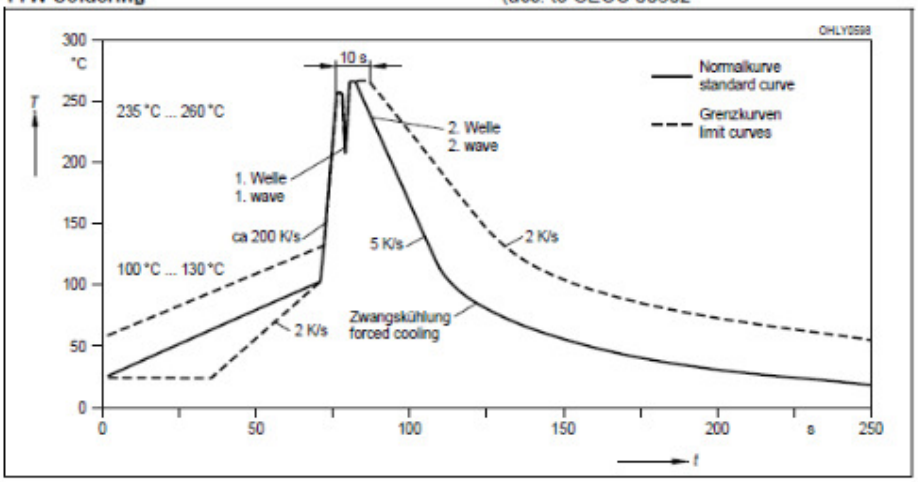

Ordering number : ENN6913A

SANYO Semiconductors
DATA SHEET

2SA2040 / 2SC5707 — PNP / NPN Epitaxial Planar Silicon Transistors
High Current Switching Applications

Applications
- DC / DC converter, relay drivers, lamp drivers, motor drivers, flash.

Features
- Adoption of FBET and MBIT processes.
- Large current capacitance.
- Low collector-to-emitter saturation voltage.
- High-speed switching.
- High allowable power dissipation.

Specifications ( ) : 2SA2040

Absolute Maximum Ratings at Ta=25°C

Parameter	Symbol	Conditions	Ratings	Unit
Collector-to-Base Voltage	V_{CBO}		(-50)100	V
Collector-to-Emitter Voltage	V_{CES}		(-50)100	V
Collector-to-Emitter Voltage	V_{CEO}		(-)50	V
Emitter-to-Base Voltage	V_{EBO}		(-)6	V
Collector Current	I_C		(-)8	A
Collector Current (Pulse)	I_{CP}		(-)11	A
Base Current	I_B		(-)2	A
Collector Dissipation	P_C		1.0	W
		Tc=25°C	15	W
Junction Temperature	Tj		150	°C
Storage Temperature	Tstg		-55 to +150	°C

Electrical Characteristics at Ta=25°C

Parameter	Symbol	Conditions	Ratings			Unit
			min	typ	max	
Collector Cutoff Current	I_{CBO}	V_{CB}=(-)40V, I_E=0A			(-)0.1	μA
Emitter Cutoff Current	I_{EBO}	V_{EB}=(-)4V, I_C=0A			(-)0.1	μA
DC Current Gain	hFE	V_{CE}=(-)2V, I_C=(-)500mA	200		560	
Gain-Bandwidth Product	fT	V_{CE}=(-)10V, I_C=(-)500mA		(290)330		MHz

Continued on next page.

SANYO Electric Co.,Ltd. Semiconductor Company
TOKYO OFFICE Tokyo Bldg., 1-10, 1 Chome, Ueno, Taito-ku, TOKYO, 110-8534 JAPAN

62405EA MS IM TB-00001403 / 30101 TS IM TA-3233 No.6913-1/5

Continued from preceding page.

Parameter	Symbol	Conditions	Ratings			Unit
			min	typ	max	
Output Capacitance	Cob	VCB=(-)10V, f=1MHz		(50)28		pF
Collector-to-Emitter Saturation Voltage	V_{CE}(sat)1	I_C=(-)3.5A, I_B=(-)175mA		(-230)160	(-390)240	mV
	V_{CE}(sat)2	I_C=(-)2A, I_B=(-)40mA		(-240)110	(-400)170	mV
Base-to-Emitter Saturation Voltage	V_{BE}(sat)	I_C=(-)2A, I_B=(-)40mA		(-)0.83	(-)1.2	V
Collector-to-Base Breakdown Voltage	$V_{(BR)CBO}$	I_C=(-)10μA, I_E=0A	(-50)100			V
Collector-to-Emitter Breakdown Voltage	$V_{(BR)CES}$	I_C=(-)100μA, R_{BE}=0Ω	(-50)100			V
Collector-to-Emitter Breakdown Voltage	$V_{(BR)CEO}$	I_C=(-)1mA, R_{BE}=∞	(-)50			V
Emitter-to-Base Breakdown Voltage	$V_{(BR)EBO}$	I_E=(-)10μA, I_C=0A	(-)6			V
Turn-On Time	t_{on}	See specified Test Circuit.		(40)30		ns
Storage Time	t_{stg}	See specified Test Circuit.		(225)420		ns
Fall Time	t_f	See specified Test Circuit.		25		ns

Package Dimensions

unit : mm

7518-003

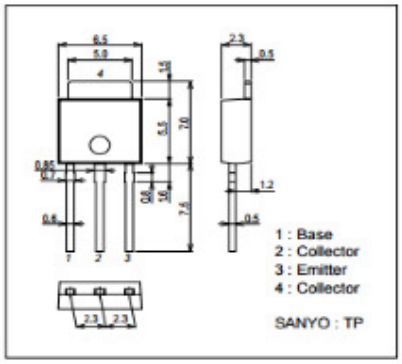

Package Dimensions

unit : mm

7003-003

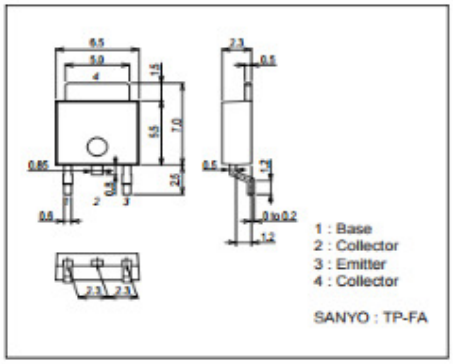

Switching Time Test Circuit

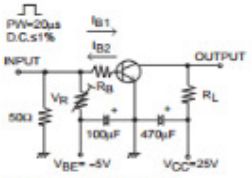

$20I_{B1}$= -$20I_{B2}$=I_C=2.5A

For PNP, the polarity is reversed.

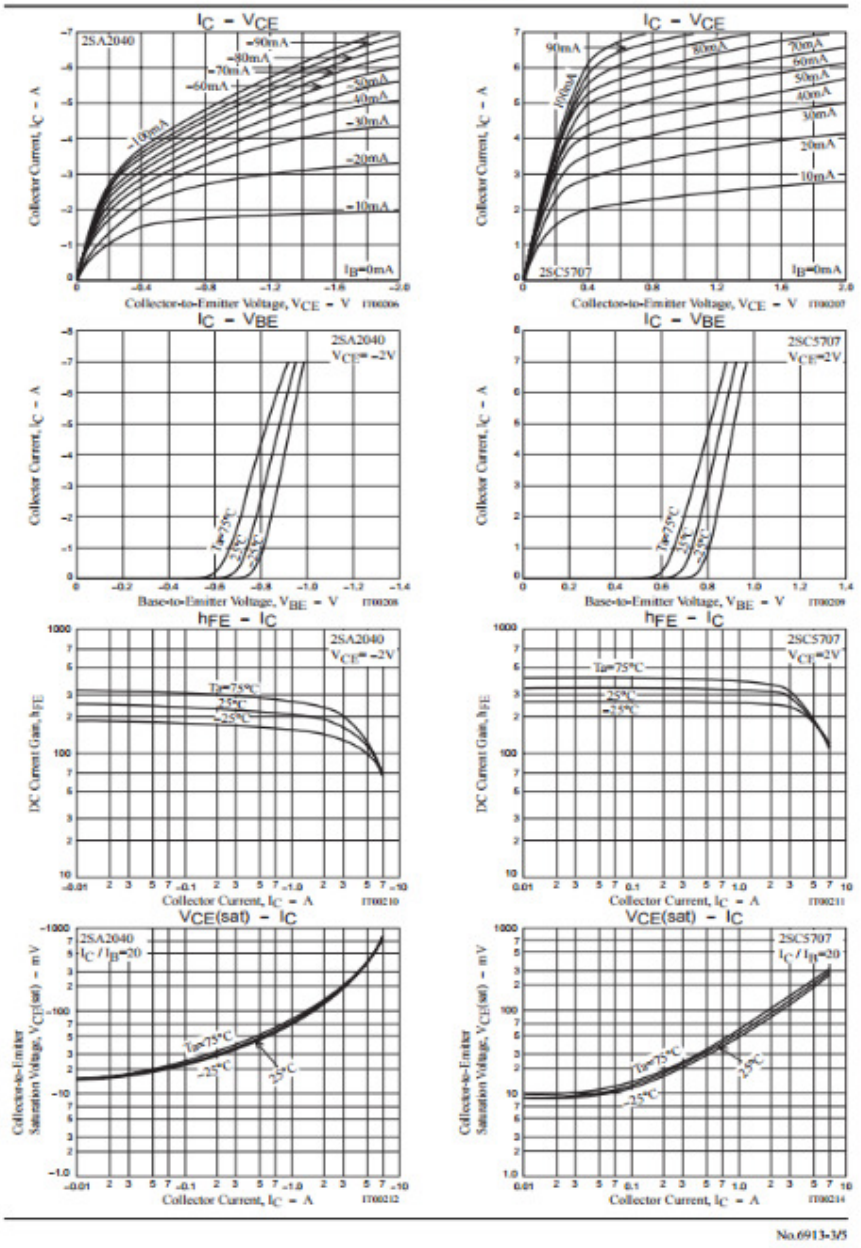
IC – VCE
2SA2040
–90mA
–80mA
–70mA
–60mA
–50mA
–40mA
–30mA
–20mA
–10mA
IB=0mA
Collector Current, IC – A
Collector-to-Emitter Voltage, VCE – V
IT00206
IC – VCE
2SC5707
90mA
80mA
70mA
60mA
50mA
40mA
30mA
20mA
10mA
IB=0mA
Collector Current, IC – A
Collector-to-Emitter Voltage, VCE – V
IT00207
IC – VBE
2SA2040
VCE= –2V
Ta=75°C
25°C
–25°C
Collector Current, IC – A
Base-to-Emitter Voltage, VBE – V
IT00208
IC – VBE
2SC5707
VCE=2V
Ta=75°C
25°C
–25°C
Collector Current, IC – A
Base-to-Emitter Voltage, VBE – V
IT00209
hFE – IC
2SA2040
VCE= –2V
Ta=75°C
25°C
–25°C
DC Current Gain, hFE
Collector Current, IC – A
IT00210
hFE – IC
2SC5707
VCE=2V
Ta=75°C
25°C
–25°C
DC Current Gain, hFE
Collector Current, IC – A
IT00211
VCE(sat) – IC
2SA2040
IC / IB=20
Ta=75°C
–25°C
25°C
Collector-to-Emitter Saturation Voltage, VCE(sat) – mV
Collector Current, IC – A
IT00212
VCE(sat) – IC
2SC5707
IC / IB=20
Ta=75°C
25°C
–25°C
Collector-to-Emitter Saturation Voltage, VCE(sat) – mV
Collector Current, IC – A
IT00214

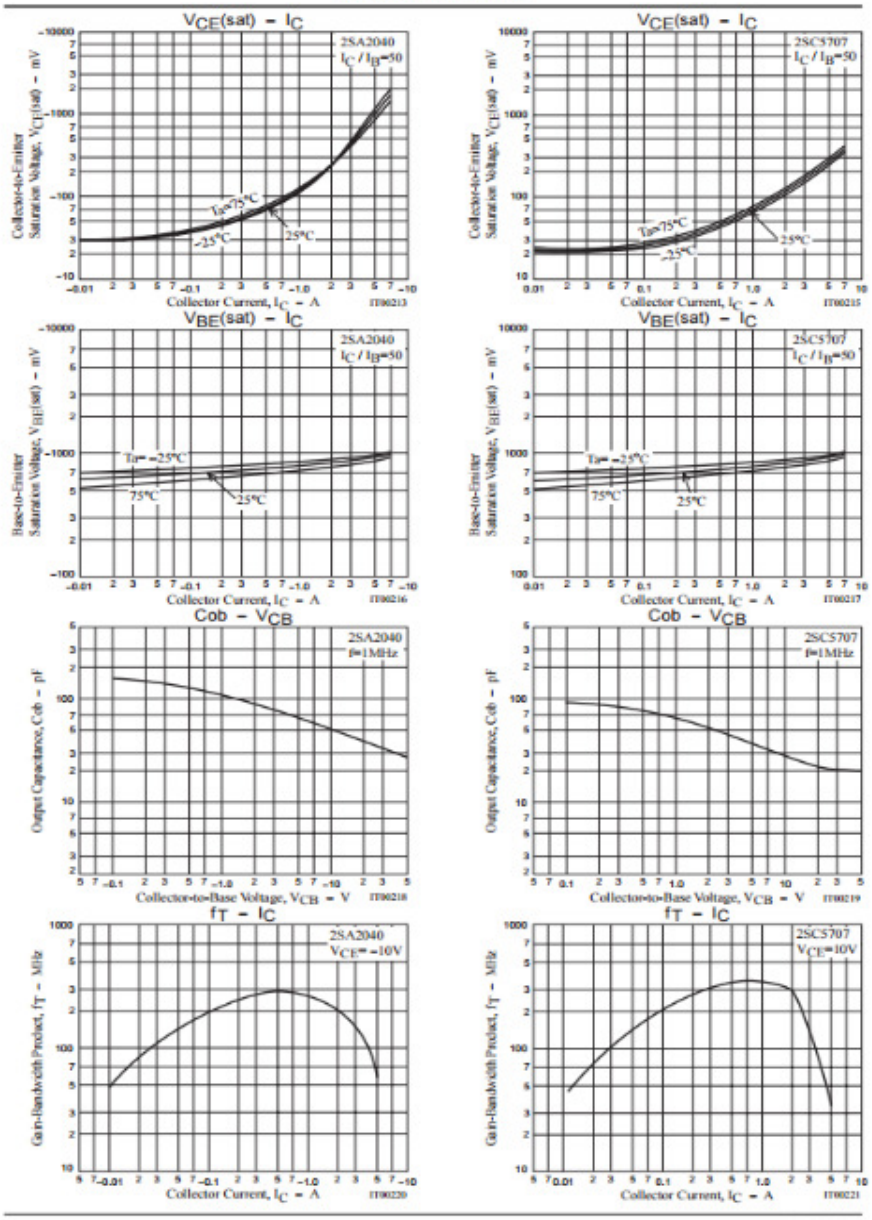
VCE(sat) – IC
2SA2040
IC / IB=50
Collector-to-Emitter Saturation Voltage, VCE(sat) – mV
Ta=75°C
–25°C
25°C
Collector Current, IC – A
IT00213
VCE(sat) – IC
2SC5707
IC / IB=50
Collector-to-Emitter Saturation Voltage, VCE(sat) – mV
Ta=75°C
–25°C
25°C
Collector Current, IC – A
IT00215
VBE(sat) – IC
2SA2040
IC / IB=50
Base-to-Emitter Saturation Voltage, VBE(sat) – mV
Ta=–25°C
75°C
25°C
Collector Current, IC – A
IT00216
VBE(sat) – IC
2SC5707
IC / IB=50
Base-to-Emitter Saturation Voltage, VBE(sat) – mV
Ta=–25°C
75°C
25°C
Collector Current, IC – A
IT00217
Cob – VCB
2SA2040
f=1MHz
Output Capacitance, Cob – pF
Collector-to-Base Voltage, VCB – V
IT00218
Cob – VCB
2SC5707
f=1MHz
Output Capacitance, Cob – pF
Collector-to-Base Voltage, VCB – V
IT00219
fT – IC
2SA2040
VCE=–10V
Gain-Bandwidth Product, fT – MHz
Collector Current, IC – A
IT00220
fT – IC
2SC5707
VCE=10V
Gain-Bandwidth Product, fT – MHz
Collector Current, IC – A
IT00221

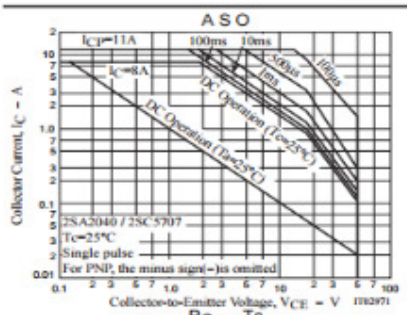

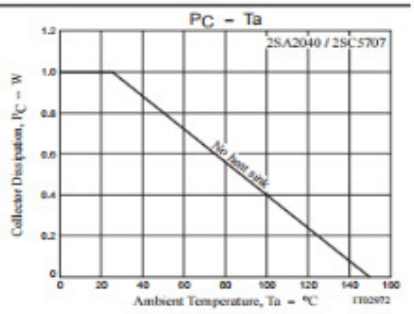

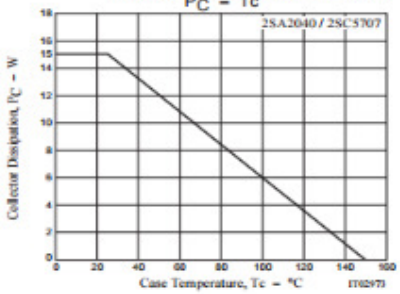

PS No.6913-5/5

Appendix C

Calculation to estimate number of reflections in bent tubes based on Snell's Law

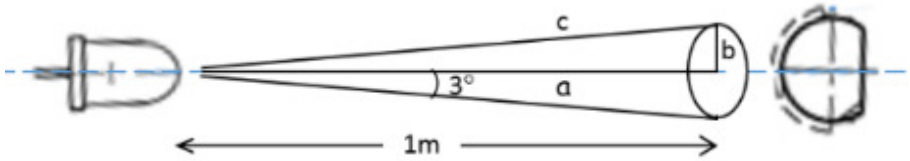

According to the above diagram, the first reflections within the tube are calculated as

	20 mm tube	35 mm tube	40 mm tube
Given	b = 10 mm θ = 3°	b = 17.5 mm θ = 3°	b = 20 mm θ = 3°
Thus, first reflection occur at	$\sin\theta = \frac{10\ mm}{c}$ $\therefore c = \frac{10\ mm}{\sin 3°}$ $= 190\ mm$	$\sin\theta = \frac{17.5\ mm}{c}$ $\therefore c = \frac{17.5\ mm}{\sin 3°}$ $= 333.92\ mm$	$\sin\theta = \frac{10\ mm}{c}$ $\therefore c = \frac{20\ mm}{\sin 3°}$ $= 381.62\ mm$

Example calculation for 20 mm tube at 30° bend

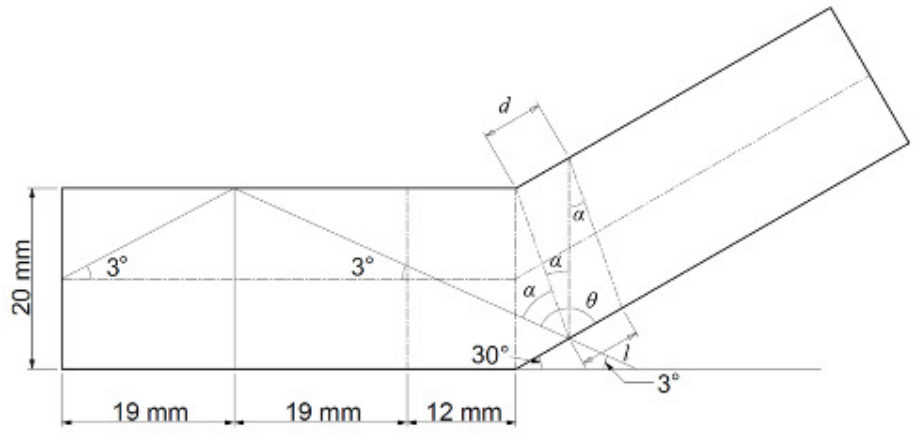

Figure 7-17 Determination of the number of reflections in bent tube.

$\theta = 180° - bend\ angle - IRLED\ half\ angle$

$\theta = 180° - 30° - 3° = 147°$

$\alpha = \theta - 90° = 147° - 90° = 57°$

$$\tan\alpha = \frac{l}{tube\ diameter}$$

$\therefore l = (tube\ diameter)x(\tan\alpha) = (20\ \text{mm})\text{x}\ (\tan 57°) = 3.08\ cm$

Thus, the number of reflections in 20 mm tube are estimated as

$$\therefore no\ of\ reflections = \frac{length\ of\ tube}{2l} = \frac{50\ cm}{2\ x\ (3.08cm)} = 8.11\ reflections$$